RSC Chemical Biology

ROYAL SOCIETY OF CHEMISTRY

REVIEW

View Article Online
View Journal | View Issue

Cite this: *RSC Chem. Biol.*, 2026, 7, 536

Illuminating microtubule functions with small molecules: past, present and future of fluorescent tubulin-binding probes

R. París-Ogáyar, †[ab] D. Lucena-Agell, †[b] K.-H. Altmann, [c] V. Palomo *[ade] and J. F. Díaz *[b]

Developing tools for the real-time visualization of tubulin, microtubules, and their dynamics is essential for studying key cellular processes such as cell division, migration, and differentiation. In this context, fluorescent small-molecule probes that bind to distinct and specific sites on microtubules have significantly advanced our understanding of tubulin dynamics and functions. In addition, fluorescent probes targeting tubulin have enabled the development of high-throughput screening assays to identify novel anti-tubulin compounds. In this review, we present a comprehensive overview of currently available fluorescent molecules that bind to tubulin, detailing their chemical structures, binding sites, development strategies and relevance to the study of microtubule functions. We also explore future directions in this field and highlight key fluorescent probes that are still lacking. Developing these tools would enable the investigation of tubulin's diverse cellular roles in even greater depth and support the advancement of tubulin-targeted therapeutics.

Received 11th December 2025,
Accepted 4th February 2026

DOI: 10.1039/d5cb00321k

rsc.li/rsc-chembio

[a] *Instituto Madrileño de Estudios Avanzados en Nanociencia (IMDEA Nanociencia), Madrid, Spain. E-mail: valle.palomo@imdea.org*
[b] *Unit for the Development of Biological, Immunological and Chemical Drugs, Centro de Investigaciones Biológicas Margarita Salas – CSIC, Madrid, Spain. E-mail: fer@cib.csic.es*
[c] *Department of Chemistry and Applied Biosciences, ETH Zürich, Zürich, Switzerland*
[d] *Biomedical Research Networking Centre on Neurodegenerative Diseases (CIBERNED), Instituto de Salud Carlos III, Madrid, Spain*
[e] *Unidad de Nanobiotecnología asociada al Centro Nacional de Biotecnología (CNB-CSIC), Madrid, Spain*
† These authors have equally contributed.

R. París-Ogáyar

Rebeca París Ogáyar (BSc in Chemistry, MSc in Drug Discovery) is a PhD candidate in Medicinal Chemistry at the Centro de Investigaciones Biológicas Margarita Salas (CSIC) and IMDEA Nanociencia, under the supervision of Dr. Fernando Díaz and Dr. Valle Palomo. Her doctoral research focuses on the development of fluorescent tubulin-targeting probes and on characterizing MAP-microtubule interactions in the presence of microtubule-targeting agents. She has completed her predoctoral research at ETH Zurich under the supervision of Karl-Heinz Altmann and at Biocev Prague in the Lánský and Braun laboratory.

D. Lucena-Agell

Daniel Lucena-Agell (BSc in Biology, MSc in Microbiology) obtained his PhD in Microbiology at Centro de Investigaciones Biológicas Margarita Salas in 2014. In 2015, he joined the Microtubule Stabilizing Agents lab (currently known as Structure and Function of Cytoskeleton lab) led by Dr. Fernando Díaz. He completed a postdoctoral position in 2016 at PSI under the supervision of Prof. Michel Steinmetz. Focusing his research on the microtubule field with special emphasis on the biochemical and structural characterization of novel microtubule-targeting agents, he has participated in the development and application of different microtubule-targeting agent-derived fluorescent probes.

Introduction

Microtubules are cytoskeletal polymers formed by the polarized assembly of α/β-tubulin heterodimers, and their behavior is tightly regulated at multiple levels. Through their dynamic properties, microtubules perform essential cellular functions including ensuring proper chromosome segregation during mitosis, facilitating intracellular transport *via* motor proteins, forming specialized motile structures such as cilia and flagella, and enabling cells to acquire and maintain their specific shapes. Given their central role in cell division, shaping and angiogenesis, microtubules are crucial for cell proliferation and migration (extensively reviewed in a previous study[1]), one of the hallmarks of cancer, along with the need for vascular support. Consequently, microtubule-targeting agents (MTAs) have been among the most successful classes of drugs used in cancer therapy (reviewed in previous works[2–4]). These compounds are broadly categorized as microtubule stabilizers (MSAs) or destabilizers (MDAs) (including tubulin degradation inducers) based on their overall effect on the equilibrium between soluble tubulin and microtubule polymers. To date, eight distinct ligand-binding sites on tubulin have been described, allowing MTAs to be classified by their specific binding domain.[5–7] Named after the first compound discovered to bind to each specific region, these druggable sites in tubulin are the colchicine site (1), the vinca domain (2), the taxane binding site (3), the maytansine binding site (4), the laulimalide/peloruside binding site (5), the pironetin binding site (6), the gatorbulin binding site (7), and the todalam binding site (8) (Fig. 1). Despite their efficacy, MTAs often have limited clinical use due to their adverse effects, particularly neurotoxicity and myelosuppression, which hinder their broader applications in other tubulin-related pathologies (reviewed in previous studies[8–10]). Hence, a better understanding of the action of MTAs at the molecular, cellular, and organismal levels is essential for developing safer and more effective compounds.

Historically, studying microtubules and the effects of small molecules on their dynamics has required a multidisciplinary approach. The discovery of tubulin itself was enabled by its interactions with colchicine, which led to tubulin purification and allowed biochemical characterization of microtubules.[11,12] The development of tubulin-specific antibodies allowed the visualization of the cytoskeleton and the evaluation of drug effects on microtubule's functions.[13–16] However, this method requires cell fixation and permeabilization, thus limiting dynamic studies. Early live-cell imaging of microtubule behavior relied on microinjecting a rhodamine-labeled tubulin,

K.-H. Altmann

Karl-Heinz Altmann is a Professor Emeritus at the ETH Zurich, where he held a chair in pharmaceutical biology from 2003 to 2022. Before joining ETH, Prof. Altmann spent 13 years in industrial drug discovery research (Ciba-Geigy, Novartis), where his latest role was that of acting head of Global Discovery Chemistry of the Novartis Institutes for Biomedical Research. Prof. Altmann's research interests are centered on the chemical synthesis of pharmaceutically relevant natural products/natural product analogs and their biological evaluation, with a particular focus on leads for anticancer and antibacterial drug discovery.

V. Palomo

Valle Palomo is a tenured researcher and Head of the Biosensors in Neuroscience Lab at IMDEA Nanociencia (Madrid, Spain). She obtained her PhD in Chemistry at the Medicinal Chemistry Institute (CSIC, Madrid) and completed postdoctoral training at The Scripps Research Institute (La Jolla, USA). Her research integrates medicinal chemistry, nanotechnology, and biosensor development to advance therapies and biomarkers for neurodegenerative diseases. Her work has delivered innovative chemical tools, patented technologies, and translational applications, with current efforts focused on early diagnosis and disease-modifying strategies using patient-derived models.

J. F. Díaz

J. Fernando Díaz is a Senior Scientist at Centro de Investigaciones Biológicas Margarita Salas (CSIC). He obtained his PhD at the Universidad Complutense de Madrid, conducting his doctoral research at CIB (Spain) and at SERC (UK). He then pursued postdoctoral training and served as an associated researcher at the Catholic University of Leuven (1993-1999). His research in chemical biology focuses on tubulin/microtubules, integrating structural biology, biophysics, and medicinal chemistry to develop chemical microtubule probes and modulators. His work has delivered landmark structural insights, patents, and translational applications, with future efforts aimed at decoding microtubule structural signaling in disease and therapy.

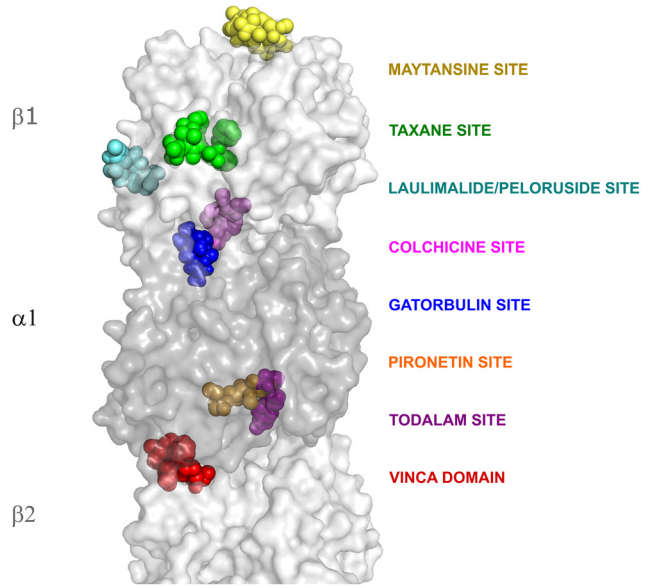

Fig. 1 Binding sites described for small-molecule ligands that can interfere with microtubule functions. Space-filling model of a representative ligand for each binding site is shown in different colors, with the site name in the same color. α-tubulin is shown in dark grey and β-tubulin in light grey.

a technically challenging method requiring tubulin isolation, labeling and reintroduction into cells.[17–19] A major breakthrough came in the late 1990s with the introduction of plasmids encoding green fluorescent protein (GFP)-tagged cytoskeletal proteins into eukaryotic cells (reviewed in a previous study[20]), leading to the first cell lines stably expressing GFP-α-tubulin.[21] However, while the impact of this technique on the field has been significant, overexpression and tag placement can alter the tubulin isotype composition and microtubule dynamics, which limits the interpretability of results obtained with these systems.[21–23] To overcome these shortcomings, more recent studies have used fluorescent tags embedded within the tubulin sequence to preserve the native isotype expression.[24] Moreover, gene-editing technologies now enable endogenous tagging of tubulin, avoiding disturbances in tubulin homeostasis and allowing the implementation of single-molecule imaging.[25–27]

An alternative approach has been fusing fluorescent proteins to microtubule-associated proteins (MAPs) for indirect microtubule visualization and simultaneous study of MAP-microtubule interactions both biochemically and in cells.[28,29] Recently, fluorescent peptides derived from MAPs have been developed to probe microtubule functions with minimal perturbation.[30]

Furthermore, alternative peptide-based approaches have encompassed the identification of short peptide sequences *via* phage display, in which the authors conjugated them to different fluorophores to suit specific experimental requirements.[31]

In addition to protein-based approaches, biologically active fluorescent probes derived from tubulin-binding drugs or other ligands have proven to be effective for visualizing and studying microtubules. Although these compounds must be carefully selected and dosed to avoid interference with microtubule dynamics, they offer significant advantages. Their versatile synthetic accessibility and increasingly improving photophysical properties provide a high signal-to-noise ratio that enables single-molecule sensing. The conjugation of low molecular weight fluorophores to target-specific recognition elements enables the labeling of molecular structures with extraordinary levels of precision. Furthermore, low molecular weight probes provide access to the nanometer scale, thus allowing to reach confined environments that could remain inaccessible to macromolecular options. Finally, fluorescent tubulin probes can be used for the *in vitro* screening and characterization of novel compounds, particularly to determine drug-binding sites *via* competition assays based on the changes in fluorescence signal. It is also worth pointing out that some compounds exhibit intrinsic fluorescence upon binding to tubulin, enabling straightforward and precise affinity measurements.[32]

Although ligand-derived molecular scaffolds provide excellent templates for fluorescent tubulin probes, their development remains a challenge due to synthetic and biochemical hurdles. However, major methodological advances have been reported in the field in recent years, which are summarized in this review together with their impact on cytoskeletal research. Fluorescent probes will be grouped together according to their binding site on tubulin, which will be discussed following the chronological order of their discovery. In addition to reviewing the data on tubulin-directed fluorescent probes reported in the relevant literature, we report previously unpublished data from our own laboratory, including hitherto unavailable equilibrium-binding constants (K_b) for several commercially available fluorescent tubulin probes. We believe that binding constants are essential parameters to be considered when choosing an appropriate probe. Finally, our account includes a tabulated summary of the most relevant probes, detailing their chemical structures, binding affinities (where available), and reported applications. This data collection is intended to support the informed selection of molecular tools for experimental design in tubulin/microtubule research.

It should be noted here that, in addition to fluorescent probes based on small molecules that target the well-characterized binding sites in tubulin, our analysis of the literature has identified other compounds reported to associate with tubulin. For example, DAPI, a DNA intercalator commonly used for nuclear staining (reviewed in a previous study[33]), has also been shown to bind to tubulin,[34] and it has been employed in *in vitro* studies of polymerization dynamics.[35] Similarly, other fluorescent compounds such as bis-ANS,[36] DCVJ,[37] Nile red,[38] and prodan[39] have been shown to interact with tubulin and have been used in various *in vitro* experimental settings. However, these compounds are neither MSAs nor MDAs, and their binding to tubulin is not specific. For these reasons, they will not be further discussed in this review.

Colchicine site

Colchicine is a microtubule destabilizer and the first microtubule-targeting agent ever identified. In fact, colchicine

enabled the discovery of tubulin as the main structural component of microtubules by Borisy and Taylor in 1967.[40,41] They characterized tubulin as a protein capable of binding to colchicine and concluded that this protein served as the fundamental building block of microtubules. Although numerous compounds have since been identified to bind to the colchicine site, none of these have proven suitable for cancer clinical applications, due to their high toxicity and narrow therapeutic window.[42] However, colchicine itself is currently used for the treatment of gout and various autoimmune diseases. Additionally, some azoles such as mebendazole and albendazole are employed as anthelmintics (reviewed in previous studies[43,44]). Finally, podophyllotoxin has been widely used in the topical treatment of genital warts[45,46] and infections caused by *Molluscum contagiosum* virus.[47,48]

Structurally, the colchicine site is located within a sizable hydrophobic pocket at the interface of the α- and β-tubulin subunits within the same heterodimer. This pocket is defined by helices H7 and H8, the T7 loop, and strands S8, S9 and S10 of the two tubulin β-sheets, and it is completed by the T5 loop of α-tubulin[49] (Fig. 2). The compound's accommodation in this site generates several conformational adjustments that explain its inhibitory activity. The most significant of these is a switch in the T7 loop that flips to accommodate the ligand, thus blocking the curved-to-straight transition necessary for microtubule assembly, thereby inhibiting polymerization.[50,51] The colchicine binding site can be subdivided into three zones.[52] Zone 2 serves as the primary binding pocket and accommodates most ligand structures. Zones 1 and 3 are auxiliary, with very few ligands occupying both simultaneously. Zone 1 lies at the interface with the α-subunit, while zone 3 extends deeper into the β-subunit. Ligands with a globular or butterfly-like conformation, referred to as classical colchicine site inhibitors (CBSIs), typically interact with zones 1 and 2, mimicking colchicine's binding mode. In contrast, non-classical CBSIs, which exhibit more planar structures, tend to bind deeper within the β-subunit, covering zones 2 and 3.[53–57]

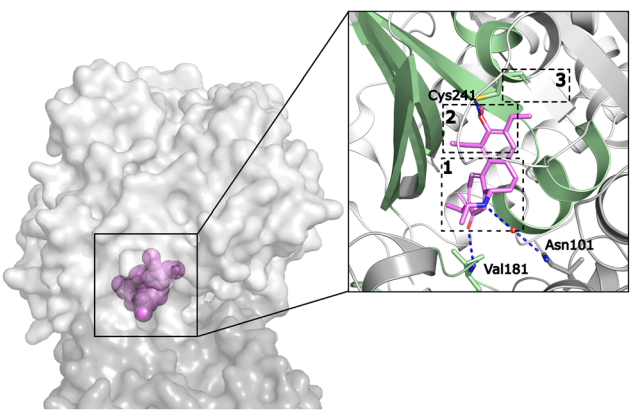

Fig. 2 Structure of colchicine-bound tubulin. (PDB: 5XIW). In the inset, the colchicine site is delineated by pale green ribbons and zones 1, 2 and 3 are boxed in dashed squares. Main interactions between colchicine and α-tubulin are shown by dashed lines. Highlighted are the hydrogen bonds with α-Val181 and β-Cys241 and a water-mediated hydrogen bond with α-Asn101. Oxygen and nitrogen atoms participating in the main interactions are shown in TV-red and blue, respectively.

Colchicine (**1a**) itself fluoresces upon binding to tubulin, and therefore, it is described as the first fluorogenic probe to target this protein. This property was first reported by Arai and Okuyama in 1973[58,59] and independently confirmed by Bhattacharyya and Wolff in 1974.[60] This feature allowed the biochemical determination of the behavior of this ligand when interacting with tubulin. However, colchicine presents a low kinetic dissociation constant and almost irreversibly binds to tubulin, which limits its applicability for the characterization of novel compounds in competitive experiments. To address this shortcoming, a new fluorescent compound, 2-methoxy-5-(2′,3′,4′-trimethoxyphenyl)tropone (also known as MTC, **1b**) was developed by Fitzgerald.[61] This compound, lacking the ring B of colchicine, retains the fluorescence properties of the parent compound but exhibits faster reversible binding[62] (K_b of 4.9×10^5 M^{-1}).[63] This probe has been widely employed to characterize both the colchicine site and its binders, allowing the identification and characterization of many novel ligands of this domain.[64–69]

As an alternative to exploiting the intrinsic fluorescence of colchicine and derivatives, different fluorophores have been attached to the molecule to allow a broader use *in cells* and *ex vivo* scenarios (Fig. 3). In 1978, Clark and Garland attached a fluorescein molecule at C7,[70] resulting in a probe (**1c**) that showed similar biological behavior as the parent compound. However, in 1999, Craenenbroeck and Engelborghs demonstrated that the fluorescein group altered the binding behavior, thereby identifying a secondary colchicine-binding site and classifying the probe as a conformation-dependent binder.[71] Despite this limitation, the fluorescein-colchicine probe has been extensively used to characterize colchicine analogues.[72–74] In 2018, Zvereva and collaborators employed the same fluorescent tag in a fluorescence anisotropy immunoassay to monitor colchicine levels in biological fluids.[75]

To improve the probe performance, Arnold *et al.* synthesized two BODIPY–colchicine conjugates (**1d-1e**) in 2008, which proved effective in both biochemical assays and live-cell imaging.[76] Other fluorophoric groups such as dansyl[77] or nitrobenzoxadiazole (NBD)[78] moieties have also been attached to colchicine (**1f-1g**) or its analogue colcemid (**1h**). It is worth mentioning that in the context of high-resolution microscopy, Zhang and co-workers developed a new colchicine photoswitchable fluorescent probe (**1i**) in 2015 by attaching a spiropyran derivative to the secondary amino group on ring B of colchicine.[79] They validated this probe for high-resolution microscopy to quantitatively monitor trace amounts of tubulin in cancer cells.

Recently, Jurášek and colleagues reported a novel, green-emitting BODIPY–colchicine (**1j**) with high potency in order to unveil the involvement of different cellular membrane-based compartments in the inhibition of microtubule cytoskeleton dynamics by colchicine.[80]

Beyond colchicine-based fluorescent probes, Leynadier and co-workers developed in 1993 two pteridine analogues, (*S*)-(−)- and

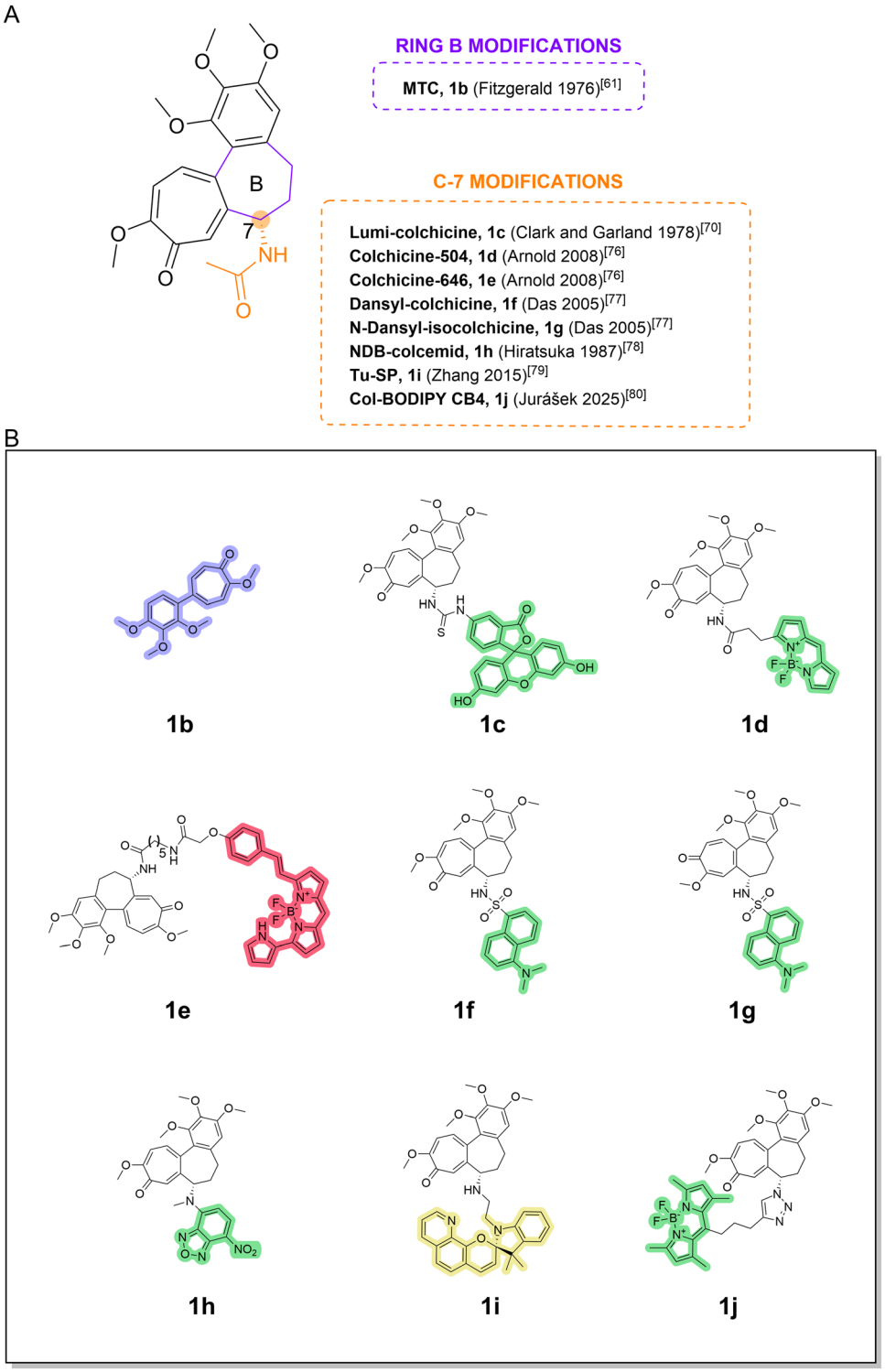

Fig. 3 Chemical structures of colchicine-based fluorescent probes. (A) Modification sites for fluorophore attachment on the colchicine core to yield biologically active fluorescent probes. (B) Chemical structures of colchicine-based fluorescent probes. The color of the highlighted regions represents the range of color emission of the corresponding fluorophore. RGB color codes assigned to represent each fluorescent emission range are as follows: UV (172,172,255); green (126,226,149); yellow (243,237,156); and far-red (251,98,124).

(*R*)-(+)-ethyl(5-amino-1,2-dihydro-2-methyl-3-phenylpyrido[3,4-*b*]-pyrazin-7-yl)carbamate (**2a** and **2b**, respectively) that bind to the colchicine site. These molecules fluoresce upon binding, with affinities surpassing that of MTC (4.1×10^6 M^{-1} for the (*S*)-isomer (**2a**) and 3.2×10^6 M^{-1} for the (*R*)-isomer (**2b**[81])) (Fig. 4). The (*R*)-isomer in particular has become a widely used tool for

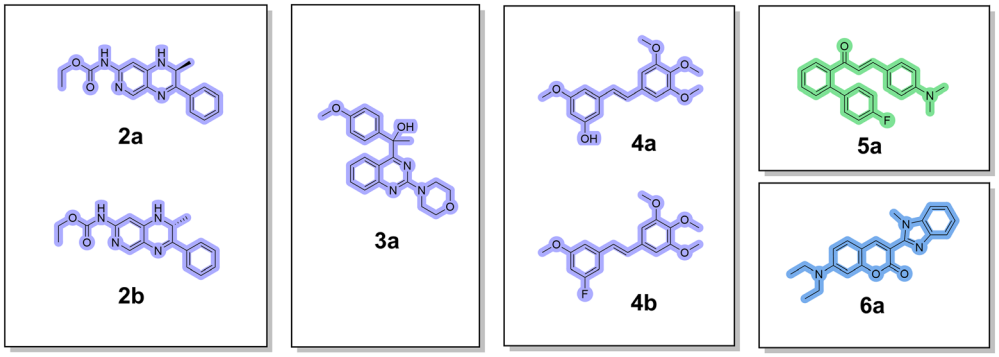

Fig. 4 Chemical structures of colchicine site fluorescent probes not based on the colchicine structure. Pteridines **2a** and **2b**, quinazoline **3a**, combretastatins **4a** and **4b**, chalcone OC9 **5a** and coumarin-30 **6a** are shown. RGB color codes assigned to represent each fluorescent emission range are as follows: UV (172,172,255); blue (119,173,237); and green (126,226,149).

identifying and characterizing high-affinity colchicine site binders.[49,82–84] PM534, a novel colchicine site tubulin assembly inhibitor that occupies the entire binding pocket, was partially characterized using a competition assay with this fluorescent probe.[57] Additionally, Suzuki *et al.* developed a family of fluorescent quinazolines (**3a**) that bind the colchicine site both *in vitro* and in cellular systems.[85]

Combretastatins—another group of colchicine site binders—exhibit potent antiproliferative activity. Among them, *Z*-isomers are more biologically active, but only the *E*-isomers exhibit fluorescence (**4a-4b**) (UV region). Leveraging this property, Bisby *et al.*[86] monitored compound uptake and intracellular distribution by means of fluorescence measurements (Fig. 4).

Additionally, in 2014[87] a series of *ortho*-aryl chalcones were characterized as a novel chemotype exhibiting tubulin-binding activity, with one derivative (OC9,[88] **5a**) displaying particularly potent antiproliferative capacity in both *in vitro* and *in vivo* experimental models. Furthermore, this compound exhibited fluorescence upon tubulin binding, thereby enabling its application as a fluorogenic probe for its spatial localization within the colchicine pocket in tubulin by fluorescent competitive assay. The authors employed this probe to efficiently characterize tubulin dynamics in different types of cancer cells.

Finally, a recent study[89] has identified coumarin-30 (**6a**), a laser dye, as a competitive ligand for the colchicine-binding site on tubulin. This compound exhibits substantially enhanced fluorescence properties, which make it a more versatile probe. This new ligand enabled the authors to identify and characterize a series of tubulin binders of the canonical colchicine-binding site and discover ligands that interact with other, less characterized binding pockets (*i.e.* "βαI" site).

Vinca domain

First isolated from the Madagascar periwinkle (*Catharanthus roseus*, previously *Vinca rosea*) in the mid-1950s by Cutts, Beer and Noble, vinblastine is one of the first anticancer agents used clinically.[90] The discovery of the compound traces back to the use of teas made from periwinkle leaves in folk medicine, which were supposed to have antidiabetic properties. In an attempt to validate this assumption, Cutts, Beer and Noble administered extracts from *C. roseus* leaves to rats, but they did not observe any lowering in the blood glucose levels. Rather, the animals exhibited severe leukopenia and bone marrow suppression. Activity-guided fractionation of the crude extract eventually led to the isolation of a crystalline compound with chemotherapeutic potential, which was named vincaleukoblastine, now known as vinblastine. Vinblastine was approved for cancer treatment in 1961, while vincristine, another vinca alkaloid, was approved in 1963.[91] Following these discoveries, second-generation vinca alkaloids were developed, including vindesine (only approved in some countries) and vinorelbine (reviewed in a previous study[92]). These compounds act as microtubule destabilizers and bind to the vinca domain of tubulin, a site located at the interface between two αβ-tubulin heterodimers. Compounds targeting the vinca domain inhibit microtubule assembly by acting as structural wedges at the longitudinal interface between tubulin dimers (reviewed in previous studies[3,93]).

As is the case for most of the tubulin-binding sites for low-molecular weight ligands, the vinca domain is structurally promiscuous. Besides vinca alkaloids, structurally unrelated compounds that target the vinca domain and exhibit similar microtubule-destabilizing activity have been identified. These include halichondrins,[94] auristatins and dolastatins.[95,96] Among them, eribulin, a synthetic analogue of the marine natural product halichondrin B, was approved by the FDA in 2010 for the treatment of breast cancer (https://www.accessdata.fda.gov/scripts/cder/daf/index.cfm?event=overview.process&ApplNo=201532).

The vinca domain extends across regions from two adjacent tubulin heterodimers and includes overlapping regions targeted by both vinblastine and dolastatins.[5] As part of microtubules, the domain faces the inner lumen and is involved in longitudinal protofilament contacts. The vinblastine-binding pocket is enclosed by the T7 loop, helix H10, and strand S9 of the α-subunit together with the C-terminal turn of helix H6 and the T5 and H6–H7 loops of β-tubulin from the adjacent heterodimer.[97,98] In contrast, the dolastatin site extends towards helix H1 of the β-subunit and typically accommodates

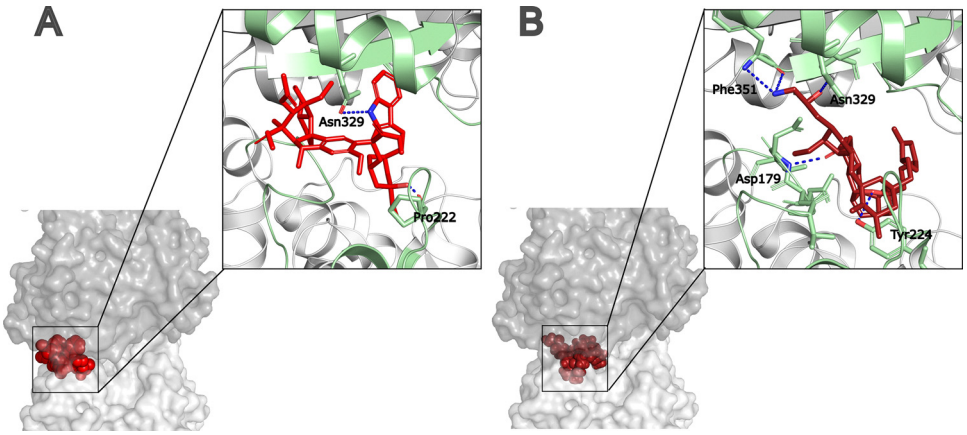

Fig. 5 Structures of vinca domain ligand-bound tubulin. Structure of (A) vinblastine-bound tubulin (PDB: 8CLE) and (B) eribulin-bound tubulin (PDB: 5JH7). In the inset, the vinca domain is delineated by pale green ribbons. Main interactions with α- and β-tubulin are shown as dashed lines. Highlighted are the (A) hydrogen bonds with β-Pro222 and α-Asn329 and (B) hydrogen bonds with β-Asp179, β-Tyr224, α-Asn329 and α-Phe351. Oxygen and nitrogen atoms participating in the main interactions are shown in TV-red and blue, respectively.

flexible peptides of three or more amino acid residues[99] (Fig. 5). The binding of vinca site ligands to this site stabilizes curved tubulin oligomers that are incompatible with the straight conformation required for microtubule polymerization. Additionally, some vinca site ligands disrupt GDP-GTP exchange in tubulin by interacting with β-Tyr224, a residue that stabilizes the guanine base interaction with the protein.[99,100]

Several fluorescent probes have been developed based on vinblastine to study its binding site and interactions with tubulin (Fig. 6). In 1996, Rai and Wolff[101] created the first fluorescent probe for the vinca site, a vinblastine-4′-anthranilate conjugate (**7a**), which fluoresces when binding to tubulin. Upon UV excitation at the absorption maximum of the anthranilate, the probe forms a covalent adduct with tubulin, enabling the localization of the vinca site, years before the first vinblastine-tubulin crystal structure was solved in 2005.[97]

In 2002, Chatterjee *et al.*[102] synthesized a coumarin-conjugated vinblastine (**7b**) to characterize its interaction with tubulin. Around the same time, BODIPY–vinblastine conjugates began to emerge. A commercially available version (originally developed by Molecular Probes, now Thermo-Fisher, but since discontinued (Cat. No. V12390)) became widely used (**7c**). Jiang *et al.*[72] employed it in 1998 to assess whether a novel tubulin binder, 3-(iodoacetamido)benzoylurea, could compete for the vinca site. In 2002, Gruol, King, and Kuehne used the same probe to study P-glycoprotein interactions with vinca alkaloids,[103] and Lin and Chen later applied it to test the ligands of the pregnane X receptor (PXR), a key player in drug-drug interactions.[104] In 2014, they developed a high-affinity BODIPY-vindoline conjugate (**7d**) for further PXR-targeted screenings.[105]

In the same year, Carney *et al.* synthesized a series of potent vinblastine analogues and characterized them using BODIPY–vinblastine (**7c**).[106] Several other studies have employed this BODIPY-vinblastine to some extent.[107,108] Meimetis and colleagues[109] later designed additional BODIPY- and SiR–vinblastine derivatives (**7e–7j**) to investigate their cellular uptake and distribution.

In 2014, the first fluorescent eribulin probe, which incorporates a BODIPY fluorophore attached to the C35-amino group, was reported by Laughney *et al.* (eribulin-BFL, **8a**).[110] The probe retained biological activity, disrupted microtubules, and induced mitotic arrest in cancer cells. Nabekura *et al.*[111] used it to study the mechanisms of resistance to eribulin, demonstrating the direct link between eribulin resistance and MDR1 activity. Moreover, they showed that intravenous co-treatment with a nanoparticle-encapsulated MDR1 inhibitor enhanced eribulin–BFL accumulation in tumors. These results suggested that previous failures to overcome MDR1-mediated resistance were primarily due to the poor pharmacokinetic properties of MDR1 inhibitors, rather than the insufficient pharmacodynamic effect. In summary, the probe provided new insights into the mechanism of resistance against eribulin *in vitro* and *in vivo*, enabling the development of a strategy to overcome this problem.

More recently, a second fluorescent eribulin probe has been synthesized to explore drug resistance and microtubule dynamics (Fig. 7). Doodhi *et al.*[112] conjugated eribulin to Alexa Fluor 488 at the C35 position (**8b**), which based on the structural data of the tubulin-eribulin complex had been identified as an ideal site for fluorophore attachment. Using this probe, it was demonstrated that eribulin specifically binds to the plus end of microtubules, inhibiting growth at this end. Interestingly, while the minus ends were not blocked, they exhibited prolonged pauses. At nanomolar concentrations, single-molecule binding to protofilament ends was visualized, revealing how eribulin promotes microtubule catastrophe and disrupts dynamic instability.

Taxane binding site

The taxane binding site is an extended cavity situated on the luminal surface of β-tubulin, primarily constituted by

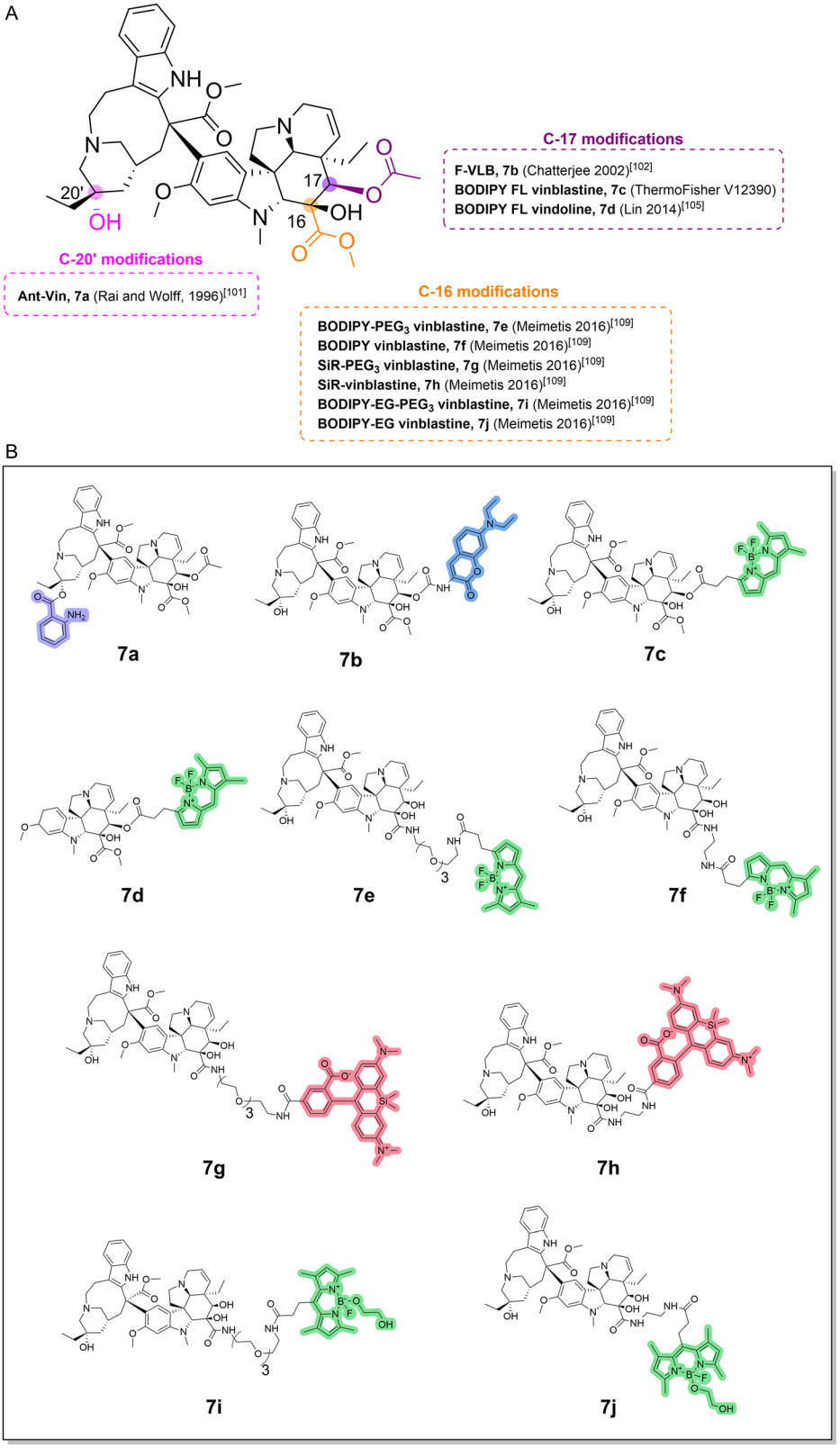

Fig. 6 Chemical structures of vinblastine-based fluorescent probes. (A) Modification sites for fluorophore attachment on the vinblastine core to yield biologically active fluorescent probes. (B) Chemical structures of these probes, with the color of the highlighted regions representing the range of color emissions of each attached fluorophore. RGB color codes assigned to represent each fluorescent emission range are as follows: UV (172,172,255); blue (119,173,237); green (126,226,149); and red (252,139,159).

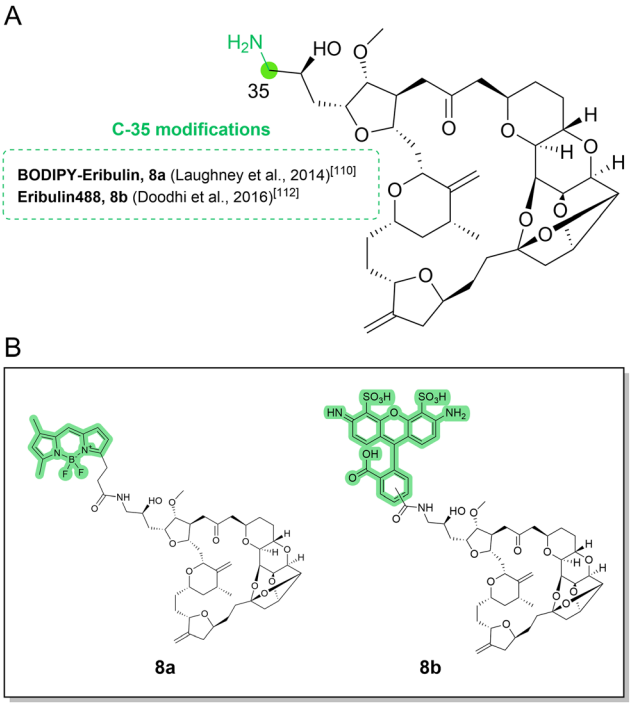

Fig. 7 Chemical structures of eribulin-based fluorescent probes. (A) Modification sites for fluorophore attachment on the eribulin core to yield biologically active fluorescent probes. (B) Chemical structures of these probes, with the color of the highlighted regions representing the range of color emission of each attached fluorophore. RGB color code assigned to represent green fluorescent emission range is (126,226,149).

hydrophobic residues from helices H1, H6, and H7, as well as the S9–S10 loop, the H6–H7 loop, and the M-loop (connecting S7 and H9). A predominant effect of ligands binding to this site is the outward repositioning of the M-loop toward adjacent protofilaments, promoting favourable lateral contacts, and thus, stabilizing the microtubule and preventing its disassembly.[7,113]

Several chemotypes have been shown to bind to this site in β-tubulin, with paclitaxel being the most extensively studied compound targeting this specific pocket. Since its clinical approval in 1992,[114] the potent anticancer activity of paclitaxel has driven the development of a wide array of fluorescent taxane derivatives. These molecular tools have significantly advanced our understanding of taxane binding mechanisms and microtubule dynamics across various biological contexts. They have been instrumental in elucidating processes such as mitotic progression, cytoskeletal organization and cellular differentiation in diverse experimental models. Furthermore, these fluorescent probes have facilitated the identification and characterization of novel microtubule-targeting agents, contributing to the discovery of compounds with improved pharmacological profiles and reduced toxicity.

Similar to the vinca site, the taxane binding site is structurally promiscuous, and it accommodates the binding of several families of compounds, whose structures are not based on the taxane scaffold (Fig. 8). Notably, taccalonolides,[115] zampanolides,[116] epothilones[117] and discodermolide[118] have all demonstrated potent *in vitro* inhibition of cancer cell proliferation through this shared mechanism of microtubule stabilization.[5,119] The discovery and characterization of these compounds have spurred the development of numerous structural analogues and derivatives,[120–123] designed to improve the pharmacological properties and enhance the

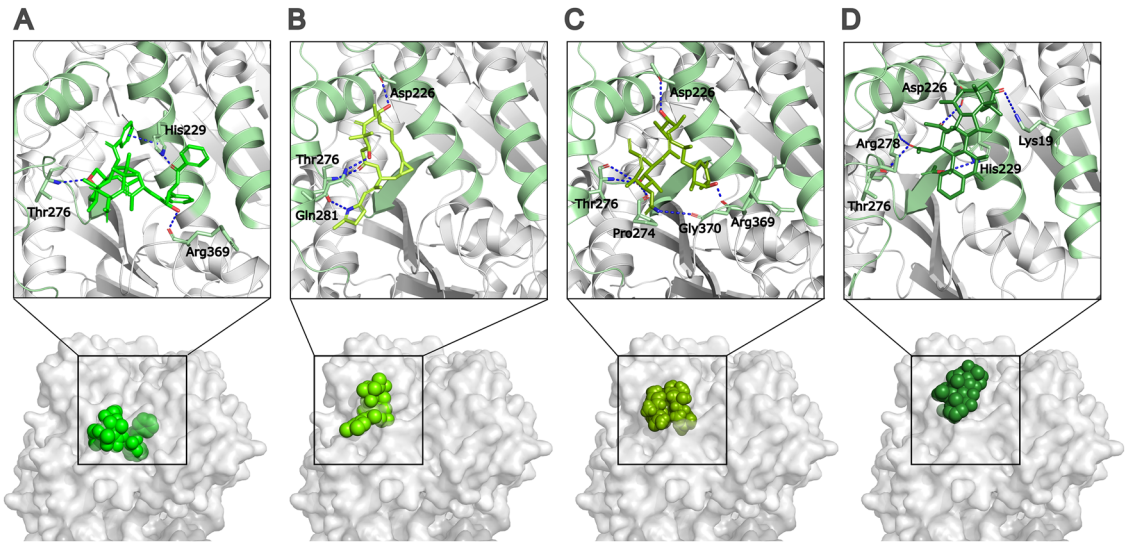

Fig. 8 Structures of taxane site ligand-bound tubulin. Structure of (A) paclitaxel-bound tubulin (PDB: 6WVR), (B) epothilone-bound tubulin (PDB: 4I50), (C) discodermolide-bound tubulin (PDB: 5LXT) and (D) taccalonolide-bound tubulin (PDB: 5EZY). In the inset, the taxane site is delineated by pale green ribbons. Main interactions with β-tubulin are shown as dashed lines. Highlighted are the (A) hydrogen bonds with β-Thr276, β-Arg369 and β-His229 and π-stacking with β-His229, (B) hydrogen bonds with β-Asp226, β-Thr276 and β-Gln281, (C) hydrogen bonds with β-Asp226, β-Thr276, β-Pro274 and β-Arg369, and (D) hydrogen bonds with β-Asp226, β-His229, β-Thr276 and β-Arg278 and a covalent bond with β-Asp226. Oxygen and nitrogen atoms participating in the main interactions are shown in red and blue, respectively.

synthetic accessibility. Fluorescent probes that are derived from taxanes, epothilones, discodermolide, or taccalonolides have been developed; however, probes based on the zampanolide scaffold are still missing at this point.

Taxanes. Paclitaxel was first discovered in the 1960s during a plant screening program conducted by the National Cancer Institute and the United States Department of Agriculture. It was isolated from the bark of the Pacific yew (*Taxus brevifolia*) and was approved by the FDA for the treatment of ovarian cancer in 1992. It was subsequently approved for breast cancer (1994) and non-small cell lung cancer (1999) (reviewed in a previous study[114]).

Although the detailed cellular and antitumoral mechanisms of action of paclitaxel remain subjects of ongoing investigations, it was demonstrated by Schiff *et al.* in 1979 that paclitaxel promotes microtubule polymerization.[124] Since then, paclitaxel has become one of the most successful drugs in the history of chemotherapy, and it has paved the way for the development of other taxanes as effective chemotherapeutic agents such docetaxel, approved in 1996, and cabazitaxel approved in 2010 (https://www.accessdata.fda.gov/scripts/cder/daf/index.cfm?event=overview.process&ApplNo=020449 and https://www.accessdata.fda.gov/scripts/cder/daf/index.cfm?event=overview.process&ApplNo=201023, respectively).

As one of the most widely used tubulin-targeting compounds, paclitaxel's binding mode has been extensively studied and exploited for the development of fluorescent derivatives. Investigations into the molecular mechanism of tubulin binding,[125–127] and the structural environment in the binding site have inspired the synthesis of multiple fluorescent paclitaxel derivatives that retain biological activity (Fig. 9). Given paclitaxel's synthetic complexity, which is a common feature among MTAs, a compromise must be reached between synthetic feasibility and biological activity preservation.

Paclitaxel anchors in a deep hydrophobic cleft where it establishes hydrogen bonds and hydrophobic interactions, primarily involving the C3′ side chain, C2, and C4 moieties. These interactions stabilize microtubules by reinforcing lateral protofilament association and inhibit depolymerization by precluding the straight-to-curved transition.[128]

The total synthesis of paclitaxel became a hallmark challenge in organic chemistry, culminating in 1994 in the first successful total syntheses reported independently by the groups of Nicolaou and Holton, respectively.[125,129] The pursuit of efficient synthetic routes remained ongoing in subsequent years, yielding 11 total syntheses reported to date, the most recent being published in 2021.[130] The current industrial production route of paclitaxel involves a semisynthetic approach that relies on 10-deacetyl baccatin III as the starting material; the latter is a natural product extracted from the leaves of the European yew (*Taxus baccata*).[131,132]

Although the creation of high-affinity fluorescent probes does not require *de novo* total synthesis, the development of such derivatives needs meticulously designed synthetic strategies, including the use of appropriate protecting groups and optimized reaction conditions. In this section, we group fluorescent derivatives according to the fluorophore attachment site on the taxane core.

C7 modifications

The C7 position emerged as the most useful site for chemical modification, yielding the highest number of biologically active, high-affinity fluorescent derivatives (Fig. 9). The C7 hydroxy group can be readily derivatized by means of esterification and is structurally positioned in such a way that its modification does not substantially impair the tubulin-binding affinity. The earliest example of a C7-modified fluorescent paclitaxel derivative was reported by Kingston *et al.* in 1991,[131] who synthesized a dansyl-labeled paclitaxel (Dan-PTX, **9a**) using a β-alanyl linker to connect the fluorophore to the C7 hydroxy group. Although this compound exhibited low fluorescence, it marks a foundational step in the field.

The first major breakthrough came with the development of flutax-1 (**9b**), synthesized by Souto *et al.* in 1996.[133] This derivative incorporated carboxyfluorescein and was obtained by reacting the free amino group of 7-(β-alanyl)paclitaxel[134] with the N-hydroxysuccinimidyl ester of 4′-carboxyfluorescein. Flutax-1 was later employed by Evangelio *et al.* (1998)[135] in pioneering studies that demonstrated the utility of fluorescent taxanes for specific, efficient, and precise labeling of cellular microtubules.

In parallel, Evangelio *et al.* also evaluated other C7-modified derivatives with worse biochemical and biological properties and fluorescence intensity, including cutax,[133] 2′AcFlutax[136] and NBD derivatives of docetaxel modified at positions 3 and 7, which exhibited minimal biological activity.[137] A rhodamine-conjugated derivative named rotax (**9c**)[138] showed some potential in promoting microtubule assembly. However, its use in live, unfixed cells led to non-specific staining, including labeling of non-microtubular vesicles, highlighting the challenge of achieving specificity and retention of potent biological activity properties in probe design. As a result, the development of a C7-modified red-emitting paclitaxel probe remained an unmet need in the field for several years.

Further optimization of flutax-1 led to the synthesis of a difluoro-fluorescein-conjugated taxane derivative, flutax-2 (**9d**),[139] which exhibited enhanced photostability and slightly higher affinity than first-generation **9b**. Initial kinetic studies of flutax-1 and flutax-2 binding to microtubules revealed that the paclitaxel-binding site was readily accessible to these fluorescent taxanes, an unexpected finding given that the site is located within the microtubule lumen. These findings, supported by the use of both flutax-1 and flutax-2, prompted the development of an alternative model wherein paclitaxel accesses its luminal binding site through lateral diffusion across the microtubule lattice rather than through end-on diffusion from the microtubule tip.[140]

Further evidence for this model came from the use of a more recent fluorescent derivative featuring a six-carbon linker between the amino group of 7-(β-alanyl)paclitaxel and the fluorophore (hexaflutax, **9e**),[141] which provided robust support for the localization of these fluorescent taxoids at a

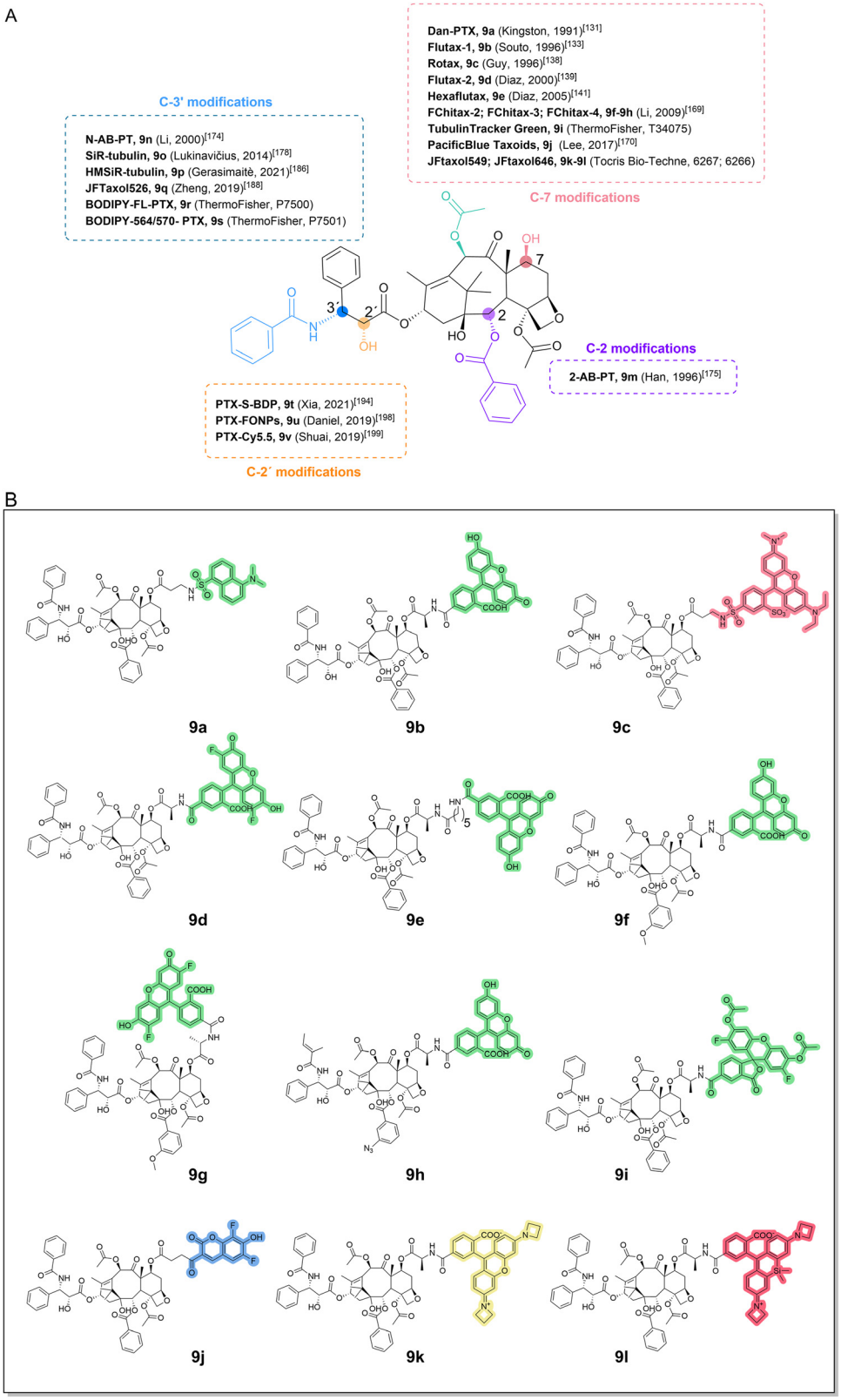

Fig. 9 Chemical structures of taxane-based fluorescent probes (I). (A) Modification sites for fluorophore attachment on the paclitaxel core to yield biologically active fluorescent probes. (B) Chemical structures of C7-modified probes, with the color of the highlighted regions representing the range of color emission of each attached fluorophore. RGB color codes assigned to represent each fluorescent emission range are as follows: blue (119,173,237); green (126,226,149); yellow (243,237,156); red (252,139,159); and far-red (251,98,124).

surface-accessible site that overlaps with the canonical paclitaxel binding pocket.[142–144]

Among its many applications, flutax-2 has proven particularly useful in efficient identification of novel compounds targeting the paclitaxel binding site.[145–147] When used with glutaraldehyde-stabilized microtubules,[148] flutax-2 enables robust competitive binding assays for evaluating MSAs.[149] Fluorescence anisotropy readouts from these assays allow the indirect determination of binding constants (K_b) for novel ligands with high accuracy and reproducibility.

In combination with sedimentation assays, flutax-2 has also facilitated the biochemical and kinetic characterization of ligand–tubulin and ligand–microtubule interactions for a wide array of compounds. These comprise cyclostreptin[142] epothilones,[150,151] dactylolides[152] and zampanolides,[62,122,147] and other taxane analogues developed by Matesanz and colleagues.[153,154] Importantly, other MSAs such as peloruside and laulimalide did not displace flutax-2 from microtubules, thus revealing the existence of an alternative site within β-tubulin, now recognized as the laulimalide/peloruside binding site.[155–157]

Since it was first introduced, flutax-2 has been widely adopted not only to investigate the cellular effects of paclitaxel but also to study the microtubule dynamics[158,159] and the intracellular distribution of microtubules in different model systems.[160,161] It has also enabled studies on cellular uptake, trafficking, and accumulation kinetics of taxanes,[162,163] and has provided insights into microtubule-MAP interactions[164] and multidrug resistance (MDR) mechanisms.[165–168]

However, accurate thermodynamic characterization using competitive binding assays with flutax-2 is limited to ligands whose affinities lie within three orders of magnitude of the probe. While flutax-2 can identify high-affinity binders, it cannot reliably determine their exact K_b values. Addressing this issue, Li *et al.*[169] developed a new series of high-affinity fluorescent probes, collectively named Fchitax. These derivatives incorporate fluorescein (**9f**) or oregon green (**9g**) fluorophores and were built upon paclitaxel scaffolds bearing methoxy substitutions at the meta-position in the phenyl ring of the C2-benzoyl moiety. In parallel, cephalomannine-based probes were synthesized by introducing an azide group at the same position (**9h**). These probes allow high-sensitivity detection at sub-nanomolar concentrations while improving the precision of affinity measurements for high-affinity taxane ligands.

Thermo-Fisher commercializes flutax-2 under the designation *Paclitaxel Oregon Green* (Cat. No. P22310), as well as a structurally related analogue featuring biacetylation of the phenolic hydroxyl groups within the fluorophore moiety, marketed as *Tubulin Tracker Green*, **9i** (Cat. No. T34075). This last derivative is an uncharged, non-fluorescent and more membrane-permeable compound compared to flutax-2. Upon cellular entry, the hydrolysis of ester bonds by endogenous nonspecific esterases removes the lipophilic acetyl groups, releasing the charged, green-fluorescent paclitaxel conjugate, i.e., flutax-2. Of note, the commercial kit of **9i** also includes pluronic acid, to further enhance the cellular uptake of the probe.

In 2017, Lee and colleagues[170] expanded the fluorophore toolkit by attaching pacific blue (PB), a coumarin-based fluorophore, to the C7-hydroxy group of paclitaxel. The resulting PB-taxane probes emit at 447 nm, broadening the spectral range for multicolor imaging. Lee and coworkers systematically tested different linkers, glycine, β-alanine, and γ-aminobutyric acid (GABA), and found that the derivative with the shortest linker (PB-Gly-TXL, **9j**) conferred the highest affinity for microtubules.[171] These PB-based probes were shown to be highly sensitive to cellular efflux mechanisms and required efflux pump inhibitors such as verapamil, which enhances intracellular retention, to achieve effective cytotoxicity in HeLa cells. Despite their size and spectral advantages,[172] the cellular uptake of PB probes was less efficient than that of flutax-2, which demonstrated effective microtubule labeling without efflux modulation.

Lastly, C7-modified taxane probes incorporating Janelia Fluor (JF) dyes are now commercially available from Tocris Bio-Techne. These include JFtaxol549 (**9k**) (Cat. No. 6267) and JFtaxol646 (**9l**) (Cat. No. 6266), which emit in the yellow and far-red regions, respectively. Tocris also offers another taxane-binding probe, JFtaxol526, that shares similar optical properties. Notably, unlike the previous two conjugates, this compound is modified at the C3′ position. The latter will be discussed in the next section.

C3′, C2′, C2 and C10 modifications

In addition to C7 labeling, several studies have explored fluorescent tagging of the paclitaxel molecule at alternative positions (Fig. 10), including C3′ (Sengupta 1995,[173] Li 2000[174]), C2 (Han 1996[175]), or C10 (Baloglu 2001,[176] Sengupta 1997[177]). In this context, it is worth mentioning the development of two minimal probes, 2-AB-PT[175] (**9m**) and N-AB-PT[174] (**9n**), containing an aniline group at C2 and C3, respectively. The studies of these probes paved the way for the development of SiR-tubulin (**9o**),[178] which enabled a significant advancement in microtubule imaging. This probe is based on docetaxel modified at the C3′ position with silicon-rhodamine (SiR), a fluorophore in which the oxygen at position 10 of the xanthene ring system is replaced by silicon. The resulting Si–C bond imparts enhanced photostability and quantum yield, making SiR a highly attractive fluorophore for advanced imaging applications.[179–181]

SiR-tubulin has been widely employed to investigate the microtubule structure and dynamics across a wide range of experimental models.[182,183] Magliocca *et al.*,[184] for instance, used SiR-tubulin alongside SiR-actin[178] to study the interplay between actin and microtubule dynamics in induced pluripotent stem cells (iPSCs) and their neuronal derivatives. Their findings highlighted a reciprocal relationship between these cytoskeletal elements during differentiation.

More recently, Shen *et al.*[185] have utilized SiR-tubulin to analyze cytoskeletal remodeling in response to changes in osmolarity and molecular crowding. This work revealed that

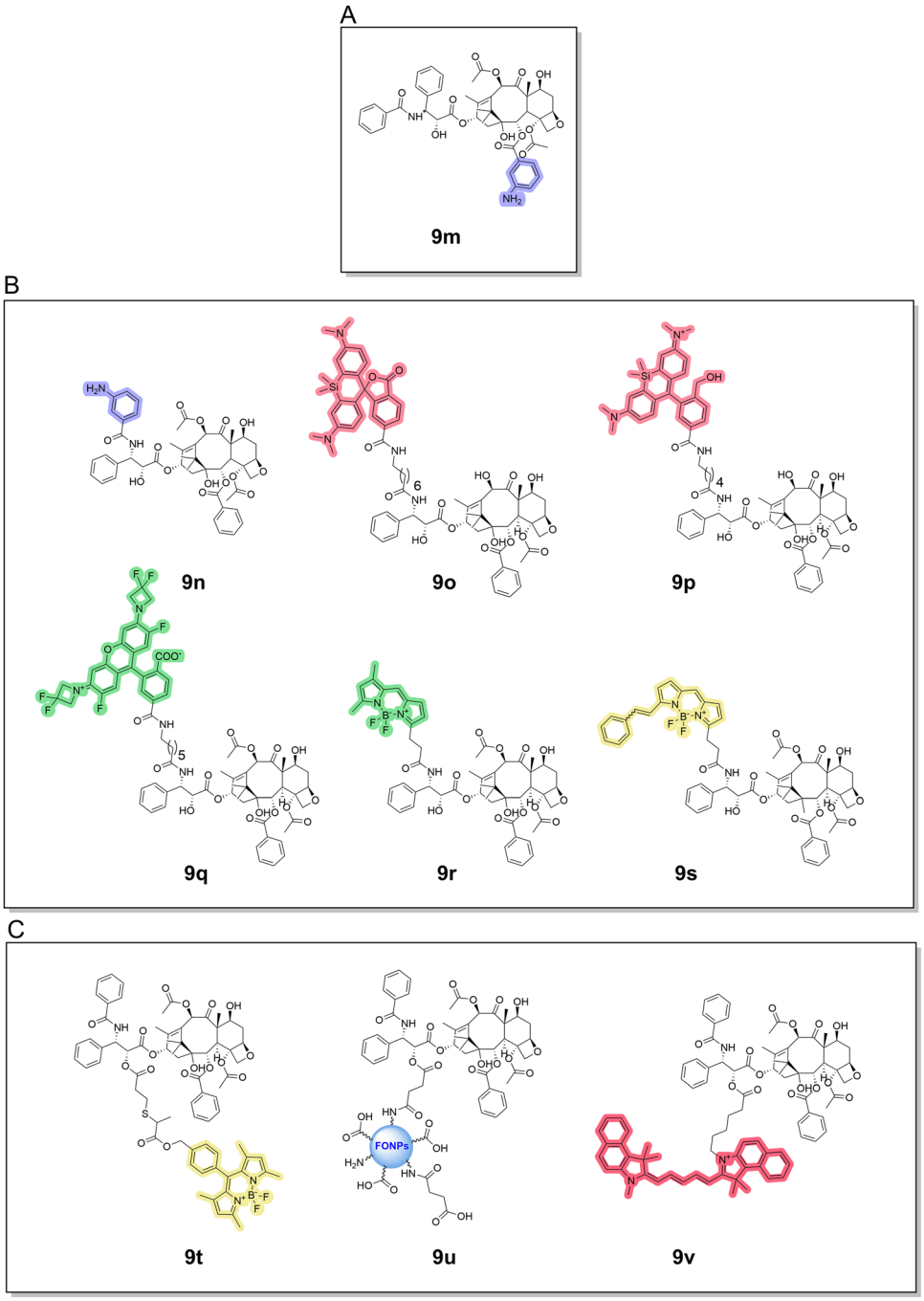

Fig. 10 Chemical structures of taxane-based fluorescent compounds (II). Chemical structures of (A) C3′-, (B) C2- and (C) C2′-modified probes, with the color of the highlighted regions representing the range of color emission of each attached fluorophore. RGB color codes assigned to represent each fluorescent emission range are as follows: UV (172,172,255); green (126,226,149); yellow (243,237,156); red (252,139,159); and far-red (251,98,124).

the cytoskeleton exhibits a highly dynamic capacity to respond to environmental stimuli through post-translational modifications such as acetylation and detyrosination, as well as through the regulated recruitment or release of microtubule-associated proteins, notably MAP7.

In 2021, a comparative study[186] focused on the coupling of various taxanes to hydroxymethyl silicon-rhodamine (HMSiR). The latter is a far-red dye known for its spontaneous blinking properties *via* intramolecular spirocyclization,[187] making it well-suited for super-resolution techniques. The authors evaluated conjugates of different taxanes, including docetaxel, cabazitaxel, and larotaxel, ultimately identifying an optimal probe for nanoscopy applications. The most effective construct, cabazitaxel linked to the 6′-regioisomer of HMSiR *via* a six-carbon spacer (**9p**), enabled high-resolution visualization of microtubule ultrastructure, including the resolution of the

inner microtubule diameter, using techniques such as single-molecule localization microscopy (SMLM), stimulated emission depletion (STED), and MINFLUX nanoscopy.

In addition to SiR and HMSiR-based probes, Zheng *et al.*[188] developed a novel fluorogenic paclitaxel-site probe using Janelia Fluor 526 (JF526),[189,190] yielding JFtaxol526 (**9q**). This probe is based on fluorophore attachment *via* C3′ of the paclitaxel side chain, and it incorporates a green-emitting fluorophore exhibiting fluorogenic behavior analogous to SiR dyes *via* a lactone-zwitterion equilibrium. JF526 spontaneously transitions from a non-fluorescent spiroether form to a fluorescent zwitterionic state upon protonation at physiological pH. *In vitro* assays demonstrated that JFtaxol526 promotes tubulin polymerization, consistent with the mechanism of paclitaxel and its analogues. In live-cell experiments, the probe specifically stained microtubules in the presence of verapamil. However, detailed thermodynamic binding characterization was not reported by Zheng *et al*.[188]

JFtaxol526 is now commercially available through Tocris Bio-Techne, along with JFtaxol549 and JFtaxol646, which emit in the yellow and far-red spectral ranges, respectively (*vide supra*).

Finally, Thermo-Fisher has also previously commercialized paclitaxel-BODIPY conjugates, including BODIPY-FL (**9r**) (green emission; Cat. No. P7500) and BODIPY 564/570 (**9s**) (orange emission; Cat. No. P7501); however, these products have recently been discontinued. Despite limited characterization in the literature, these probes, which are known to be substrates of P-glycoprotein,[191] have contributed to our understanding of MSAs in cellular environments.[192] For instance, a 2002 study employing BODIPY-FL-paclitaxel demonstrated that P-gp is a major barrier to paclitaxel transport across the blood–brain barrier.[193]

Recent advancements in BODIPY-based probes have also facilitated new drug delivery strategies. Notably, Xia *et al.*[194] engineered a photoactivatable paclitaxel-BODIPY prodrug (PTX-S-BDP, **9t**) incorporating a redox-sensitive linker in C2′ to enable fluorescence imaging-guided chemotherapy. Formulated as nanoparticles using pluronic F-127,[195] PTX-S-BDP exhibited improved aqueous solubility, high colloidal stability, and cytotoxicity comparable to unmodified paclitaxel. A key innovation of this system is the use of a sulfide [or thioether] linker sensitive to intracellular glutathione and hydrogen peroxide levels, facilitating selective activation in the tumor microenvironment.[196,197]

Within the context of taxane-based nanoparticle systems, two additional formulations incorporating fluorescent paclitaxel derivatives have been previously developed. In 2019, Daniel *et al.* conjugated fluorescent organic nanoparticles, synthesized from citric acid and diethylenetriamine, to the 2′-hydroxy group of paclitaxel (**9u**).[198] The resulting water-soluble probe demonstrated preferential uptake by glioblastoma cells in two-photon fluorescence imaging assays. The second reported nanoparticle formulation consists of paclitaxel conjugated to Cy5.5 (**9v**), also *via* the C2′ position.[199] This study, which primarily focused on evaluating the biodistribution of paclitaxel, employed various nanoparticle formulations. Following intravenous administration in Bel-7402 tumor-bearing mice, the fluorescent conjugate enabled visualization of the tissue distribution of paclitaxel.

Fluorescent taxanes with unknown structures

In addition to the previously mentioned fluorescent taxanes whose structures are publicly accessible, several commercial entities have introduced fluorescent taxane-derived probes whose chemical structure is not available. For instance, Tubulin Tracker Deep Red (**9w**) (Invitrogen, now Thermo-Fisher) is a far-red-emitting derivative of docetaxel, but its exact chemical structure remains undisclosed. The lack of biochemical and biological characterization data (*e.g.*, binding affinity, polymerization activity, IC_{50}) limits a thorough understanding of the biological effects of this probe. Nevertheless, the manufacturer reports rapid and specific microtubule labeling in live cells within 30 minutes, with no measurable cytotoxicity observed after 24 hours of incubation at working concentrations. The commercial kit includes probenecid to block organic anion transporters and improve probe retention.

Biotium has also developed a suite of fluorescent paclitaxel-based probes under the ViaFluor brand (**9x**). These include ViaFluor 405 (blue emission; Cat. No. 70064), ViaFluor 488 (green; Cat. No. 70062), and ViaFluor 647 (far-red; Cat. No. 70063). Although their exact chemical structures remain undisclosed, these probes are described as paclitaxel-derived and reported to exert minimal perturbation of microtubule dynamics and cell division, presumably due to low microtubule affinity. However, quantitative data regarding binding affinities or other biochemical and biological parameters are not publicly available.

In 2020, Logan and McCartney[200] conducted a comparative study using *Drosophila* oogenesis to assess the performance of three far-red microtubule probes: Tubulin Tracker Deep Red, ViaFluor 647, and SiR-Tubulin. All three probes successfully labeled microtubules, but Tubulin Tracker Deep Red exhibited the highest fluorescence intensity, best signal-to-noise ratio, and fastest cellular uptake. It also maintained effective labeling at lower concentrations that minimized the disruption of F-actin (probably because it did not require the use of verapamil). Interestingly, although verapamil improved probe retention, it also increased actin cytoskeleton defects, suggesting potential off-target effects.

Merck, in turn, offers a green-labeled taxane under the trade name BioTracker488 (**9y**) (Cat. No. SCT142). However, the chemical structure of this compound and its biochemical and biological characterization have not been disclosed.

Besides, Spirochrome offers a series of paclitaxel-derived fluorescent probes trademarked as SPY-tubulin (**9z**), including SPY-555 tubulin (Cat. No. SC203), SPY-650 tubulin (Cat. No. SC503), and SPY-700 tubulin (Cat. No. SC603). The product datasheets supplied by the manufacturer do not include any additional structural, biochemical or biological data. It is worth mentioning that SPY555-tubulin and SPY650-tubulin have been increasingly employed to visualize microtubule architecture

and dynamics in live-cell imaging. Each probe has been cited in over 30 studies, contributing to critical insights across a wide range of biological systems and cellular processes.[201–204]

Despite the growing availability of these fluorescent tools, significant challenges remain in correlating the molecular effects of these probes on microtubules with their broader cellular impacts. In the absence of comprehensive characterization, it is difficult to interpret cellular phenotypes following probe incubation. A notable example is flutax-2, which induces the formation of microtubules with altered interdimer spacings and protofilament numbers compared to paclitaxel (Bonato *et al.* 2025, in press). Furthermore, cells treated with flutax-2 display distinct phenotypes, underscoring that observed effects may stem not only from the MTA itself but also from the attached fluorophore or linker moiety.

Finally, the widespread adoption of the commercial probes is limited by their considerable cost, which restricts accessibility for many laboratories.

Importantly, to conclude the section on fluorescent taxanes, we note that last year, Wen *et al.*[205] reported a series of docetaxel-derived probes leveraging the concept of bioorthogonal chemistry. They developed a functionalized C3′ derivative bearing an azide handle, enabling *in situ* post-fixation reaction with fluorophores containing strained alkynes such as DBCO. In combination with super-resolution microscopy of mitotic spindles, this strategy revealed dark spindle zones undetectable by immunolabelling and preserved fluorescence after fixation.

This approach holds considerable promise, with potential applications across various contexts and as inspiration for developing new probes from other scaffolds based on the same concept.

Epothilones. Epothilones are a class of natural macrocyclic lactones originally isolated from the myxobacterium *Sorangium cellulosum*.[206] Among naturally occurring epothilones, the epoxide-containing epothilones A and B are the most abundant. The corresponding olefins, epothilones C and D, are still highly active, but they are approximately 10-fold less potent cell growth inhibitors than epothilones A and B, respectively (reviewed in a previous study[207]). Epothilones bind to the taxane site on β-tubulin and promote microtubule polymerization and stabilization. Their potent antiproliferative activity led to the development of ixabepilone, a semisynthetic lactam analogue of epothilone B that was approved in 2007 for the treatment of metastatic breast cancer (https://www.accessdata.fda.gov/scripts/cder/daf/index.cfm?event=overview.process&ApplNo=022065). Unlike paclitaxel, ixabepilone is a poor substrate of multidrug resistance (MDR) efflux pumps and is effective against several tubulin isotypes, including the taxane-resistant βIII-tubulin isotype.[208]

Structurally, all epothilones share a conserved binding mode in which they form hydrogen-bonding networks with residues Thr276 and Gln281 of the M-loop. These interactions stabilize lateral contacts between adjacent β-tubulin monomers by engaging the M-loop of one monomer with the H1–S2 loop of the neighboring protofilament. In addition, they establish several hydrophobic contacts within the taxane pocket.[113,209]

The first fluorescently labeled epothilone derivatives (Fig. 11) were reported by Ganesh *et al.* in 2003, who introduced a meta-*N,N*-dimethylaminobenzoic acid moiety at C26 of epothilone D (**10a**) or C26 of C21-hydroxy epothilone D (**10b**), respectively. While being substantially less active than the parent compound epothilone D, these probes retained sufficient biological activity to enable fluorescence-based mechanistic investigations.[210]

A significant advance was made by Gertsch *et al.* in 2009, who synthesized a fluorescent azathilone probe, where an NBD fluorophore was attached to a backbone-modified epothilone core (12-aza-epothilone) (**10c**).[211] In this scaffold, the epoxide oxygen in epothilone A is removed and C12 is replaced by nitrogen, thus creating a functional handle for the easy attachment of exocyclic substituent groups, including fluorophoric moieties. The corresponding NBD conjugate exhibits a binding constant (K_b) for microtubule binding of 2.2×10^6 M^{-1} and retains microtubule specificity, while the cytotoxicity of the compound was 40- to 100-fold lower than that of epothilone A. Cytotoxicity was slightly diminished (approximately 3-fold) in a cell line overexpressing P-glycoprotein, indicating moderate susceptibility to efflux-based resistance.

In 2020, Rai *et al.* reported an AlexaFluor 488-containing epothilone B-derived probe (**10d**),[159] originating from the group of Altmann at ETH Zurich.[212] In this probe, the fluorophore-linker construct was attached to C6 of the epothilone macrocycle, which had been deduced to be a favorable site for the perturbation-free attachment of bulky groups based on SAR studies[213,214] and structural data for tubulin-epothilone complexes.[209] The assembly of this conjugate involved the synthesis of an epothilone B analogue incorporating a 5-hexynyl group at position C6 of the epothilone macrocycle instead of the natural methyl group and subsequent conjugation with the fluorophore *via* Huisgen cycloaddition. The Alexa-labeled compound showed a K_b value of 1.5×10^8 M^{-1} for microtubule binding. However, no data on live-cell staining or cytotoxicity have been reported for the compound. Using the same modified epothilone B analogue as a precursor, a fluorescein-containing probe (**10e**) was also prepared, which, however, exhibited approximately 300-fold lower affinity for microtubules than the Alexa Fluor 488 conjugate.[212] The disparity in affinity has been attributed to the differences in the linker length between the triazole moiety and the fluorophore, although this hypothesis awaits experimental confirmation.

Discodermolide. Discodermolide is a complex polyketide first isolated in 1990 from the marine sponge *Discodermia dissoluta*.[215] It exhibits potent antiproliferative activity[216] and stabilizes microtubules through binding to the taxane site on β-tubulin.[217] Due to its scarcity and the difficulty of sourcing the compound from natural specimens, numerous synthetic efforts have been undertaken to achieve its total synthesis.[118,218–222]

The first high-resolution structural insight into discodermolide–tubulin interactions was provided by Prota *et al.* in 2017.[223] Their study revealed that discodermolide binds deeply within the taxane pocket of β-tubulin, forming hydrogen bonds with residues Asp226, Ser232, Pro274, Thr276, and Arg369.

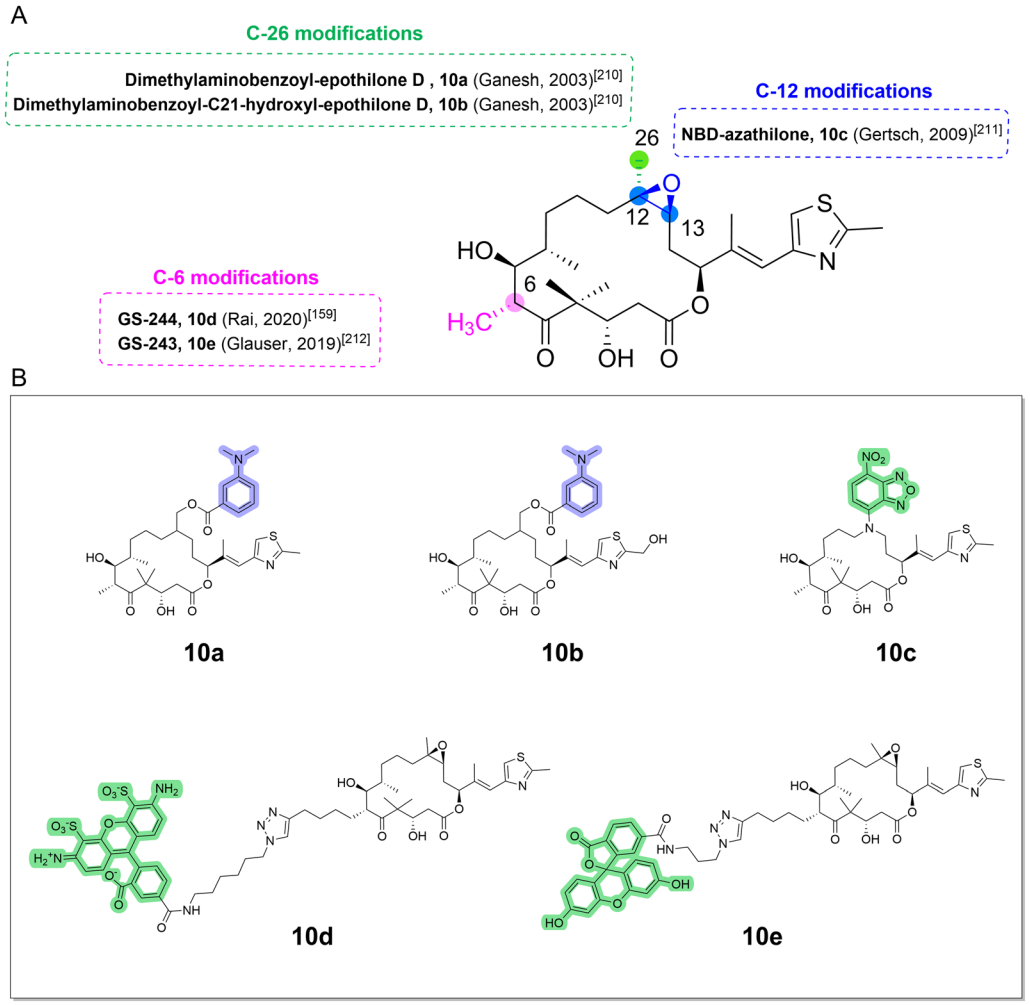

Fig. 11 Chemical structures of epothilone B-based fluorescent probes. (A) Modification sites for fluorophore attachment on the epothilone B core to yield biologically active fluorescent probes. (B) Chemical structures of these probes, with the color of the highlighted regions representing the range of color emission of each attached fluorophore. RGB color codes assigned to represent each fluorescent emission range are as follows: UV (172,172,255) and green (126,226,149).

Additional interactions involve the diene moiety engaging with Thr276 and a guanidyl group interacting with Arg278. These contacts contribute to the stabilization of the N-terminal segment of the M-loop by forming an α-helical conformation, a critical region for lateral protofilament contacts in microtubules. Moreover, van der Waals and hydrophobic interactions further anchor the compound within the binding pocket.

The first fluorescently labeled discodermolide derivatives (Fig. 12) were reported in 2005 by Smith *et al.* (**11a-11b**) alongside a series of five photoaffinity probes.[224] The authors utilized a highly advanced intermediate from the total synthesis to generate two distinct fluorescent probes. One probe was obtained *via* chemoselective esterification of the primary hydroxy group of a partially protected discodermolide analogue with a hexanoic acid derivative bearing a dansyl fluorophore. The resulting construct retained both tubulin-polymerizing activity and cytotoxicity comparable to natural discodermolide. The second probe was obtained by the conjugation of *N*-6-aminohexyl dansylsulfonamide to the C19 position *via* a carbamate linkage, producing a derivative with slightly diminished tubulin-polymerizing activity but enhanced cytotoxicity.

Subsequently, in 2011, a novel fluorescent derivative of a chemically simplified discodermolide analogue incorporating a dimethylaminobenzoyl (DMAB) moiety was developed (**11c**).[225] This compound was designed to probe the microenvironment of the discodermolide binding site on tubulin and has potential utility in competitive binding assays for ligands with low affinity.

Taccalonolides. Taccalonolides are a family of microtubule-stabilizing compounds isolated from various *Tacca* species.[226,227] Despite their ability to induce microtubule alterations reminiscent of paclitaxel's effects in live-cell systems at relatively high concentrations (5–10 μM),[115] their ability to affect microtubule polymerization *in vitro* has been found to be negligible.[228] In 2017, Wang *et al.* solved the crystal structure of taccalonolide AJ bound to tubulin, which showed that the compound formed a covalent bond with tubulin by reaction between its epoxide group and β-Asp226.[229]

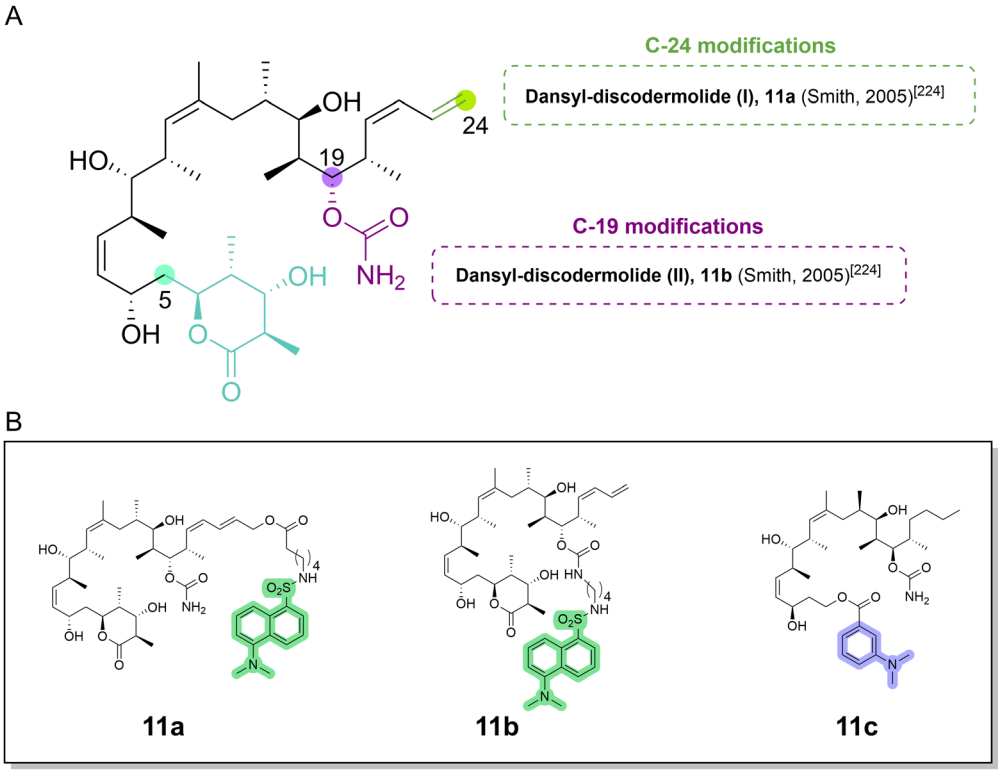

Fig. 12 Chemical structures of discodermolide-based fluorescent probes. (A) Modification sites for fluorophore attachment on the discodermolide core to yield biologically active fluorescent probes. (B) Chemical structures of these probes, with the color of the highlighted regions representing the range of color emission of each attached fluorophore. RGB color codes assigned to represent each fluorescent emission range are as follows: UV (172,172,255) and green (126,226,149).

Taccalonolides do not significantly enhance tubulin assembly and show poor competition with flutax-2 for microtubule binding.[149,229] Nevertheless, they have attracted substantial interest in oncology due to their ability to circumvent resistance mechanisms commonly observed with taxane-based therapies. Notably, taccalonolides A, B, E, and N have been demonstrated in both *in vitro* and animal models to overcome resistance associated with P-glycoprotein overexpression, multidrug resistance-associated Protein 7, and βIII-tubulin.[230,231] A striking feature of these compounds is their *in vivo* potency, which surpasses expectations based on their *in vitro* activity.

In 2019, Du and colleagues identified C6 as an optimal position for fluorophore conjugation and they synthesized a taccalonolide–fluorescein conjugate (**12a**) through site-specific modification at this carbon.[232] Although this probe exhibited diminished cytotoxic potency in cellular assays, it retained comparable microtubule-binding capacity to the parental compound, laying the foundation for the development of future fluorescent taccalonolide probes.

Further work by the same group led to the synthesis of additional fluorescent derivatives that preserved both biochemical activity and cellular potency (Fig. 13).[233] However, the applicability of these probes in live-cell imaging is limited by their irreversible binding to tubulin. Among the newly developed derivatives, Flu-Tacca-7 (**12b**), a C6-conjugated compound derived from taccalonolide AJ incorporating a bis-pivaloyl-protected carboxyfluorescein, showed the most promising labeling properties. Flu-Tacca-7 confirmed β-tubulin as the primary molecular target of taccalonolide AJ and demonstrated robust labeling performance, particularly in contexts where non-covalent probes are ineffective, such as in drug-resistant cell lines expressing efflux transporters.

Maytansine site

Since its discovery in 1972,[234] maytansine and related compounds have attracted attention as potent antiproliferative agents due to their unique mechanism of action on microtubules. However, only two maytansinoid-based compounds have been approved to date for clinical applications, both of which are antibody–drug conjugates (ADCs): trastuzumab emtansine (commercialized as Kadcyla™) consists of a maytansinoid linked to the monoclonal antibody trastuzumab, while mirvetuximab soravtansine-gynx (commercialized as Elahere™) is a first-in-class antibody–maytansine conjugate targeting the folate receptor α (FRα).[235] These ADCs have been approved for clinical use in HER2-positive metastatic breast cancer[236] and FRα-positive, platinum-resistant ovarian cancer,[237] respectively. Research continues to discover novel ligands targeting this binding site for potential clinical applications.

Maytansine-site ligands can bind to both curved and straight tubulin conformations and modulate microtubule dynamics through two distinct mechanisms. At high

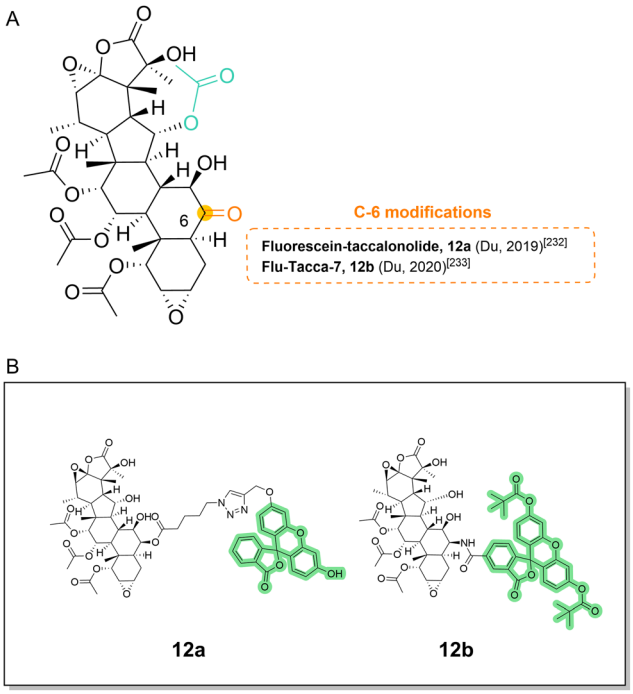

Fig. 13 Chemical structures of taccalonolide AJ-based fluorescent probes. (A) Modification sites for fluorophore attachment on the taccalonolide AJ core to yield biologically active fluorescent probes. (B) Chemical structures of these probes, with the color of the highlighted regions representing the range of color emission of each attached fluorophore. RGB color code assigned to represent green fluorescent emission range is (126,226,149).

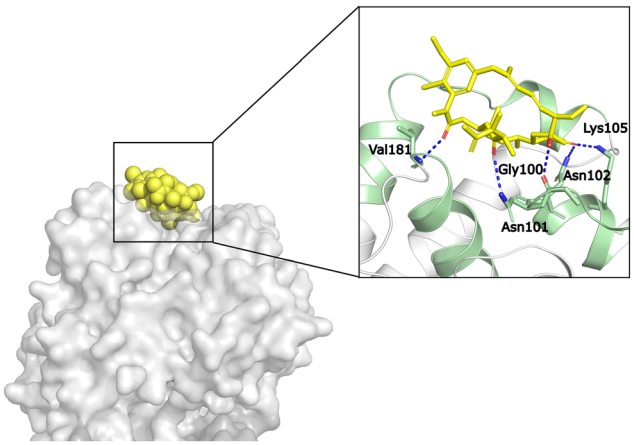

Fig. 14 Structure of maytansine-bound tubulin. (PDB: 4TV8). In the inset, the maytansine site is delineated by pale green ribbons. Main interactions with α-tubulin are shown as dashed lines. Highlighted are the hydrogen bonds with β-Gly100, β-Asn101, β-Asn102, β-Lys105, and β-Val181. Oxygen and nitrogen atoms participating in the main interactions are shown in TV-red and blue, respectively.

concentrations, they sequester free tubulin into assembly-incompetent complexes. At sub-stoichiometric concentrations, they inhibit microtubule polymerization by sterically blocking the longitudinal addition of tubulin subunits at microtubule plus ends, thereby impairing polymer growth.[238]

Structural studies have clarified previous controversies regarding the mutually exclusive tubulin binding of maytansine and vinca domain ligands. It was unclear whether this inhibition was competitive or non-competitive. Crystallographic analyses by Prota and colleagues in 2014 resolved this paradox by demonstrating that maytansinoid binding hinders the complete assembly of the vinca domain, while the formation of the full vinca domain interferes with access to the maytansine site, indicating a mutually exclusive but non-competitive binding relationship.[239] The maytansine binding pocket (Fig. 14) is located exclusively within β-tubulin and is formed by hydrophobic and polar residues from helices H3, H5, H11 and H11′, and loops T3 and T11–11′.

The first fluorescent probe targeting this site (Fig. 15) was developed in 1993 from the 20-demethoxy-20-hydroxy derivative of ansamitocin P-3 (PDM-3).[240] The conjugation of the phenolic hydroxy group with a dansyl derivative *via* a 3-carbon spacer yielded a fluorescent compound (**13a**) used in competitive assays to validate its binding specificity.

In 2015, BODIPY-labeled maytansinoids were introduced to facilitate the determination of drug-to-antibody ratios in ADCs.[241] Two widely studied maytansinoids, namely DM1 and DM4, were conjugated through their thiol group at the terminus of the C3 side chain (**13b-13e**). One derivative displayed unexpectedly low fluorescence, probably due to photoinduced electron transfer quenching between the maytansinoid core and BODIPY.

A more functionally robust fluorescent probe was developed by Menchon *et al.* in 2018,[242] who synthesized a fluorescein-labeled maytansinol derivative *via* the conjugation of the fluorescent moiety to an ester of maytansinol with hept-6-ynoic acid by means of a click reaction with an azide-functionalized fluorescein derivative (**13f**). This probe demonstrated high affinity for tubulin ($K_b = 1.5 \times 10^8\ M^{-1}$) and faithfully mimicked the binding profile of maytansine. It was subsequently used to characterize the binding of compounds with unclear interactions, including spongistatin, disorazole Z, and PM060184.[242] Owing to its favorable properties, this probe has since been adopted in multiple studies,[243,244] including the work by Bold *et al.*,[245] who applied it to characterize a structurally simplified disorazole Z analogue.

Future perspectives. Developing biologically active probes derived from MTAs is a challenging task. Thus far, fluorescent probes have been developed for only 4 of the 8 druggable sites found in tubulin. Why are such molecular tools for the remaining four sites still lacking? While the gatorbulin and todalam sites have been discovered only recently, molecular probes are also absent for the laulimalide/peloruside site and the pironetin site, both of which have been known for much longer.

The laulimalide/peloruside site deserves special attention. The discovery of laulimalide and isolaulimalide (also named fijanolide B and A, respectively), independently reported by Corley *et al.*[246] and Quiñoà *et al.*[247] in 1988, introduced a new class of marine-derived macrolides with cytotoxic activity against tumor-derived KB cell lines, with laulimalide being the

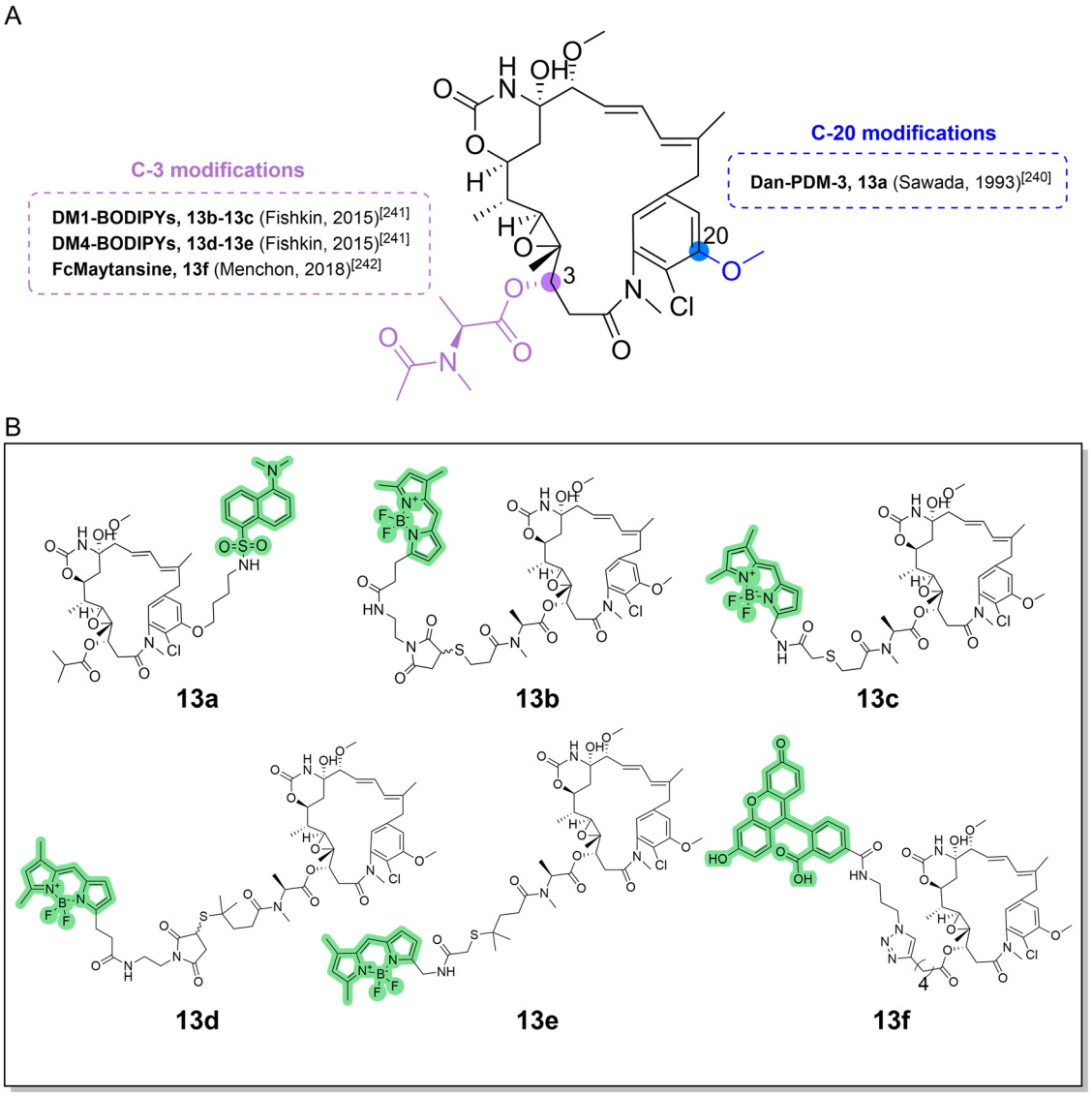

Fig. 15 Chemical structures of maytansine-based fluorescent probes. (A) Modification sites for fluorophore attachment on the maytansine core to yield biologically active fluorescent probes. (B) Chemical structures of these probes, with the color of the highlighted regions representing the range of color emission of each attached fluorophore. RGB color code assigned to represent green fluorescent emission range is (126,226,149).

more potent congener. Subsequent studies by Mooberry *et al.* in 1999 demonstrated that laulimalide stabilizes microtubules in cells and is a poor substrate of P-glycoprotein efflux pump.[248]

The marine macrolide peloruside A was first isolated from *Mycale* sp. by Northcote and co-workers[249] in 2000. The same group subsequently demonstrated in 2002 that the compound possessed microtubule-stabilizing activity.[250]

By the early 2000s, laulimalide[155] and peloruside A[157] were hypothesized to bind to a shared site on microtubules that was distinct from the taxane pocket, based on competitive displacement assays. This hypothesis was later supported through multiple additional studies.[251–255] In 2014, Prota *et al.* solved the crystal structures of tubulin in complex with both compounds, confirming the existence of a novel outer surface binding pocket that is spatially distinct from the lumen-facing taxane site. This configuration allows for the simultaneous binding of ligands at both sites without steric conflict.[156]

Recently, Estévez-Gallego *et al.* described microtubule structural signals arising from the binding of laulimalide and peloruside.[256] While the binding of taxanes leads to a longitudinal expansion of the tubulin dimer, laulimalide/peloruside is neutral with respect to dimer expansion/compression. In addition, it was shown that the structural effects of pelophen B,[257] a synthetic analogue of peloruside A, do not even affect the lateral parameters of the microtubule lattice, thus extending the spectrum of compounds with potential clinical utility.

Notwithstanding the promising pharmacological relevance of laulimalide/peloruside, several challenges hinder probe development:

- The difficulty of chemical derivatization and limited availability of natural laulimalide and peloruside A.

• The synthetic complexity of *de novo* total synthesis of both parent compounds and suitably modified analogues.[258–260]

• The tight steric environment surrounding the binding pocket, which complicates fluorophore incorporation.

• The limited accessibility of functional groups that are not directly involved in tubulin interactions, making derivatization chemically restrictive.

The pironetin site likewise remains unaddressed in the development of fluorescent probes. Pironetin was first isolated in 1994 by Kobayashi *et al.* from a *Streptomyces* sp. culture.[261–263] While the compound was initially characterized as a plant growth regulator, subsequent studies by Osada and co-workers revealed its antiproliferative properties and its ability to induce cell cycle arrest.[264] In 1999, Osada's group demonstrated that pironetin suppresses microtubule assembly.[265] This compound covalently binds to a pocket in α-tubulin and destabilizes microtubules *via* two proposed mechanisms: (i) at high concentrations, pironetin forms assembly-incompetent tubulin-ligand complexes with free tubulin dimers and (ii) at low concentrations, it binds to the minus end of microtubules, where α-tubulin subunits are exposed, blocking further dimer addition. The development of probes targeting this site remains a compelling goal to advance the structural and pharmacological characterization of this unique binding pocket. The reason may lie in the site's location *per se*, which is set deeply embedded in the tubulin structure. This positioning limits both the diversity of molecular scaffolds reported to bind to this site and the possible chemical modifications of the pironetin scaffold that preserve its activity.

As pointed out above, compared to the laulimalide/peloruside and pironetin sites, the gartobulin and todalam sites have been discovered more recently. This may partly explain why no fluorescent probes have been developed for these sites yet.

The gatorbulin site is named after the cyclic depsipeptide gatorbulin, which was isolated from the marine cyanobacterium *Lyngbya cf. confervoides* in 2021 by Mathew *et al.*[266] The compound exhibits potent antiproliferative activity across several cancer cell lines by inhibiting microtubule dynamics. While the MTC probe (*vide supra*) has been employed to assess the affinity of gatorbulin and related analogues for tubulin,[267] no site-specific fluorescent probe has yet been developed for its binding pocket. Although the gatorbulin site structurally overlaps with the colchicine site, the two sites are functionally divergent. Thus, the rational design of fluorescent ligands specific for the gatorbulin site would not only refine its biochemical characterization, but also allow spatiotemporal drug tracking in live-cell systems.

The only notable molecule reported so far to interact with the todalam site in α-tubulin is todalam itself, as discovered in 2022 by Mühlethaler *et al.* through a systematic approach combining high-throughput fragment-based crystallographic screening, iterative structure-based design, and extensive structure-activity relationship (SAR) analyses.[268] Todalam has strong microtubule-depolymerizing activity, induces G2/M arrest in cells, and promotes apoptosis. This molecule acts through a dual mechanism: being a dimer hijacker and functioning as a wedge, thus blocking the curved-to-straight transition and, hence, microtubule dynamics. In principle, the distinct location and mechanism of todalam offer a promising foundation for the rational development of site-specific imaging agents, which could provide novel tools for investigating microtubule dynamics and drug-target engagement in real time.

As this review demonstrates, a multitude of fluorescent probes binding to tubulin/microtubules have been developed over the years, which have enabled significant advances in our understanding of tubulin biochemistry and biology. The constant improvement of these probes required continuous optimization of both the linker moiety and the fluorophore. Early fluorophores, which incorporated simple polyaromatic systems or aromatic rings bearing electron-donating substituents (such as aniline), lacked the photophysical properties required for cytoskeletal visualization in advanced imaging applications. The development of probes incorporating more sophisticated fluorophores has now enabled the visualization of the cytoskeleton using techniques such as TIRF and high-resolution microscopy, which have revolutionized the microtubule field. In this context, numerous studies have employed diverse fluorescent probes to investigate the structural and dynamic properties of microtubules in the presence of various MTAs[112,159,269] and associated proteins.[270] However, it must still be kept in mind that modifying a parental MTA by the incorporation of a fluorophore can produce relevant unexpected effects, even if binding affinity and mode of interaction are maintained. An illustrative example is the case of flutax-2, which exhibits distinct effects on microtubules from the parent drug paclitaxel. Among other differences, flutax-2-assembled microtubules have a different structure than those stabilized by paclitaxel, resulting in different biochemical properties (Bonato *et al.* 2025, *in press*).

It also needs to be remembered that the fluorescent probes presented in this article are all derivatives of parent molecules with microtubule-stabilizing or -destabilizing activity, and thus, they exert microtubule-stabilizing or -destabilizing effects themselves. These effects need to be taken into account in order to ensure reliable results in cellular experiments. The optimal use of these molecular probes requires rigorous determination of non-cytotoxic concentration ranges, evaluation of potential off-target effects, and assessment of probe-induced cellular perturbations that may appear in experimental outcomes. The development of fluorescent microtubule-binding probes that exhibit high-affinity target engagement without perturbing polymerization dynamics remains an unmet need, but research on this question is currently ongoing. As we have shown here, there is already a compound (pelophen B) that minimally alters the microtubule lattice; however, this molecule still retains the capacity to modulate microtubule dynamics.[256]

As a final point, the evolving landscape of microtubule pharmacology asks for continuous advancements in molecular tool development. For example, we are currently witnessing a

Table 1 Table of MTA-derived fluorescent probes[61,63,70,71,76–81,85–87,89,100,102,104,105,109,110,112,131,133,138,139,141,159,169,170,174,175,178,186,188,194,198,199,210–212,224,225,232,233,240–242,274]

	Name	Structure	Fluorophore	Chemical scaffold and modification site	Binding affinity (M^{-1})[c]	Ref.[d]
COLCHICINE SITE						
1a	Colchicine	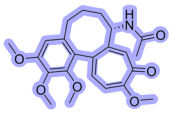	--	Colchicine	1.2×10^7 [274]	
1b	MTC	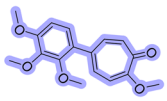	--	Colchicine ring B	4.9×10^5 [63]	61
1c	Lumi-colchicine	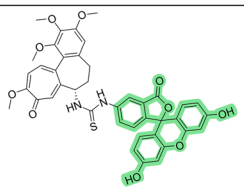	Fluorescein	Colchicine C7	2.0×10^5 [70]; 4.5×10^4 [71]	70
1d	Colchicine -504[a]	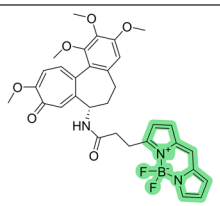	BODIPY-504	Colchicine C7	1.7×10^5	76
1e	Colchicine -646[a]	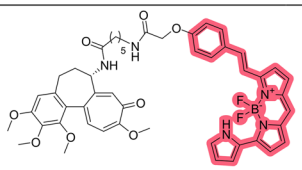	BODIPY-646	Colchicine C7	1.3×10^5	76
1f	Dansyl-colchicine	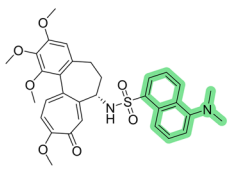	Dansyl	Colchicine C7	2.2×10^5	77
1g	N-Dansyl-isocolchicine	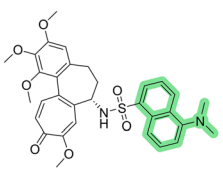	Dansyl	Isocolchicine C7	7.0×10^4	77
1h	NBD-colcemid[a]	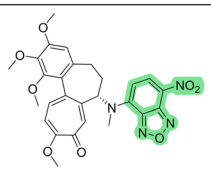	NBD	Colcemid C7	$2.0\text{-}5.7 \times 10^5$	78
1i	Tu-SP	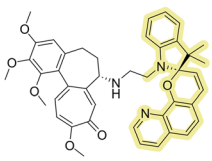	Spiropyrane derivative	Colchicine C7	Not reported	79

Table 1 (*continued*)

	Name	Structure	Fluorophore	Chemical scaffold and modification site	Binding affinity (M^{-1})[c]	Ref.[d]
1j	Col-BODIPY CB4	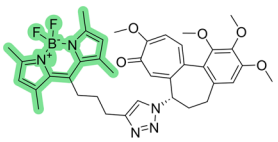	BODIPY	Colchicine C7	6.0×10^4	80
2a	NSC 613862	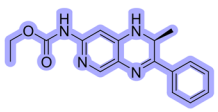	---	Pteridine	4.1×10^6	81
2b	NSC 613863	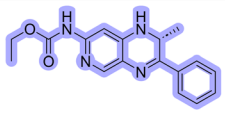	---	Pteridine	3.2×10^6	81
3a	Morpholino - quinazoline	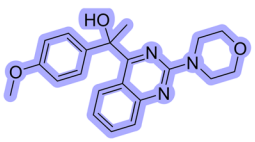	---	Quinazoline C2	Not reported	85
4a	CA4	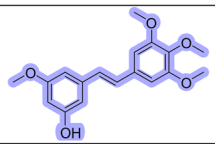	---	E-Combretastatin	Not reported	86
4b	CA4F	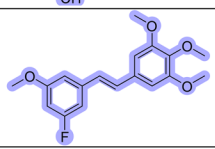	---	E-Combretastatin	Not reported	86
5a	OC9	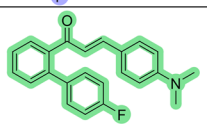	---	Chalcone	5.9×10^7 [88]	87
6a	Coumarin-30	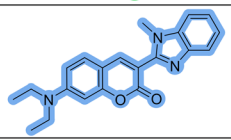	Coumarin-30	Coumarin	3.1×10^5	89
		VINCA DOMAIN				
7a	Vinblastin e-4´-anthranilate[a]	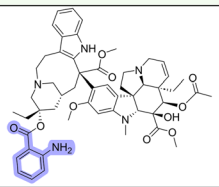	Anthranilate	Vinblastine C20'	2.5×10^4	100
7b	F-VLB	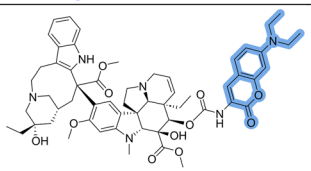	Coumarin	Vinblastine C17	7.7×10^4	102
7c	BODIPY FL vinblastine[a]	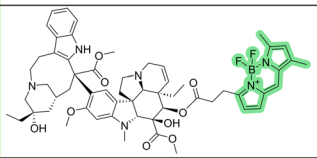	BODIPY FL	Vinblastine C17	1.5×10^6 [104]	TF

Table 1 (*continued*)

	Name	Structure	Fluorophore	Chemical scaffold and modification site	Binding affinity (M^{-1})[c]	Ref.[d]
7d	BODIPY FL vindoline[a]	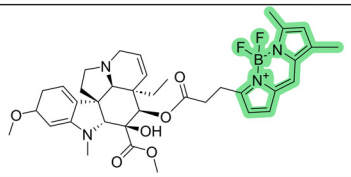	BODIPY FL	Vindoline C17	3.9×10^6	105
7e	BODIPY-PEG_3 vinblastine	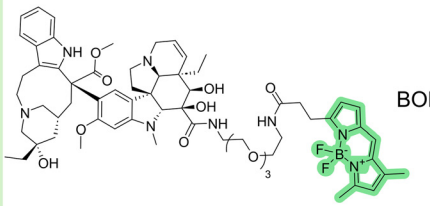	BODIPY FL	Vinblastine C16	Not reported	109
7f	BODIPY vinblastine	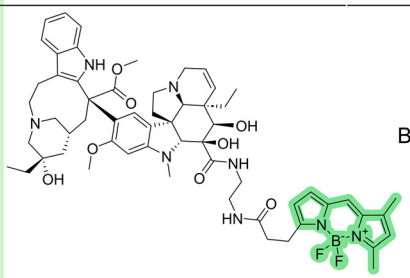	BODIPY FL	Vinblastine C16	Not reported	109
7g	SiR-PEG_3 vinblastine	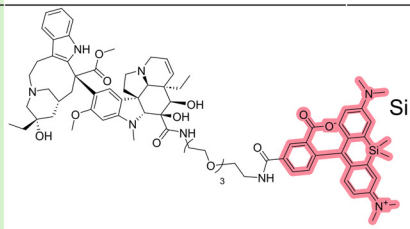	SiRhodamine	Vinblastine C16	Not reported	109
7h	SiR-vinblastine	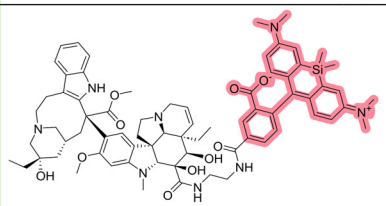	SiRhodamine	Vinblastine C16	Not reported	109
7i	BODIPY-EG-PEG_3 vinblastine	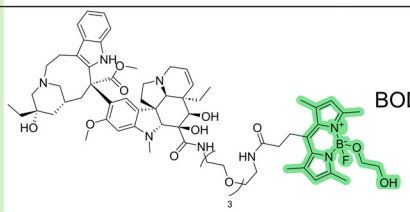	BODIPY(EG) FL	Vinblastine C16	Not reported	109
7j	BODIPY-EG vinblastine	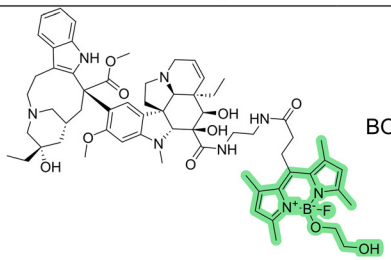	BODIPY(EG) FL	Vinblastine C16	Not reported	109

Table 1 (*continued*)

	Name	Structure	Fluorophore	Chemical scaffold and modification site	Binding affinity (M^{-1})[c]	Ref.[d]
8a	BODIPY-Eribulin	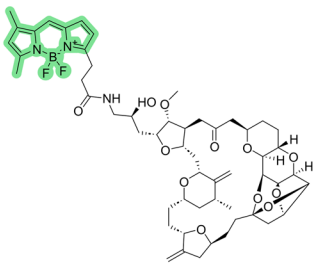	BODIPY FL	Eribulin C35	Not reported	110
8b	Eribulin488[a]	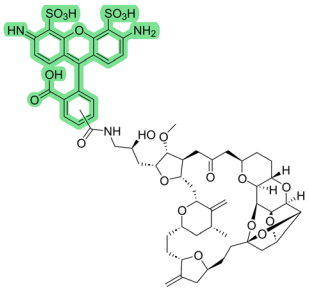	AlexaFluor 488	Eribulin C35	2.9×10^7	112
		TAXANE SITE				
9a	Dan-PTX	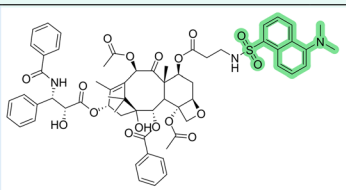	Dansyl	Paclitaxel C7	Not reported	131
9b	Flutax-1	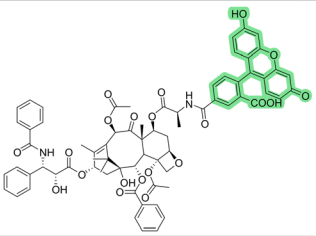	Fluorescein	Paclitaxel C7	2.9×10^7 [139]	133
9c	Rotax	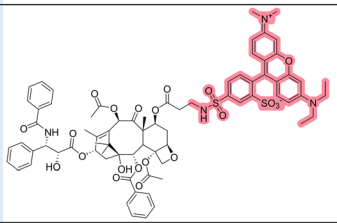	Rhodamine	Paclitaxel C7	Not reported	138
9d	Flutax-2[b]	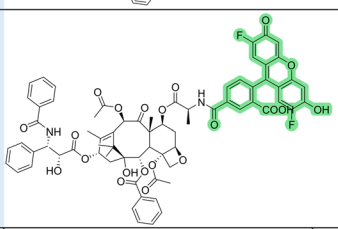	Oregon green	Paclitaxel C7	2.2×10^7	139
9e	Hexaflutax	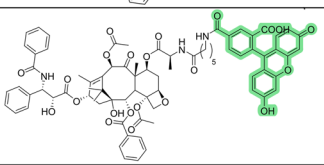	Fluorescein	Paclitaxel C7	7.2×10^5	141

Table 1 (*continued*)

	Name	Structure	Fluorophore	Chemical scaffold and modification site	Binding affinity (M^{-1})[c]	Ref.[d]
9f	FChitax-2	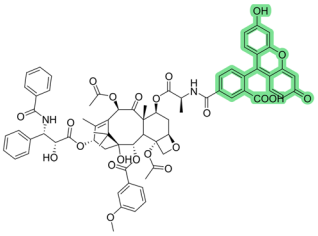	Fluorescein	Chitax-11 C7	4.4×10^8	169
9g	FChitax-3	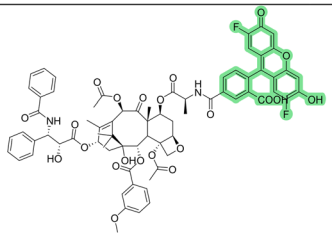	Oregon green	Chitax-11 C7	6.8×10^8	169
9h	FChitax-4	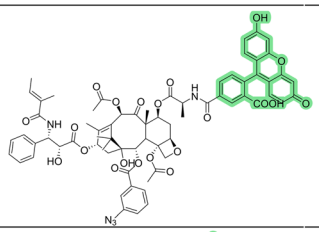	Fluorescein	Cephalomannine C7	1.2×10^9	169
9i	Tubulin Tracker Green[b]	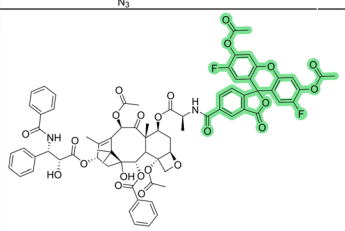	Oregon green	Paclitaxel C7	Not reported	TF
9j	PB-Gly-TXL[a]	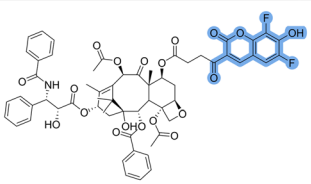	Pacific Blue	Paclitaxel C7	2.9×10^7	170
9k	JFtaxol549[b]	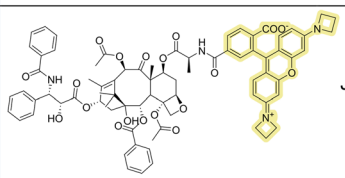	Janelia Fluor 549	Paclitaxel C7	Not reported	T
9l	JFtaxol646[b]	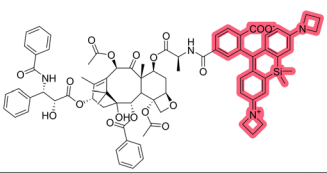	Janelia Fluor 646	Paclitaxel C7	1.1×10^6 (SM)	T
9m	2-AB-PT	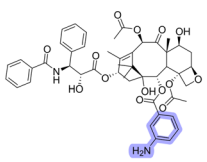	Anilin	Paclitaxel C2	2.0×10^7	174

Table 1 (*continued*)

	Name	Structure	Fluorophore	Chemical scaffold and modification site	Binding affinity (M^{-1})[c]	Ref.[d]
9n	N-AB-PT[a]	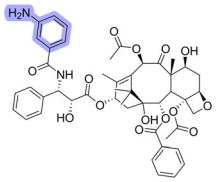	Anilin	Paclitaxel C3′	4.0×10^5	175
9o	SiR-tubulin[b]	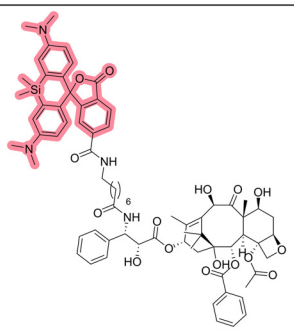	SiRhodamine	Docetaxel C3′	1.4×10^7 (SM)	178
9p	HMSiR-tubulin[a]	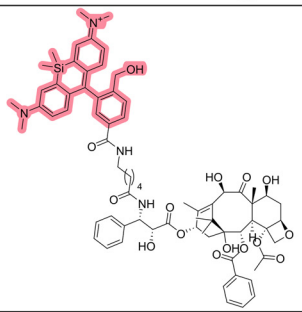	HMSi Rhodamine	Docetaxel C3′	8.3×10^6	186
9q	JFtaxol526[b]	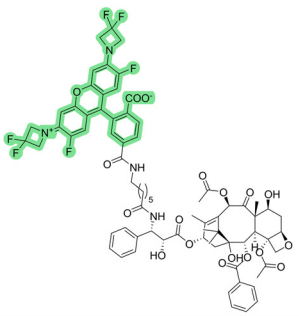	Janelia Fluor 526	Paclitaxel C3′	Not reported	188
9r	BODIPY-FL-PTX	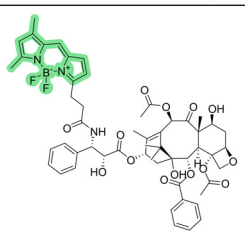	BODIPY- FL	Paclitaxel C3′	Not reported	TF
9s	BODIPY 564/570-PTX	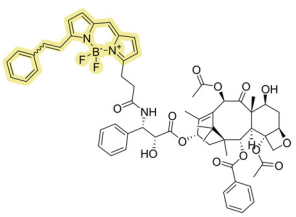	BODIPY 564/570	Paclitaxel C3′	Not reported	TF

Table 1 (*continued*)

	Name	Structure	Fluorophore	Chemical scaffold and modification site	Binding affinity (M^{-1})[c]	Ref.[d]
9t	PTX-S-BDP	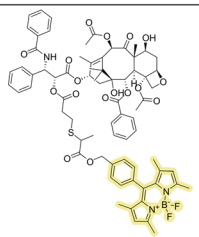	BODIPY OH	Paclitaxel C2′	Not reported	194
9u	PTX-FONPs	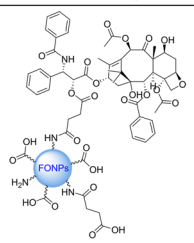	FONPs	Paclitaxel C2′	Not reported	198
9v	PTX-Cy5.5	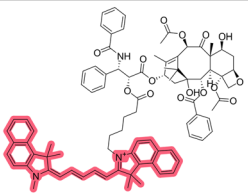	Cy5.5	Paclitaxel C2′	Not reported	199
9w	Tubulin Tracker Deep Red[b]	N/A	N/A	N/A	1.3×10^6 (SM)	TF
9x	Via Fluor 405/488/647[b]	N/A	Alexa Fluor, Texas Red, and DyLight	N/A	Not reported	B
9y	BioTracker 488[b]	N/A	N/A	N/A	Not reported	M
9z	SPY 555/650/700b -tubulin[b]	N/A	SPY 555/650/700	N/A	Not reported	S
10a	Dimethylaminobenzoyl-epothilone D	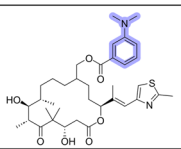	Dimethylaminobenzoyl	Epothilone D C26	Not reported	210
10b	Dimethylaminobenzoyl-C21-hydroxy epothilone D	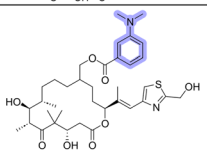	Dimethylaminobenzoyl	Epothilone D C26	Not reported	210
10c	NBD-azathilone[a]	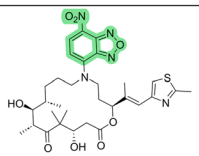	NBD	Aza-epothilone C12	2.2×10^6	211
10d	GS244	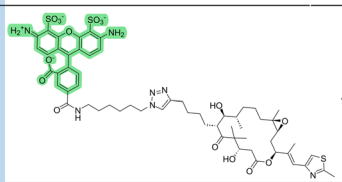	AlexaFluor 488	Epothilone B C6′	1.5×10^8 212	159

Table 1 (*continued*)

	Name	Structure	Fluorophore	Chemical scaffold and modification site	Binding affinity (M^{-1})[c]	Ref.[d]
10e	GS243	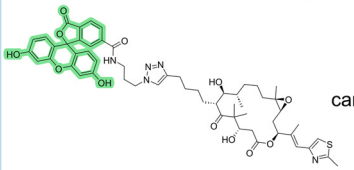	6-carboxifluorescein	Epothilone B C6′	2.7×10^5	212
11a	Dansyl-discodermolide	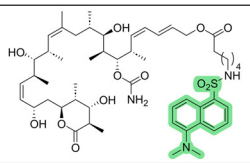	Dansyl	Discodermolide C24	Not reported	224
11b	Dansyl-discodermolide	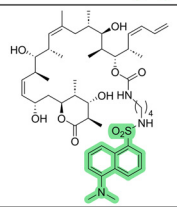	Dansyl	Discodermolide C19	Not reported	224
11c	Dimethylaminobenzoyl-discodermolide[a]	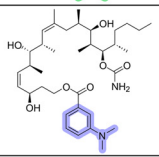	Dimethylaminobenzoyl	Discodermolide C5	4.1×10^4	225
12a	Fluorescein-taccalonolide	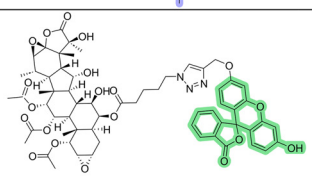	Fluorescein	Taccalonolide AJ C6	Not reported	232
12b	Flu-Tacca-7	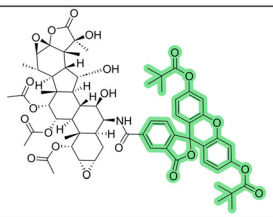	Dipivaloyl-carboxifluorescein	Taccalonolide AJ C6	Not reported	233
		MAYTANSINE SITE				
13a	Dan-PDM-3	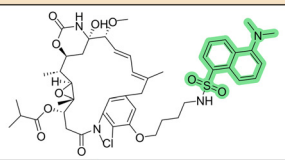	Dansyl	PDM-3 C20	Not reported	240
13b	DM1-mal-BODIPY	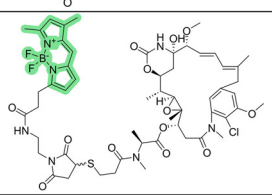	BODIPY X	DM1 C3	Not reported	241
13c	DM1-acetamide-BODIPY	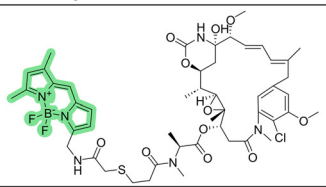	BODIPY X	DM1 C3	Not reported	241

Table 1 (*continued*)

	Name	Structure	Fluorophore	Chemical scaffold and modification site	Binding affinity (M^{-1})[c]	Ref.[d]
13d	DM4-mal-BODIPY	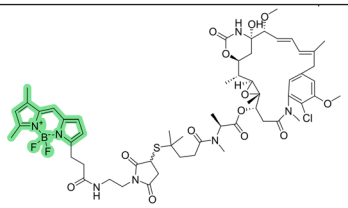	BODIPY X	DM4 C3	Not reported	241
13e	DM4-BODIPY	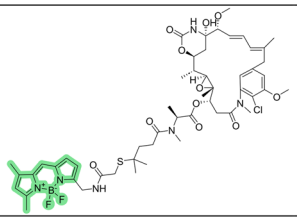	BODIPY X	DM4 C3	Not reported	241
13f	FcMaytansine[a]	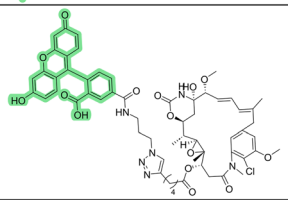	Fluorescein	Maytansinol C3	1.5×10^8	242

[a] The binding constant was calculated from the dissociation constant found in the literature following the equation: $K_b = \frac{1}{K_d}$. [b] Commercially available. TF (Thermo-Fisher), T (Tocris), B (Biotium), M (Merck) and S (Spirochrome). [c] References correspond to the publication reporting the binding or dissociation constant when this value is not provided in the probe discovery manuscript. [d] References correspond to the original publication in which the probe was first reported.RGB color codes assigned to represent each fluorescent emission range are as follows: UV (172,172,255); blue (119,173,237); green (126,226,149); yellow (243,237,156); red (252,139,159); and far-red (251,98,124).

paradigm shift in tubulin-directed drug discovery, with a new focus on the tubulin code, tubulin isotype composition and post-translational modifications. This emerging research focus demands not only the identification of isotype-selective ligands[271] but also their derivatization into fluorescent probes capable of elucidating structure-function relationships within distinct tubulin populations and facilitating the discovery of next-generation therapeutic candidates. Moreover, the generation of probes capable of selectively recognizing microtubules bearing distinct post-translational modifications could revolutionize the field not only from a drug discovery perspective, but also by enabling detailed research into how these modifications regulate microtubule functions, thereby providing a deeper understanding of all aspects of tubulin biology.

The probes discussed in this review provide the foundational framework for the rational design of next-generation tools with potential clinical applications. Future progress will be based on the interplay of continuous advances in imaging technologies, the discovery and tailored synthesis of fluorophores with superior photophysical properties, and the development of safer and more effective drugs, enabled in part by the molecular probes described herein in this review.

Conclusions and expert opinion

Microtubules are highly dynamic cytoskeletal polymers essential for processes such as mitosis, intracellular transport and neuronal homeostasis. Small fluorescent molecules targeting defined binding sites on tubulin and microtubules have become powerful tools to visualize and interrogate microtubule organization and dynamics in living systems, providing unprecedented spatial and temporal resolution and significantly advancing both fundamental and applied research.

Despite their utility, these probes present an intrinsic and often underappreciated limitation: their unavoidable impact on the equilibrium between assembled microtubules and unassembled tubulin implies that small molecules interacting with tubulin cannot be considered passive observers. Because they bind to functionally relevant sites, small fluorescent ligands inherently alter polymerization dynamics and, in the case of stabilizing agents, they can also modify the microtubule lattice structure,[272] thereby affecting microtubule-associated protein recognition. Depending on their binding mode, such compounds may promote assembly, suppress catastrophe, or induce depolymerization, meaning that the fluorescent signal itself can perturb the system under observation. From an expert perspective, this dual role, as both the reporter and modulator,

constitutes a fundamental caveat that must be explicitly considered when interpreting experimental data.

Circumventing this limitation is inherently difficult and, in principle, incompatible with microtubule-destabilizing agents. By definition, these compounds act by blocking essential structural transitions, such as the curved-to-straight conformational change of tubulin at the colchicine or gatorbulin sites, or by masking critical interaction surfaces, as do ligands targeting the pironetin, maytansine, or vinca sites. Their use as fluorescent probes therefore unavoidably perturbs the assembly equilibrium. In contrast, microtubule-stabilizing agents provide a more tractable framework for rational probe design. For ligands binding the laulimalide–peloruside site, which stabilize microtubules by bridging adjacent protofilaments, structural perturbations can be minimized through careful selection of the binding moiety of the fluorescent probe. Moreover, recent work from our group has demonstrated that taxane-site ligands can be engineered to be structurally neutral,[272,273] or by suppressing certain chemical features biologically inactive, by avoiding enforcement of the straight lattice conformation while retaining microtubule binding.[128]

In conclusion, fluorescent small molecules targeting microtubule sites remain invaluable tools, but their use requires a rigorous and critical experimental framework. Future efforts should prioritize the development of probes that minimize perturbation of polymerization equilibrium, together with standardized biophysical and cellular assays to quantify their effects. Only through such careful design and validation can fluorescent microtubule ligands reliably illuminate cytoskeletal biology without introducing unintended functional interference.

Materials and methods

Determination of the binding constants of fluorescent taxanes

Taxane binding sites in stabilized microtubules were prepared as described in a previous study.[140] Flutax-2 was synthesized as described previously.[139] The binding constants of JFTaxol646, Tubulin Tracker Deep Red and SiR-tubulin (Table 1) were determined by competition with flutax-2 as described previously.[148]

Added in proofs

Glauser *et al.* recently reported the synthesis of a novel far-red fluorescent epothilone probe in conjunction with the synthesis of GS244 (**10d**) and their precursor.[275] The new conjugate, functionalized with a PEG_3 linker and a Janelia Fluor 646 fluorophore, demonstrates binding to microtubules with an association constant (Kb) of 3.3×10^7 M. Moreover, this probe efficiently labels cellular microtubules, thereby expanding the repertoire of far-red fluorescent taxane-site probes available for advanced microscopy applications.

Author contributions

RP-O, DL-A, VP, and JFD contributed to the concept and design of the manuscript. RP-O and DL-A contributed to the writing. VP, JFD and KHA critically revised the manuscript and contributed to the writing. All authors contributed to the article and approved the submitted version.

Conflicts of interest

The authors declare that the research was conducted in the absence of any commercial or financial relationships that could be construed as a potential conflict of interest.

Data availability

No primary research results, software or code have been included and no new data were generated or analysed as part of this review, with the exception of newly determined binding constants for three commercial compounds, which are presented in Table 1.

Acknowledgements

This work was partially funded by grants RYC2019-027489-I (VP), PID2021-128340OA-I00 (VP) and PID2022-136765OB-I00 (JFD) from the Ministerio de Ciencia e Innovación (MICIN) and FEDER as well as CNS2022-135852 (VP) from MCIN/AEI/10.13039/501100011033, FSE invierte en tu futuro, and the European Union NextGenerationEU/PRTR. We thank Dr. Beatriz Álvarez Bernad for her invaluable support and advice. We apologize to any authors whose work we may have unintentionally omitted from this review.

References

1 D. Hanahan, Hallmarks of Cancer: New Dimensions, *Cancer Discovery*, 2022, **12**(1), 31–46, DOI: 10.1158/2159-8290.CD-21-1059.
2 X. Wang, B. Gigant and X. Zheng, *et al.*, Microtubule-targeting agents for cancer treatment: Seven binding sites and three strategies, *MedComm: Oncol.*, 2023, **2**(3), e46, DOI: 10.1002/mog2.46.
3 M. O. Steinmetz and A. E. Prota, Microtubule-Targeting Agents: Strategies To Hijack the Cytoskeleton, *Trends Cell Biol.*, 2018, **28**(10), 776–792, DOI: 10.1016/j.tcb.2018.05.001.
4 V. Čermák, V. Dostál and M. Jelínek, *et al.*, Microtubule-targeting agents and their impact on cancer treatment, *Eur. J. Cell Biol.*, 2020, **99**(4), 151075, DOI: 10.1016/j.ejcb.2020.151075.
5 D. Alpízar-Pedraza, A. Veulens, N. de la and E. C. Araujo, *et al.*, Microtubules destabilizing agents binding sites in tubulin, *J. Mol. Struct.*, 2022, 1259, DOI: 10.1016/j.molstruc.2022.132723.
6 T. Mühlethaler, D. Gioia and A. E. Prota, *et al.*, Comprehensive Analysis of Binding Sites in Tubulin, *Angew. Chem., Int. Ed.*, 2021, **60**(24), 13331–13342, DOI: 10.1002/anie.202100273.
7 J. J. Field, J. F. Díaz and J. H. Miller, The binding sites of microtubule-stabilizing agents, *Chem. Biol.*, 2013, **20**(3), 301–315, DOI: 10.1016/j.chembiol.2013.01.014.

8 A. Sferra, E. Bertini and G. Haase, Editorial: Tubulinopathies: fundamental and clinical challenges, *Front. Cell. Neurosci.*, 2023, **17**, 1296958, DOI: 10.3389/fncel.2023.1296958.
9 Z. Cyske, L. Gaffke and K. Pierzynowska, *et al.*, Tubulin Cytoskeleton in Neurodegenerative Diseases–not Only Primary Tubulinopathies, *Cell. Mol. Neurobiol.*, 2023, **43**(5), 1867–1884, DOI: 10.1007/s10571-022-01304-6.
10 K. J. Hoff, A. J. Neumann and J. K. Moore, The molecular biology of tubulinopathies: Understanding the impact of variants on tubulin structure and microtubule regulation, *Front. Cell. Neurosci.*, 2022, **16**, 102367, DOI: 10.3389/fncel.2022.1023267.
11 R. C. Weisenberg, Microtubule Formation in vitro in Solutions Containing Low Calcium Concentrations, *Science*, 1972, **177**(4054), 1104–1105, DOI: 10.1126/science.177.4054.1104.
12 R. C. Weisenberg, G. G. Borisy and E. W. Taylor, Colchicine-binding protein of mammalian brain and its relation to microtubules, *Biochemistry*, 1968, **7**(12), 4466–4479, DOI: 10.1021/bi00852a043.
13 P. B. Schiff and S. B. Horwitz, Taxol stabilizes microtubules in mouse fibroblast cells, *Proc Natl. Acad. Sci. U. S. A.*, 1980, **77**(3), 1561–1565, DOI: 10.1073/pnas.77.3.1561.
14 M. A. Jordan, R. J. Toso and D. Thrower, *et al.*, Mechanism of mitotic block and inhibition of cell proliferation by taxol at low concentrations, *Proc Natl. Acad. Sci. U. S. A.*, 1993, **90**(20), 9552–9556, DOI: 10.1073/pnas.90.20.9552.
15 M. A. Jordan, D. Thrower and L. Wilson, Effects of vinblastine, podophyllotoxin and nocodazole on mitotic spindles: Implications for the role of microtubule dynamics in mitosis, *J. Cell Sci.*, 1992, **102**(3), 401–416, DOI: 10.1242/jcs.102.3.401.
16 M. A. Jordan, D. Thrower and L. Wilson, Mechanism of inhibition of cell proliferation by Vinca alkaloids, *Cancer Res.*, 1991, **51**(8), 2212–2222.
17 C. M. Waterman-Storer and E. D. Salmon, Actomyosin-based Retrograde Flow of Microtubules in the Lamella of Migrating Epithelial Cells Influences Microtubule Dynamic Instability and Turnover and Is Associated with Microtubule Breakage and Treadmilling, *J. Cell Biol.*, 1997, **139**(2), 417–434, DOI: 10.1083/jcb.139.2.417.
18 A.-M. C. Yvon and P. Wadsworth, Non-centrosomal microtubule formation and measurement of minus end microtubule dynamics in A498 cells, *J. Cell Sci.*, 1997, **110**(19), 2391–2401, DOI: 10.1242/jcs.110.19.2391.
19 A. Hyman, D. Drechsel, D. Kellogg, *et al.*, *Preparation of Modified Tubulins*, 1991, pp. 478–485, DOI: 10.1016/0076-6879(91)96041-O.
20 B. Ludin and A. Matus, GFP illuminates the cytoskeleton, *Trends Cell Biol.*, 1998, **8**(2), 72–77, DOI: 10.1016/S0962-8924(98)80015-9.
21 N. M. Rusan, C. J. Fagerstrom and A.-M. C. Yvon, *et al.*, Cell Cycle-Dependent Changes in Microtubule Dynamics in Living Cells Expressing Green Fluorescent Protein-α Tubulin, *Mol. Biol. Cell*, 2001, **12**(4), 971–980, DOI: 10.1091/mbc.12.4.971.
22 Y. Honda, K. Tsuchiya and E. Sumiyoshi, *et al.*, Tubulin isotype substitution revealed that isotype combination modulates microtubule dynamics in C. elegans embryos, *J. Cell Sci.*, 2017, **130**(9), 1652–1661, DOI: 10.1242/jcs.200923.
23 K. Nishida, K. Tsuchiya and H. Obinata, *et al.*, Expression Patterns and Levels of All Tubulin Isotypes Analyzed in GFP Knock-In C. elegans Strains, *Cell Struct. Funct.*, 2021, **46**(1), 51–64, DOI: 10.1247/csf.21022.
24 K. Xu, Z. Li and L. Mao, *et al.*, AlphaFold2-guided engineering of split-GFP technology enables labeling of endogenous tubulins across species while preserving function, *PLoS Biol.*, 2024, **22**(8), e3002615, DOI: 10.1371/journal.pbio.3002615.
25 A. O. Khan, V. A. Simms and J. A. Pike, *et al.*, CRISPR-Cas9 Mediated Labelling Allows for Single Molecule Imaging and Resolution, *Sci. Rep.*, 2017, **7**(1), 8450, DOI: 10.1038/s41598-017-08493-x.
26 B. Roberts, A. Haupt and A. Tucker, *et al.*, Systematic gene tagging using CRISPR/Cas9 in human stem cells to illuminate cell organization, *Mol. Biol. Cell*, 2017, **28**(21), 2854–2874, DOI: 10.1091/mbc.e17-03-0209.
27 H. Khachatryan, B. Olszowy and C. A. Barrero, *et al.*, Identification of Inhibitors of Tubulin Polymerization Using a CRISPR-Edited Cell Line with Endogenous Fluorescent Tagging of β-Tubulin and Histone H1, *Biomolecules*, 2023, **13**(2), 249, DOI: 10.3390/biom13020249.
28 T. Scherson, T. E. Kreis and J. Schlessinger, *et al.*, Dynamic interactions of fluorescently labeled microtubule-associated proteins in living cells, *J. Cell Biol.*, 1984, **99**(2), 425–434, DOI: 10.1083/jcb.99.2.425.
29 C. Gell, V. Bormuth, G. J. Brouhard, *et al.*, *Microtubule Dynamics Reconstituted In Vitro and Imaged by Single-Molecule Fluorescence Microscopy*, 2010, pp. 221–245, DOI: 10.1016/S0091-679X(10)95013-9.
30 H. Inaba, T. Yamamoto and T. Iwasaki, *et al.*, Fluorescent Tau-derived Peptide for Monitoring Microtubules in Living Cells, *ACS Omega*, 2019, **4**(6), 11245–11250, DOI: 10.1021/acsomega.9b01089.
31 S. Xie, J. Li and S. Sun, *et al.*, TUBright: A Peptide Probe for Imaging Microtubules, *Anal. Chem.*, 2022, **94**(32), 11168–11174, DOI: 10.1021/acs.analchem.2c01285.
32 M. D. Canela, M. J. Pérez-Pérez and S. Noppen, *et al.*, Novel colchicine-site binders with a cyclohexanedione scaffold identified through a ligand-based virtual screening approach, *J. Med. Chem.*, 2014, **57**(10), 3924–3938, DOI: 10.1021/jm401939g.
33 J. Kapuscinski, DAPI: a DNA-Specific Fluorescent Probe, *Biotech. Histochem.*, 1995, **70**(5), 220–233, DOI: 10.3109/10520299509108199.
34 M. Mirigian, K. Mukherjee and S. L. Bane, *et al.*, Measurement of In Vitro Microtubule Polymerization by Turbidity and Fluorescence, *Methods Cell Biol.*, 2013, **115**, 215–229, DOI: 10.1016/B978-0-12-407757-7.00014-1.
35 D. M. Barron, S. K. Chatterjee and R. Ravindra, *et al.*, A fluorescence-based high-throughput assay for antimicrotubule drugs, *Anal. Biochem.*, 2003, **315**(1), 49–56, DOI: 10.1016/S0003-2697(02)00691-7.
36 P. Horowitz, V. Prasad and R. F. Luduena, Bis(1,8-anilinonaphthalenesulfonate). A novel and potent

inhibitor of microtubule assembly, *J. Biol. Chem.*, 1984, **259**(23), 14647–14650, DOI: 10.1016/S0021-9258(17)42651-2.
37 C. E. Kung and J. K. Reed, Fluorescent molecular rotors: a new class of probes for tubulin structure and assembly, *Biochemistry*, 1989, **28**(16), 6678–6686, DOI: 10.1021/bi00442a022.
38 D. L. Sackett, J. R. Knutson and J. Wolff, Hydrophobic surfaces of tubulin probed by time-resolved and steady-state fluorescence of nile red, *J. Biol. Chem.*, 1990, **265**(25), 14899–14906, DOI: 10.1016/S0021-9258(18)77201-3.
39 M. Mazumdar, P. K. Parrack and B. Bhattacharyya, Interaction of Prodan with tubulin, *Eur. J. Biochem.*, 1992, **204**(1), 127–132, DOI: 10.1111/j.1432-1033.1992.tb16614.x.
40 G. G. Borisy and E. W. Taylor, The mechanism of action of colchicine, *J. Cell Biol.*, 1967, **34**(2), 525–533, DOI: 10.1083/jcb.34.2.525.
41 G. G. Borisy and E. W. Taylor, The mechanism of action of colchicine, *J. Cell Biol.*, 1967, **34**(2), 535–548, DOI: 10.1083/jcb.34.2.535.
42 E. C. McLoughlin and N. M. O'Boyle, Colchicine-Binding Site Inhibitors from Chemistry to Clinic: A Review, *Pharmaceuticals*, 2020, **13**(8), 1–43, DOI: 10.3390/ph13010008.
43 J.-Y. Chai, B.-K. Jung and S.-J. Hong, Albendazole and Mebendazole as Anti-Parasitic and Anti-Cancer Agents: an Update, *Korean J. Parasitol.*, 2021, **59**(3), 189–225, DOI: 10.3347/kjp.2021.59.3.189.
44 T. Bekele, L. Lachisa and A. Tsegaye, *et al.*, Efficacy of Albendazole and Mebendazole Against Soil Transmitted Infections among Pre-School and School Age Children: A Systematic Review and Meta-Analysis, *J. Epidemiol. Global Health*, 2024, **14**(3), 884–904, DOI: 10.1007/s44197-024-00231-7.
45 D. Hellberg, T. Svarrer and S. Nilsson, *et al.*, Self-Treatment of Female External Genital Warts with 0.5% Podophyllotoxin Cream (Condyline®) vs Weekly Applications of 20% Podophyllin Solution, *Int. J. STD AIDS*, 1995, **6**(4), 257–261, DOI: 10.1177/095646249500600407.
46 A. Edwards, A. Atma-Ram and R. N. Thin, Podophyllotoxin 0.5% v podophyllin 20% to treat penile warts, *Sex Transm. Infect.*, 1988, **64**(4), 263–265, DOI: 10.1136/sti.64.4.263.
47 Y.-C. Chao, M.-J. Ko and W.-C. Tsai, *et al.*, Comparative efficacy of treatments for molluscum contagiosum: A systematic review and network meta-analysis, *J. Dtsch. Dermatol. Ges.*, 2023, **21**(6), 587–597, DOI: 10.1111/ddg.15063.
48 T. A. Syed, S. Lundin and M. Ahmad, Topical 0.3% and 0.5% Podophyllotoxin Cream for Self-Treatment of Molluscum contagiosum in Males, *Dermatology*, 1994, **189**(1), 65–68, DOI: 10.1159/000246787.
49 O. Bueno, J. E. Gallego and S. Martins, *et al.*, High-affinity ligands of the colchicine domain in tubulin based on a structure-guided design, *Sci. Rep.*, 2018, **8**(1), 4242, DOI: 10.1038/s41598-018-22382-x.
50 S. Chattopadhyaya, D. Chakravorty and G. Basu, A collective motion description of tubulin βT7 loop dynamics, *Biophys. Physicobiol.*, 2019, **16**, 264–273, DOI: 10.2142/biophysico.16.0_264.
51 L. X. Peng, M. T. Hsu and M. Bonomi, *et al.*, The Free Energy Profile of Tubulin Straight-Bent Conformational Changes, with Implications for Microtubule Assembly and Drug Discovery, *PLoS Comput. Biol.*, 2014, **10**(2), e1003464, DOI: 10.1371/journal.pcbi.1003464.
52 A. Massarotti, A. Coluccia and R. Silvestri, *et al.*, The tubulin colchicine domain: A molecular modeling perspective, *ChemMedChem*, 2012, **7**(1), 33–42, DOI: 10.1002/cmdc.201100361.
53 L. Wang, Y. Zheng and D. Li, *et al.*, Design, Synthesis, and Bioactivity Evaluation of Dual-Target Inhibitors of Tubulin and Src Kinase Guided by Crystal Structure, *J. Med. Chem.*, 2021, **64**(12), 8127–8141, DOI: 10.1021/acs.jmedchem.0c01961.
54 Y. Wang, H. Zhang and B. Gigant, *et al.*, Structures of a diverse set of colchicine binding site inhibitors in complex with tubulin provide a rationale for drug discovery, *FEBS J.*, 2016, **283**(1), 102–111, DOI: 10.1111/febs.13555.
55 L. Niu, J. Yang and W. Yan, *et al.*, Reversible binding of the anticancer drug KXO1 (tirbanibulin) to the colchicine-binding site of β-tubulin explains KXO1's low clinical toxicity, *J. Biol. Chem.*, 2019, **294**(48), 18099–18108, DOI: 10.1074/jbc.RA119.010732.
56 A. Fallah-Tafti, A. Foroumadi and R. Tiwari, *et al.*, Thiazolyl N-benzyl-substituted acetamide derivatives: Synthesis, Src kinase inhibitory and anticancer activities, *Eur. J. Med. Chem.*, 2011, **46**(10), 4853–4858, DOI: 10.1016/j.ejmech.2011.07.050.
57 D. Lucena-Agell, M. J. Guillén and R. Matesanz, *et al.*, PM534, an Optimized Target-Protein Interaction Strategy through the Colchicine Site of Tubulin, *J. Med. Chem.*, 2024, **67**(4), 2619–2630, DOI: 10.1021/acs.jmedchem.3c01775.
58 T. Arai, Purification and properties of the colchicine binding protein from bovine brain (Japanese), *Biochem. Soc.*, 1973, **45**(1), 19–29.
59 T. Arai and T. Okuyama, Fluorometric assay of tubulin-colchicine complex, *Anal. Biochem.*, 1975, **69**(2), 443–450, DOI: 10.1016/0003-2697(75)90146-3.
60 B. Bhattacharyya and J. Wolff, Promotion of Fluorescence upon Binding of Colchicine to Tubulin, *Proc Natl. Acad. Sci. U. S. A.*, 1974, **71**(7), 2627–2631, DOI: 10.1073/pnas.71.7.2627.
61 T. J. Fitzgerald, Molecular features of colchicine associated with antimitotic activity and inhibition of tubulin polymerization, *Biochem. Pharmacol.*, 1976, **25**(12), 1383–1387, DOI: 10.1016/0006-2952(76)90108-8.
62 J. J. Field, B. Pera and J. E. Gallego, *et al.*, Zampanolide Binding to Tubulin Indicates Cross-Talk of Taxane Site with Colchicine and Nucleotide Sites, *J. Nat. Prod.*, 2018, **81**(3), 494–505, DOI: 10.1021/acs.jnatprod.7b00704.
63 J. M. Andreu, M. J. Gorbunopff and J. C. Lee, *et al.*, Interaction of tubulin with bifunctional colchicine analogs: an equilibrium study, *Biochemistry*, 1984, **23**(8), 1742–1752, DOI: 10.1021/bi00303a025.
64 V. Peyrot, D. Leynadier and M. Sarrazin, *et al.*, Mechanism of binding of the new antimitotic drug MDL 27048 to the colchicine site of tubulin: Equilibrium studies, *Biochemistry*, 1992, **31**(45), 11125–11132, DOI: 10.1021/bi00160a024.
65 A. C. Cabrera, D. Lucena-Agell and M. Redondo-Horcajo, *et al.*, Aggregated compound biological signatures

facilitate phenotypic drug discovery and target elucidation, *ACS Chem. Biol.*, 2016, **11**(11), 3024–3034, DOI: 10.1021/acschembio.6b00358.

66 N. M. Cury, T. Mühlethaler and A. B. A. Laranjeira, *et al.*, Structural Basis of Colchicine-Site targeting Acylhydrazones active against Multidrug-Resistant Acute Lymphoblastic Leukemia, *iScience*, 2019, **21**, 95–109, DOI: 10.1016/j.isci.2019.10.003.

67 B. Keenan, R. K. Finol-Urdaneta and A. Hope, *et al.*, N-alkylisatin-based microtubule destabilizers bind to the colchicine site on tubulin and retain efficacy in drug resistant acute lymphoblastic leukemia cell lines with less in vitro neurotoxicity, *Cancer Cell Int.*, 2020, **20**(170), 1–16, DOI: 10.1186/s12935-020-01251-6.

68 Anonymous, Two Antagonistic Microtubule Targeting Drugs Act Synergistically to Kill Cancer Cells, *Cancers*, DOI: 10.3390/cancers12082196.

69 M. Antúnez-Mojica, J. Rodríguez-Salarichs and M. Redondo-Horcajo, *et al.*, Structural and Biochemical Characterization of the Interaction of Tubulin with Potent Natural Analogues of Podophyllotoxin, *J. Nat. Prod.*, 2016, **79**(8), 2113–2121, DOI: 10.1021/acs.jnatprod.6b00428.

70 J. I. Clark and D. Garland, Fluorescein colchicine. Synthesis, purification, and biological activity, *J. Cell Biol.*, 1978, **76**(3), 619–627, DOI: 10.1083/jcb.76.3.619.

71 E. V. Craenenbroeck and Y. Engelborghs, Quantitative characterization of the binding of fluorescently labeled colchicine to tubulin in vitro using fluorescence correlation spectroscopy, *Biochemistry*, 1999, **38**(16), 5082–5088, DOI: 10.1021/bi9821925.

72 J. D. Jiang, A. S. Davis and K. Middleton, *et al.*, 3-(Iodoacetamido)-benzoylurea: a novel cancericidal tubulin ligand that inhibits microtubule polymerization, phosphorylates bcl-2, and induces apoptosis in tumor cells, *Cancer Res.*, 1998, **58**(23), 5389–5395.

73 T. L. Gururaja, D. Goff and T. Kinoshita, *et al.*, R-253 Disrupts Microtubule Networks in Multiple Tumor Cell Lines, *Clin. Cancer Res.*, 2006, **12**(12), 3831–3842, DOI: 10.1158/1078-0432.CCR-06-0168.

74 N. Nicolaus, J. Zapke and P. Riesterer, *et al.*, Azides Derived from Colchicine and their Use in Library Synthesis: a Practical Entry to New Bioactive Derivatives of an Old Natural Drug, *ChemMedChem*, 2010, **5**(5), 661–665, DOI: 10.1002/cmdc.201000063.

75 E. A. Zvereva, A. V. Zherdev and A. A. Formanovsky, *et al.*, Fluorescence polarization immunoassay of colchicine, *J. Pharm. Biomed. Anal.*, 2018, **159**, 326–330, DOI: 10.1016/j.jpba.2018.07.008.

76 L. A. Arnold, P. Ranaivo and R. K. Guy, Synthesis and characterization of BODIPY-labeled colchicine, *Bioorg. Med. Chem. Lett.*, 2008, **18**(22), 5867–5870, DOI: 10.1016/j.bmcl.2008.07.068.

77 L. Das, A. B. Datta and S. Gupta, *et al.*, NH-Dansyl Isocolchicine Exhibits a Significantly Improved Tubulin-Binding Affinity and Microtubule Inhibition in Comparison to Isocolchicine by Binding Tubulin through Its A and B Rings, *Biochemistry*, 2005, **44**(9), 3249–3258, DOI: 10.1021/bi048211u.

78 T. Hiratsuka and T. Kato, A fluorescent analog of colcemid, N-(7-nitrobenz-2-oxa-1,3-diazol-4-yl)-colcemid, as a probe for the colcemid-binding sites of tubulin and microtubules, *J. Biol. Chem.*, 1987, **262**(13), 6318–6322, DOI: 10.1016/s0021-9258(18)45572-x.

79 H. Zhang, C. Wang and T. Jiang, *et al.*, Microtubule-targetable fluorescent probe: Site-specific detection and super-resolution imaging of ultratrace tubulin in microtubules of living cancer cells, *Anal. Chem.*, 2015, **87**(10), 5216–5222, DOI: 10.1021/acs.analchem.5b01089.

80 M. Jurášek, E. Dráberová and J. Řehulka, *et al.*, Colchicine-BODIPY Probes: Evidence for the Involvement of Intracellular Membranes in the Targeting of Colchicine to Tubulin, *ACS Pharmacol. Transl. Sci.*, 2025, **8**(7), 1965–1985, DOI: 10.1021/acsptsci.4c00730.

81 D. Leynadier, V. Peyrot and M. Sarrazin, *et al.*, Tubulin binding of two 1-deaza-7,8-dihydropteridines with different biological properties: Enantiomers NSC 613862 (S)-(-) and NSC 613863 (R)-(+), *Biochemistry*, 1993, **32**(40), 10675–10682, DOI: 10.1021/bi00091a018.

82 M.-D. Canela, O. Bueno and S. Noppen, *et al.*, Targeting the colchicine site in tubulin through cyclohexanedione derivatives, *RSC Adv.*, 2016, **6**(23), 19492–19506, DOI: 10.1039/C5RA26807A.

83 O. Bueno, G. Tobajas and E. Quesada, *et al.*, Conformational mimetics of the α-methyl chalcone TUB091 binding tubulin: Design, synthesis and antiproliferative activity, *Eur. J. Med. Chem.*, 2018, **148**, 337–348, DOI: 10.1016/j.ejmech.2018.02.019.

84 O. Bueno, M. Gargantilla and J. Estévez-Gallego, *et al.*, Diphenyl ether derivatives occupy the expanded binding site of cyclohexanedione compounds at the colchicine site in tubulin by movement of the αT5 loop, *Eur. J. Med. Chem.*, 2019, **171**, 195–208, DOI: 10.1016/j.ejmech.2019.03.045.

85 Y. Suzuki, J. Sawada and P. Hibner, *et al.*, Fluorescent anticancer quinazolines as molecular probes for β-tubulin colchicine site competition assay and visualization of microtubules as intracellular targeting sites, *Dyes Pigm.*, 2017, **145**, 233–238, DOI: 10.1016/j.dyepig.2017.05.050.

86 R. H. Bisby, S. W. Botchway and J. A. Hadfield, *et al.*, Fluorescence lifetime imaging of E-combretastatin uptake and distribution in live mammalian cells, *Eur. J. Cancer*, 2012, **48**(12), 1896–1903, DOI: 10.1016/j.ejca.2011.11.025.

87 C. Zhu, Y. Zuo and R. Wang, *et al.*, Discovery of Potent Cytotoxic Ortho-Aryl Chalcones as New Scaffold Targeting Tubulin and Mitosis with Affinity-Based Fluorescence, *J. Med. Chem.*, 2014, **57**(15), 6364–6382, DOI: 10.1021/jm500024v.

88 C. Zhu, Y. Zuo and B. Liang, *et al.*, Distinct tubulin dynamics in cancer cells explored using a highly tubulin-specific fluorescent probe, *Chem. Commun.*, 2015, **51**(69), 13400–13403, DOI: 10.1039/C5CC04927J.

89 M. N. Anisimov, M. A. Boichenko and A. A. Sivachev, *et al.*, Coumarin-30 Enables Site-Resolved Detection of Tubulin Ligands by Microscale Thermophoresis, *Angew. Chem., Int. Ed.*, 2025, e17086, DOI: 10.1002/anie.202517086.

90 R. L. Noble, C. T. Beer and J. H. Cutts, Role of chance observations in chemotherapy: Vinca rosea, *Ann. N. Y.*

Acad. Sci., 1958, **76**(3), 882–894, DOI: 10.1111/j.1749-6632.1958.tb54906.x.

91 Y. Ren, K. DeRose and L. Li, *et al.*, Vincamine, from an antioxidant and a cerebral vasodilator to its anticancer potential, *Bioorg. Med. Chem.*, 2023, **92**, 117439, DOI: 10.1016/j.bmc.2023.117439.

92 E. Martino, G. Casamassima and S. Castiglione, *et al.*, Vinca alkaloids and analogues as anti-cancer agents: Looking back, peering ahead, *Bioorg. Med. Chem. Lett.*, 2018, **28**(17), 2816–2826, DOI: 10.1016/j.bmcl.2018.06.044.

93 A. L. Risinger and L. Du, Targeting and extending the eukaryotic druggable genome with natural products: cytoskeletal targets of natural products, *Nat. Prod. Rep.*, 2020, **37**(5), 634–652, DOI: 10.1039/C9NP00053D.

94 R. L. Bai, K. D. Paull and C. L. Herald, *et al.*, Halichondrin B and homohalichondrin B, marine natural products binding in the vinca domain of tubulin. Discovery of tubulin-based mechanism of action by analysis of differential cytotoxicity data, *J. Biol. Chem.*, 1991, **266**(24), 15882–15889, DOI: 10.1016/S0021-9258(18)98491-7.

95 R. Bai, G. R. Petit and E. Hamel, Dolastatin 10, a powerful cytostatic peptide derived from a marine animal, *Biochem. Pharmacol.*, 1990, **39**(12), 1941–1949, DOI: 10.1016/0006-2952(90)90613-P.

96 Z. Cruz-Monserrate, J. T. Mullaney and P. G. Harran, *et al.*, Dolastatin 15 binds in the vinca domain of tubulin as demonstrated by Hummel–Dreyer chromatography, *Eur. J. Biochem.*, 2003, **270**(18), 3822–3828, DOI: 10.1046/j.1432-1033.2003.03776.x.

97 B. Gigant, C. Wang and R. B. G. Ravelli, *et al.*, Structural basis for the regulation of tubulin by vinblastine, *Nature*, 2005, **435**(7041), 519–522, DOI: 10.1038/nature03566.

98 Y. Wang, F. W. Benz and Y. Wu, *et al.*, Structural Insights into the Pharmacophore of Vinca Domain Inhibitors of Microtubules, *Mol. Pharmacol.*, 2016, **89**(2), 233–242, DOI: 10.1124/mol.115.100149.

99 A. Cormier, M. Marchand and R. B. G. Ravelli, *et al.*, Structural insight into the inhibition of tubulin by vinca domain peptide ligands, *EMBO Rep.*, 2008, **9**(11), 1101–1106, DOI: 10.1038/embor.2008.171.

100 A. Cormier, M. Knossow and C. Wang, *et al.*, The Binding of Vinca Domain Agents to Tubulin, *Methods Cell Biol.*, 2010, 373–390, DOI: 10.1016/S0091-679X(10)95020-6.

101 S. S. Rai and J. Wolff, Localization of the Vinblastine-binding Site on β-Tubulin, *J. Biol. Chem.*, 1996, **271**(25), 14707–14711, DOI: 10.1074/jbc.271.25.14707.

102 S. K. Chatterjee, J. Laffray and P. Patel, *et al.*, Interaction of Tubulin with a New Fluorescent Analogue of Vinblastine, *Biochemistry*, 2002, **41**(47), 14010–14018, DOI: 10.1021/bi026182m.

103 D. J. Gruol, M. N. King and M. E. Kuehne, Evidence for the Locations of Distinct Steroid and Vinca Alkaloid Interaction Domains within the Murine mdr1b P-Glycoprotein, *Mol. Pharmacol.*, 2002, **62**(5), 1238–1248, DOI: 10.1124/mol.62.5.1238.

104 W. Lin and T. Chen, A vinblastine fluorescent probe for pregnane X receptor in a time-resolved fluorescence resonance energy transfer assay, *Anal. Biochem.*, 2013, **443**(2), 252–260, DOI: 10.1016/j.ab.2013.09.009.

105 W. Lin, J. Liu and C. Jeffries, *et al.*, Development of BODIPY FL Vindoline as a Novel and High-Affinity Pregnane X Receptor Fluorescent Probe, *Bioconjug. Chem.*, 2014, **25**(9), 1664–1677, DOI: 10.1021/bc5002856.

106 D. W. Carney, J. C. Lukesh and D. M. Brody, *et al.*, Ultrapotent vinblastines in which added molecular complexity further disrupts the target tubulin dimer–dimer interface, *Proc Natl. Acad. Sci. U. S. A.*, 2016, **113**(35), 9691–9698, DOI: 10.1073/pnas.1611405113.

107 O. Bársony, G. Szalóki and D. Türk, *et al.*, A single active catalytic site is sufficient to promote transport in P-glycoprotein, *Sci. Rep.*, 2016, **6**(1), 24810, DOI: 10.1038/srep24810.

108 H. P. Eikesdal, W. Landuyt and O. Dahl, The influence of combretastatin A-4 and vinblastine on interstitial fluid pressure in BT4An rat gliomas, *Cancer Lett.*, 2002, **178**(2), 209–217, DOI: 10.1016/S0304-3835(01)00835-7.

109 L. G. Meimetis, R. J. Giedt and H. Mikula, *et al.*, Fluorescent vinblastine probes for live cell imaging, *Chem. Commun.*, 2016, **52**(64), 9953–9956, DOI: 10.1039/C6CC04129A.

110 A. M. Laughney, E. Kim and M. M. Sprachman, *et al.*, Single-cell pharmacokinetic imaging reveals a therapeutic strategy to overcome drug resistance to the microtubule inhibitor eribulin, *Sci. Transl. Med.*, 2014, **6**(261), 1–23, DOI: 10.1126/scitranslmed.3009318.

111 T. Nabekura, T. Kawasaki and M. Jimura, *et al.*, Microtubule-targeting anticancer drug eribulin induces drug efflux transporter P-glycoprotein, *Biochem. Biophys. Rep.*, 2020, **21**(100727), 1–5, DOI: 10.1016/j.bbrep.2020.100727.

112 H. Doodhi, A. E. Prota and R. Rodríguez-García, *et al.*, Termination of Protofilament Elongation by Eribulin Induces Lattice Defects that Promote Microtubule Catastrophes, *Curr. Biol.*, 2016, **26**(13), 1713–1721, DOI: 10.1016/j.cub.2016.04.053.

113 A. E. Prota, K. Bargsten and D. Zurwerra, *et al.*, Molecular mechanism of action of microtubule-stabilizing anticancer agents, *Science*, 2013, **339**(6119), 587–590, DOI: 10.1126/science.1230582.

114 B. A. Weaver, How Taxol/paclitaxel kills cancer cells, *Mol. Biol. Cell*, 2014, **25**(18), 2677–2681, DOI: 10.1091/mbc.e14-04-0916.

115 X. Chen, A. Winstead and H. Yu, *et al.*, Taccalonolides: A novel class of microtubule-stabilizing anticancer agents, *Cancers*, 2021, **13**(4), 1–19, DOI: 10.3390/cancers13040920.

116 L. Takahashi-Ruiz, J. D. Morris and P. Crews, *et al.*, In Vivo Evaluation of (-)-Zampanolide Demonstrates Potent and Persistent Antitumor Efficacy When Targeted to the Tumor Site, *Molecules*, 2022, **27**(13), 4244, DOI: 10.3390/molecules27134244.

117 C. Villegas, I. González-Chavarría and V. Burgos, *et al.*, Epothilones as Natural Compounds for Novel Anticancer Drugs Development, *Int. J. Mol. Sci.*, 2023, **24**(7), 6063, DOI: 10.3390/ijms24076063.

118 A. B. Smith and B. S. Freeze, -Discodermolide: total synthesis, construction of novel analogues, and biological

evaluation, *Tetrahedron*, 2007, **64**(2), 261–298, DOI: 10.1016/j.tet.2007.10.039.

119 L. Lafanechère, The microtubule cytoskeleton: An old validated target for novel therapeutic drugs, *Front. Pharmacol.*, 2022, **13**, 969183, DOI: 10.3389/fphar.2022.969183.

120 C. P. Bold, M. Gut and J. Schürmann, *et al.*, Synthesis of Morpholine-Based Analogues of (−)-Zampanolide and Their Biological Activity, *Chem. - Eur. J.*, 2021, **27**(19), 5936–5943, DOI: 10.1002/chem.202003996.

121 A. Mandhare, S. Biradar and A. Gurule, Azaepothilone B and its derivatives: a patent review, *Expert Opin. Ther. Pat.*, 2016, **26**(8), 891–905, DOI: 10.1080/13543776.2016.1199688.

122 T. M. Brütsch, E. Cotter and D. Lucena-Agell, *et al.*, Synthesis and Structure-Activity Relationship Studies of C(13)-Desmethylene-(−)-Zampanolide Analogs, *Chem. - Eur. J.*, 2023, **29**(36), e20230070, DOI: 10.1002/chem.202300703.

123 K.-H. Altmann, *Semisynthetic Derivatives of Epothilones*, Springer, 2009, pp. 135–156, DOI: 10.1007/978-3-211-78207-1_4.

124 P. B. Schiff, J. Fant and S. B. Horwitz, Promotion of microtubule assembly in vitro by taxol, *Nature*, 1979, **277**(5698), 665–667, DOI: 10.1038/277665a0.

125 J. P. Snyder, J. H. Nettles and B. Cornett, *et al.*, The binding conformation of Taxol in-tubulin: A model based on electron crystallographic density, *Proc Natl. Acad. Sci. U. S. A.*, 2001, **98**(9), 5312–5316, DOI: 10.1073/pnas.051309398.

126 M. Graffe, D. Zenisek and J. W. Taraska, A marginal band of microtubules transports and organizes mitochondria in retinal bipolar synaptic terminals, *J. Gen. Physiol.*, 2015, **146**(1), 109–117, DOI: 10.1085/jgp.201511396.

127 S. Rao, S. B. Horwitz and I. Ringel, Direct Photoaffinity Labeling of Tubulin With Taxol, *J. Natl. Cancer Inst.*, 1992, **84**(10), 785–788, DOI: 10.1093/jnci/84.10.785.

128 A. E. Prota, D. Lucena-Agell and Y. Ma, *et al.*, Structural insight into the stabilization of microtubules by taxanes, *eLife*, 2023, **12**, e84791, DOI: 10.7554/eLife.84791.

129 E. Nogales, S. G. Wolf and A. Khant, *et al.*, Structure of tubulin at 6.5 A and location of the taxol-binding site, *Nature*, 1995, **375**, 424–427, DOI: 10.1038/375424a0.

130 Y. J. Hu, C. C. Gu and X. F. Wang, *et al.*, Asymmetric Total Synthesis of Taxol, *J. Am. Chem. Soc.*, 2021, **143**(42), 17862–17870, DOI: 10.1021/jacs.1c09637.

131 D. G. I. Kingston, The chemistry of taxol, *Pharmacol. Ther.*, 1991, **52**, 1–34.

132 E. Baloglu and D. G. I. Kingston, A new semisynthesis of paclitaxel from Baccatin III, *J. Nat. Prod.*, 1999, **62**(7), 1068–1071, DOI: 10.1021/np990040k.

133 A. A. Souto, A. U. Acuña and J. M. Andreu, *et al.*, New fluorescent water-soluble taxol derivatives, *Angew. Chem., Int. Ed. Engl.*, 1996, **34**(23), 2710–2712, DOI: 10.1002/anie.199527101.

134 A. E. Mathew, M. R. Mejillano and J. P. Nath, *et al.*, Synthesis and evaluation of some water-soluble prodrugs and derivatives of taxol with antitumor activity, *J. Med. Chem.*, 1992, **35**(1), 145–151, DOI: 10.1021/jm00079a019.

135 J. A. Evangelio, M. Abal and I. Barasoain, *et al.*, Fluorescent Taxoids as Probes of the Microtubule Cytoskeleton, *Cell Motil. Cytoskeleton*, 1998, **39**(1), 73–90, DOI: 10.1002/(SICI)1097-0169(1998)39:1%3C73::AID-CM7%3E3.0.CO;2-H.

136 W. Mellado, N. F. Magri and D. Kingston, *et al.*, Preparation and biological activity of taxol acetates, *Biochem. Biophys. Res. Commun.*, 1984, **124**(2), 329–336, DOI: 10.1016/0006-291x(84)91557-2.

137 J. Dubois, M.-T. Goff and F. Gutritte-Voegelein, *et al.*, Fluorescent and Biotinylated Analogues of Docetaxel Synthesis and Biological Evaluation, *Bioorg. Med. Chem.*, 1995, **3**(10), 1357–1368, DOI: 10.1016/0968-0896(95)00115-w.

138 R. K. Guy, Z. A. Scott and R. D. Sloboda, *et al.*, Fluorescent taxoids, *Chem. Biol.*, 1996, **3**(12), 1021–1031, DOI: 10.1016/s1074-5521(96)90168-4.

139 J. F. Díaz, R. Strobe and Y. Engelborghs, *et al.*, Molecular recognition of taxol by microtubules: Kinetics and thermodynamics of binding of fluorescent taxol derivatives to an exposed site, *J. Biol. Chem.*, 2000, **275**(34), 26265–26276, DOI: 10.1074/jbc.M003120200.

140 J. F. Díaz, I. Barasoain and J. M. Andreu, Fast kinetics of Taxol binding to microtubules: Effects of solution variables and microtubule-associated proteins, *J. Biol. Chem.*, 2003, **278**(10), 8407–8419, DOI: 10.1074/jbc.M211163200.

141 J. F. Díaz, I. Barasoain and A. A. Souto, *et al.*, Macromolecular accessibility of fluorescent taxoids bound at a paclitaxel binding site in the microtubule surface, *J. Biol. Chem.*, 2005, **280**(5), 3928–3937, DOI: 10.1074/jbc.M407816200.

142 R. M. Buey, E. Calvo and I. Barasoain, *et al.*, Cyclostreptin binds covalently to microtubule pores and lumenal taxoid binding sites, *Nat. Chem. Biol.*, 2007, **3**(2), 117–125, DOI: 10.1038/nchembio853.

143 I. Barasoain, A. M. García-Carril and R. Matesanz, *et al.*, Probing the Pore Drug Binding Site of Microtubules with Fluorescent Taxanes: Evidence of Two Binding Poses, *Chem. Biol.*, 2010, **17**(3), 243–253, DOI: 10.1016/j.chembiol.2010.02.006.

144 I. Barasoain, J. F. Díaz and J. M. Andreu, Fluorescent taxoid probes for microtubule research, *Methods Cell Biol.*, 2010, **95**, 353–372, DOI: 10.1016/S0091-679X(10)95019-X.

145 J. M. Andreu and I. Barasoain, The Interaction of Baccatin III with the Taxol Binding Site of Microtubules Determined by a Homogeneous Assay with Fluorescent Taxoid, *Biochemistry*, 2001, **40**, 11975–11984, DOI: 10.1021/bi010869.

146 R. Matesanz, J. Rodríguez-Salarichs and B. Pera, *et al.*, Modulation of microtubule interprotofilament interactions by modified taxanes, *Biophys. J.*, 2011, **101**(12), 2970–2980, DOI: 10.1016/j.bpj.2011.11.005.

147 J. J. Field, B. Pera and E. Calvo, *et al.*, Zampanolide, a potent new microtubule-stabilizing agent, covalently reacts with the taxane luminal site in tubulin α,β-heterodimers and microtubules, *Chem. Biol.*, 2012, **19**(6), 686–698, DOI: 10.1016/j.chembiol.2012.05.008.

148 J. F. Díaz and R. M. Buey, *Microtubule Protocols-Characterizing Ligand-Microtubule Binding by Competition Methods*, Humana, Totowa, NJ, 1st edn, 2007.

149 R. M. Buey, I. Barasoain and E. Jackson, *et al.*, Microtubule interactions with chemically diverse stabilizing agents:

Thermodynamics of binding to the paclitaxel site predicts cytotoxicity, *Chem. Biol.*, 2005, **12**(12), 1269–1279, DOI: 10.1016/j.chembiol.2005.09.010.

150 R. M. Buey, J. F. Díaz and J. M. Andreu, *et al.*, Interaction of Epothilone Analogs with the Paclitaxel Binding Site, *Chem. Biol.*, 2004, **11**, 225–236.

151 F. Z. Gaugaz, A. Chicca and M. Redondo-Horcajo, *et al.*, Synthesis, microtubule-binding affinity, and antiproliferative activity of new epothilone analogs and of an EGFR-targeted epothilone-peptide conjugate, *Int. J. Mol. Sci.*, 2019, **20**(5), 1113, DOI: 10.3390/ijms20051113.

152 A. Cutignano, I. Bruno and G. Bifulco, *et al.*, Dactylolide, a New Cytotoxic Macrolide from the Vanuatu SpongeDactylospongia sp, *Eur. J. Org. Chem.*, 2001, 775–778, DOI: 10.1002/1099-0690(200102)2001:4%3C775::AID-EJOC775%3E3.0.CO;2-Z.

153 R. Matesanz, C. Trigili and J. Rodríguez-Salarichs, *et al.*, Taxanes with high potency inducing tubulin assembly overcome tumoural cell resistances, *Bioorg. Med. Chem.*, 2015, **22**(18), 5078–5090, DOI: 10.1016/j.bmc.2014.05.048.

154 R. Matesanz, I. Barasoain and C. G. Yang, *et al.*, Optimization of Taxane Binding to Microtubules: Binding Affinity Dissection and Incremental Construction of a High-Affinity Analog of Paclitaxel, *Chem. Biol.*, 2008, **15**(6), 573–585, DOI: 10.1016/j.chembiol.2008.05.008.

155 D. E. Pryor, A. O'Brate and G. Bilcer, *et al.*, The microtubule stabilizing agent laulimalide does not bind in the taxoid site, kills cells resistant to paclitaxel and epothilones, and may not require its epoxide moiety for activity, *Biochemistry*, 2002, **41**(29), 9109–9115, DOI: 10.1021/bi020211b.

156 A. E. Prota, K. Bargsten and P. T. Northcote, *et al.*, Structural basis of microtubule stabilization by laulimalide and peloruside, *Angew. Chem., Int. Ed.*, 2014, **53**(6), 1621–1625, DOI: 10.1002/anie.201307749.

157 T. N. Gaitanos, R. M. Buey and J. F. Díaz, *et al.*, Peloruside A Does Not Bind to the Taxoid Site on β-Tubulin and Retains Its Activity in Multidrug-Resistant Cell Lines, *Cancer Res.*, 2004, **64**(15), 5063–5067, DOI: 10.1158/0008-5472.CAN-04-0771.

158 M. P. Lillo, O. Cañadas and R. E. Dale, *et al.*, Location and properties of the Taxol binding center in microtubules: A picosecond laser study with fluorescent taxoids, *Biochemistry*, 2002, **41**(41), 12436–12449, DOI: 10.1021/bi0261793.

159 A. Rai, T. Liu and S. Glauser, *et al.*, Taxanes convert regions of perturbed microtubule growth into rescue sites, *Nat. Mater.*, 2020, **19**(3), 355–365, DOI: 10.1038/s41563-019-0546-6.

160 P. B. Vieira, F. P. Borges and B. Gottardi, *et al.*, Analysis of microtubule cytoskeleton distribution using a fluorescent taxoid in two trichomonadid protozoa: Trichomonas gallinae and Tritrichomonas foetus, *Exp. Parasitol.*, 2008, **119**(1), 186–191, DOI: 10.1016/j.exppara.2007.12.011.

161 S. Hennig, S. V. D. Linde and M. Lummer, *et al.*, Instant live-cell super-resolution imaging of cellular structures by nanoinjection of fluorescent probes, *Nano Lett.*, 2015, **15**(2), 1374–1381, DOI: 10.1021/nl504660t.

162 N. Chen, C. Brachmann and X. Liu, *et al.*, Albumin-bound nanoparticle (nab) paclitaxel exhibits enhanced paclitaxel tissue distribution and tumor penetration, *Cancer Chemother. Pharmacol.*, 2015, **76**(4), 699–712, DOI: 10.1007/s00280-015-2833-5.

163 M. C. Naill, M. E. Kolewe and S. C. Roberts, Paclitaxel uptake and transport in Taxus cell suspension cultures, *Biochem. Eng. J.*, 2012, **63**, 50–56, DOI: 10.1016/j.bej.2012.01.006.

164 I. L. D. Maïo, P. Barbier and D. Allegro, *et al.*, Quantitative analysis of tau-microtubule interaction using FRET, *Int. J. Mol. Sci.*, 2014, **15**(8), 14697–14714, DOI: 10.3390/ijms150814697.

165 A. I. Marcus, A. M. O'Brate and R. M. Buey, *et al.*, Farnesyltransferase inhibitors reverse taxane resistance, *Cancer Res.*, 2006, **66**(17), 8838–8846, DOI: 10.1158/0008-5472.CAN-06-0699.

166 E. L. Kavanagh, S. Lindsay and M. Halasz, *et al.*, Protein and chemotherapy profiling of extracellular vesicles harvested from therapeutic induced senescent triple negative breast cancer cells, *Oncogenesis*, 2017, **6**(10), e388, DOI: 10.1038/ONCSIS.2017.82.

167 S. L. Feng, Z. W. Yuan and X. J. Yao, *et al.*, Tangeretin, a citrus pentamethoxyflavone, antagonizes ABCB1-mediated multidrug resistance by inhibiting its transport function, *Pharmacol. Res.*, 2016, **110**, 193–204, DOI: 10.1016/j.phrs.2016.04.003.

168 S. Feng, H. Zhou and D. Wu, *et al.*, Nobiletin and its derivatives overcome multidrug resistance (MDR) in cancer: total synthesis and discovery of potent MDR reversal agents, *Acta Pharm. Sin. B*, 2020, **10**(2), 327–343, DOI: 10.1016/j.apsb.2019.07.007.

169 X. Li, I. Barasoain and R. Matesanz, *et al.*, Synthesis and biological activities of high affinity taxane-based fluorescent probes, *Bioorg. Med. Chem. Lett.*, 2009, **19**(3), 751–754, DOI: 10.1016/j.bmcl.2008.12.018.

170 M. M. Lee, Z. Gao and B. R. Peterson, Synthesis of a Fluorescent Analogue of Paclitaxel That Selectively Binds Microtubules and Sensitively Detects Efflux by P-Glycoprotein, *Angew. Chem.*, 2017, **129**(24), 7031–7035, DOI: 10.1002/ange.201703298.

171 A. E. Andres, D. Rane and B. R. Peterson, Pacific Blue-Taxoids as Fluorescent Molecular Probes of Microtubules, *Methods Mol. Biol.*, 2022, **2430**, 449–466, DOI: 10.1007/978-1-0716-1983-4_28.

172 W.-C. Sun, K. R. Gee and R. P. Haugland, Synthesis of Novel Fluorinated Coumarins: Excellent UV-Light Excitable Fluorescent Dyes Introduction, *Bioorg. Med. Chem. Lett.*, 1998, **8**, 3107–3110, DOI: 10.1016/s0960-894x(98)00578-2%20Abstract.

173 S. Sengupta, T. C. Boge and G. I. Georg, *et al.*, Interaction of a Fluorescent Paclitaxel Analogue with Tubulin, *Biochemistry*, 1995, **34**, 11889–11890, DOI: 10.1021/bi00037a029.

174 Y. Li, R. Edsall and P. G. Jagtap, *et al.*, Equilibrium studies of a fluorescent paclitaxel derivative binding to microtubules, *Biochemistry*, 2000, **39**(3), 616–623, DOI: 10.1021/bi992044u.

175 Y. Han, A. G. Chaudhary and M. D. Chordia, *et al.*, Interaction of a Fluorescent Derivative of Paclitaxel (Taxol) with Microtubules and Tubulin-Colchicine, *Biochemistry*, 1996, **35**(45), 14173–14183, DOI: 10.1021/bi960774l.

176 E. Baloglu, D. G. I. Kingston and P. Patel, *et al.*, Synthesis and Microtubule Binding of Fluorescent Paclitaxel Derivatives, *Bioorg. Med. Chem. Lett.*, 2001, **11**(17), 2249–2252, DOI: 10.1016/s0960-894x(01)00453-x.

177 S. Sengupta, T. C. Boge and Y. Liu, *et al.*, Probing the Environment of Tubulin-Bound Paclitaxel Using Fluorescent Paclitaxel Analogues, *Biochemistry*, 1997, **36**(17), 5179–5184, DOI: 10.1021/bi962891m.

178 G. Lukinavičius, L. Reymond and E. D'Este, *et al.*, Fluorogenic probes for live-cell imaging of the cytoskeleton, *Nat. Methods*, 2014, **11**(7), 731–733, DOI: 10.1038/nmeth.2972.

179 H. Ohno, E. Sasaki and S. Yamada, *et al.*, Recent advances in Si-rhodamine-based fluorescent probes for live-cell imaging, *Org. Biomol. Chem.*, 2024, **22**(16), 3099–3108, DOI: 10.1039/d4ob00130c.

180 Y. Xiao and X. Qian, Substitution of oxygen with silicon: A big step forward for fluorescent dyes in life science, *Coord. Chem. Rev.*, 2020, **423**, 213513, DOI: 10.1016/j.ccr.2020.213513.

181 T. Wang, Q. J. Zhao and H. G. Hu, *et al.*, Spirolactonized Si-rhodamine: A novel NIR fluorophore utilized as a platform to construct Si-rhodamine-based probes, *Chem. Commun.*, 2012, **48**(70), 8781–8783, DOI: 10.1039/c2cc34159j.

182 E. Derivery, C. Seum and A. Daeden, *et al.*, Polarized endosome dynamics by spindle asymmetry during asymmetric cell division, *Nature*, 2015, **528**(7581), 280–285, DOI: 10.1038/nature16443.

183 P. S. A. Courtois and T. S. Kitajima, Triple-Color Live Imaging of Mouse Oocytes. in *Mouse Oocyte Development, Methods in Molecular Biology*, ed. Verlhac, M. H., Terret, M. E., Humana Press, vol 1818, 2018.

184 V. Magliocca, S. Petrini and T. Franchin, *et al.*, Identifying the dynamics of actin and tubulin polymerization in iPSCs and in iPSC-derived neurons, *Oncotarget*, 2017, **8**(67), 111096–111109.

185 Y. Shen and K. M. Ori-McKenney, Microtubule-associated protein MAP7 promotes tubulin posttranslational modifications and cargo transport to enable osmotic adaptation, *Dev. Cell*, 2024, **59**(12), 1553–1570, DOI: 10.1016/j.devcel.2024.03.022.

186 R. T. Gerasimaitė, J. Bucevičius and K. A. Kiszka, *et al.*, Blinking Fluorescent Probes for Tubulin Nanoscopy in Living and Fixed Cells, *ACS Chem. Biol.*, 2021, **16**(11), 2130–2136, DOI: 10.1021/acschembio.1c00538.

187 S. N. Uno, M. Kamiya and T. Yoshihara, *et al.*, A spontaneously blinking fluorophore based on intramolecular spirocyclization for live-cell super-resolution imaging, *Nat. Chem.*, 2014, **6**(8), 681–689, DOI: 10.1038/nchem.2002.

188 Q. Zheng, A. X. Ayala and I. Chung, *et al.*, Rational Design of Fluorogenic and Spontaneously Blinking Labels for Super-Resolution Imaging, *ACS Cent. Sci.*, 2019, **5**(9), 1602–1613, DOI: 10.1021/acscentsci.9b00676.

189 J. B. Grimm, B. P. English and H. Choi, *et al.*, Bright photoactivatable fluorophores for single-molecule imaging, *Nat. Methods*, 2016, **13**(12), 985–988, DOI: 10.1038/nmeth.4034.

190 J. B. Grimm, B. P. English and J. Chen, *et al.*, A general method to improve fluorophores for live-cell and single-molecule microscopy, *Nat. Methods*, 2015, **12**(3), 244–250, DOI: 10.1038/nmeth.3256.

191 L. Xu, K. G. Schaefer and G. M. King, *et al.*, Insights into interactions between taxanes and P-glycoprotein using biophysical and in silico methods, *J. Pharm. Sci.*, 2025, **114**(5), 103708, DOI: 10.1016/j.xphs.2025.103708.

192 M. A. Melan, Use of Fluorochrome-Tagged Taxol® to Produce Fluorescent Microtubules in Solution, *Biotechniques*, 1998, **25**(2), 188–192, DOI: 10.2144/98252bm02.

193 S. Fellner, B. Bauer and D. S. Miller, *et al.*, Transport of paclitaxel (Taxol) across the blood-brain barrier in vitro and in vivo, *J. Clin. Invest.*, 2002, **110**(9), 1309–1318, DOI: 10.1172/JCI15451.

194 J. Xia, Q. Pei and M. Zheng, *et al.*, An activatable fluorescent prodrug of paclitaxel and BODIPY, *J. Mater. Chem. B*, 2021, **9**(9), 2308–2313, DOI: 10.1039/d0tb02510k.

195 J. C. Gilbert, J. Hadgraft and A. Bye, *et al.*, Drug release from Pluronic F-127 gels, *Int. J. Pharm.*, 1986, **32**, 223–228, DOI: 10.1016/0378-5173(86)90182-1.

196 T. Ali, D. Li and T. N. F. Ponnamperumage, *et al.*, Generation of Hydrogen Peroxide in Cancer Cells: Advancing Therapeutic Approaches for Cancer Treatment, *Cancers*, 2024, **16**(12), 2171, DOI: 10.3390/cancers16122171.

197 M. López-Lázaro, Dual role of hydrogen peroxide in cancer: Possible relevance to cancer chemoprevention and therapy, *Cancer Lett.*, 2007, **252**(1), 1–8, DOI: 10.1016/j.canlet.2006.10.029.

198 J. Daniel, M. Montaleytang and S. Nagarajan, *et al.*, Hydrophilic Fluorescent Nanoprodrug of Paclitaxel for Glioblastoma Chemotherapy, *ACS Omega*, 2019, **4**(19), 18342–18354, DOI: 10.1021/acsomega.9b02588.

199 Q. Shuai, G. Zhao and X. Zhang, *et al.*, Selection of fluorescent dye for tracking biodistribution of paclitaxel in live imaging, *Colloids Surf., B*, 2019, **181**, 872–878, DOI: 10.1016/j.colsurfb.2019.06.035.

200 G. Logan and B. McCartney, Comparative analysis of taxol-derived fluorescent probes to assess microtubule networks in a complex live three-dimensional tissue, *Cytoskeleton*, 2020, **77**(5–6), 229–237, DOI: 10.1002/cm.21599.

201 C. So, K. Menelaou and J. Uraji, *et al.*, Mechanism of spindle pole organization and instability in human oocytes, *Science*, 2022, **375**(6581), eabj3944, DOI: 10.1126/science.abj3944.

202 M. S. Frei, B. Koch and J. Hiblot, *et al.*, Live-Cell Fluorescence Lifetime Multiplexing Using Synthetic Fluorescent Probes, *ACS Chem. Biol.*, 2022, **17**(6), 1321–1327, DOI: 10.1021/acschembio.2c00041.

203 G. Y. Liu, S.-C. Chen and G.-H. Lee, *et al.*, Precise control of microtubule disassembly in living cells, *EMBO J.*, 2022, **41**(15), e110472.

204 R. D. Pace, S. Ghosh and V. H. Ryan, *et al.*, Messenger RNA transport on lysosomal vesicles maintains axonal mitochondrial homeostasis and prevents axonal degeneration, *Nat. Neurosci.*, 2024, **27**(6), 1087–1102, DOI: 10.1038/s41593-024-01619-1.

205 G. Wen, X. Chen and P. Eiring, *et al.*, Functionalized Docetaxel Probes for Refined Visualization of Mitotic Spindles by Expansion Microscopy, *J. Am. Chem. Soc.*, 2025, **147**(8), 6604–6611, DOI: 10.1021/jacs.4c15608.

206 G. P. D. Hoefle, N. D. Bedorf, K. D. Gerth, *et al.*, Epothilones, Their Manufacturing Processes as Well as Medium Containing Them. 1993.

207 S. Forli, Epothilones: From Discovery to Clinical Trials, *Curr. Top. Med. Chem.*, 2014, **14**(20), 2312–2321, DOI: 10.2174/1568026614666141130095855.

208 F. Y. F. Lee, R. Borzilleri and C. R. Fairchild, *et al.*, Preclinical discovery of ixabepilone, a highly active antineoplastic agent, *Cancer Chemother. Pharmacol.*, 2008, **63**(1), 157–166, DOI: 10.1007/s00280-008-0724-8.

209 Q. Xiao, T. Xue and W. Shuai, *et al.*, High-resolution X-ray structure of three microtubule-stabilizing agents in complex with tubulin provide a rationale for drug design, *Biochem. Biophys. Res. Commun.*, 2021, **534**, 330–336, DOI: 10.1016/j.bbrc.2020.11.082.

210 T. Ganesh, J. K. Schilling and R. K. Palakodety, *et al.*, Synthesis and biological evaluation of fluorescently labeled epothilone analogs for tubulin binding studies, *Tetrahedron*, 2003, **59**(50), 9979–9984, DOI: 10.1016/j.tet.2003.10.024.

211 J. Gertsch, F. Feyen and A. Bützberger, *et al.*, Making epothilones fluoresce: Design, synthesis, and biological characterization of a fluorescent N12-aza-epothilone (azathilone), *ChemBioChem*, 2009, **10**(15), 2513–2521, DOI: 10.1002/cbic.200900376.

212 S. Glauser Synthesis of Monocyclic and Dioxane-Derived Zampanolide Analogues and of Highly Active Fluorescent Epothilone B Conjugates. 2019.

213 K. C. Nicolaou, A. Ritzén and K. Namoto, Recent developments in the chemistry, biology and medicine of the epothilones, *Chem. Commun.*, 2001, 1523–1535, DOI: 10.1039/b104949f.

214 K. C. Nicolaou, F. Roschangar and D. Vourloumis, Chemical Biology of Epothilones, *Angew. Chem., Int. Ed.*, 1998, **37**(15), 2014–2045, DOI: 10.1002/(SICI)1521-3773(19980817)37:15%3C2014::AID-ANIE2014%3E3.0.CO;2-2.

215 S. P. Gunasekera, M. Gunasekera and R. E. Longley, *et al.*, Discodermolide: a new bioactive polyhydroxylated lactone from the marine sponge Discodermia dissoluta, *J. Org. Chem.*, 1990, **55**(16), 4912–4915, DOI: 10.1021/jo00303a029.

216 R. E. Longley, D. Caddigan and D. Harmody, *et al.*, Discodermolide—A New, Marine-Derived Immunosuppressive Compound, *Transplantation*, 1991, **52**(4), 656–661, DOI: 10.1097/00007890-199110000-00015.

217 R. J. Kowalski, P. Giannakakou and S. P. Gunasekera, *et al.*, The Microtubule-Stabilizing Agent Discodermolide Competitively Inhibits the Binding of Paclitaxel (Taxol) to Tubulin Polymers, Enhances Tubulin Nucleation Reactions More Potently than Paclitaxel, and Inhibits the Growth of Paclitaxel-Resistant Cells, *Mol. Pharmacol.*, 1997, **52**(4), 613–622, DOI: 10.1124/mol.52.4.613.

218 I. Paterson and G. J. Florence, The Development of a Practical Total Synthesis of Discodermolide, a Promising Microtubule-Stabilizing Anticancer Agent, *Eur. J. Org. Chem.*, 2003, 2193–2208, DOI: 10.1002/ejoc.200300061.

219 Z. Yu, R. J. Ely and J. P. Morken, Synthesis of (+)-Discodermolide by Catalytic Stereoselective Borylation Reactions, *Angew. Chem., Int. Ed.*, 2014, **53**(36), 9632–9636, DOI: 10.1002/anie.201405455.

220 J. A. Marshall and B. A. Johns, Total Synthesis of (+)-Discodermolide, *J. Org. Chem.*, 1998, **63**(22), 7885–7892, DOI: 10.1021/jo9811423.

221 D. T. Hung, J. B. Nerenberg and S. L. Schreiber, Syntheses of Discodermolides Useful for Investigating Microtubule Binding and Stabilization, *J. Am. Chem. Soc.*, 1996, **118**(45), 11054–11080, DOI: 10.1021/ja961374o.

222 I. Paterson and G. J. Florence, The chemical synthesis of discodermolide, *Top. Curr. Chem.*, 2009, **286**, 73–119, DOI: 10.1007/128_2008_7.

223 A. E. Prota, K. Bargsten and M. Redondo-Horcajo, *et al.*, Structural Basis of Microtubule Stabilization by Discodermolide, *ChemBioChem*, 2017, **18**(10), 905–909, DOI: 10.1002/cbic.201600696.

224 A. B. Smith, P. V. Rucker and I. Brouard, *et al.*, Design, synthesis, and biological evaluation of potent discodermolide fluorescent and photoaffinity molecular probes, *Org. Lett.*, 2005, **7**(23), 5199–5202, DOI: 10.1021/ol0520166.

225 J. Qi, A. R. Blanden and S. Bane, *et al.*, Design, synthesis and biological evaluation of a simplified fluorescently labeled discodermolide as a molecular probe to study the binding of discodermolide to tubulin, *Bioorg. Med. Chem.*, 2011, **19**(17), 5247–5254, DOI: 10.1016/j.bmc.2011.06.082.

226 J. Li, A. L. Risinger and S. L. Mooberry, Taccalonolide microtubule stabilizers, *Bioorg. Med. Chem.*, 2015, **22**(18), 5091–5096, DOI: 10.1016/j.bmc.2014.01.012.

227 Y. Li, Y. F. Du and F. Gao, *et al.*, Taccalonolides: Structure, semi-synthesis, and biological activity, *Front. Pharmacol.*, 2022, **13**, 968061, DOI: 10.3389/fphar.2022.968061.

228 S. S. Yee, L. Du and A. L. Risinger, Taccalonolide Microtubule Stabilizers, *Prog. Chem. Org. Nat. Prod.*, 2020, **112**, 183–206, DOI: 10.1007/978-3-030-52966-6_3.

229 Y. Wang, Y. Yu and G. B. Li, *et al.*, Mechanism of microtubule stabilization by taccalonolide AJ, *Nat. Commun.*, 2017, **8**, 15787, DOI: 10.1038/ncomms15787.

230 A. L. Risinger, E. M. Jackson and L. A. Polin, *et al.*, The taccalonolides: Microtubule stabilizers that circumvent clinically relevant taxane resistance mechanisms, *Cancer Res.*, 2008, **68**(21), 8881–8888, DOI: 10.1158/0008-5472.CAN-08-2037.

231 T. L. Tinley, D. A. Randall-Hlubek and R. M. Leal, *et al.*, Taccalonolides E and A: Plant-derived steroids with microtubule-stabilizing activity, *Cancer Res.*, 2003, **63**(12), 3211–3220.

232 L. Du, A. L. Risinger and S. S. Yee, *et al.*, Identification of C-6 as a New Site for Linker Conjugation to the Taccalonolide Microtubule Stabilizers, *J. Nat. Prod.*, 2019, **82**(3), 583–588, DOI: 10.1021/acs.jnatprod.8b01036.

233 L. Du, S. S. Yee and K. Ramachandran, *et al.*, Elucidating target specificity of the taccalonolide covalent microtubule stabilizers employing a combinatorial chemical approach, *Nat. Commun.*, 2020, **11**(1), 654, DOI: 10.1038/s41467-019-14277-w.

234 S. M. Kupchan, Y. Komoda and W. A. Court, *et al.*, Tumor inhibitors. LXXIII. Maytansine, a novel antileukemic ansa macrolide from Maytenus ovatus, *J. Am. Chem. Soc.*, 1972, **94**(4), 1354–1356, DOI: 10.1021/ja00759a054.

235 O. Ab, K. R. Whiteman and L. M. Bartle, *et al.*, IMGN853, a Folate Receptor-α (FRα)–Targeting Antibody–Drug Conjugate, Exhibits Potent Targeted Antitumor Activity against FRα-Expressing Tumors, *Mol. Cancer Ther.*, 2015, **14**(7), 1605–1613, DOI: 10.1158/1535-7163.MCT-14-1095.

236 V. Diéras, D. Miles and S. Verma, *et al.*, Trastuzumab emtansine versus capecitabine plus lapatinib in patients with previously treated HER2-positive advanced breast cancer (EMILIA): a descriptive analysis of final overall survival results from a randomised, open-label, phase 3 trial, *Lancet Oncol.*, 2017, **18**(6), 732–742, DOI: 10.1016/S1470-2045(17)30312-1.

237 K. N. Moore, A. Angelergues and G. E. Konecny, *et al.*, Mirvetuximab Soravtansine in FRα-Positive, Platinum-Resistant Ovarian Cancer, *N. Engl. J. Med.*, 2023, **389**(23), 2162–2174, DOI: 10.1056/NEJMoa2309169.

238 S. Zafar, M. Armaghan and K. Khan, *et al.*, New insights into the anticancer therapeutic potential of maytansine and its derivatives, *Biomed. Pharmacother.*, 2023, **165**, 115039, DOI: 10.1016/j.biopha.2023.115039.

239 A. E. Prota, K. Bargsten and J. F. Diaz, *et al.*, A new tubulin-binding site and pharmacophore for microtubule-destabilizing anticancer drugs, *Proc. Natl. Acad. Sci. U. S. A.*, 2014, **111**(38), 13817–13821, DOI: 10.1073/pnas.1408124111.

240 T. Sawada, Y. Kato and H. Kobayashi, *et al.*, A Fluorescent Probe and a Photoaffinity Labeling Reagent To Study the Binding Site of Maytansine and Rhizoxin on Tubulin, *Bioconjugate Chem.*, 1993, **4**, 284–289, DOI: 10.1021/bc00022a006.

241 N. Fishkin, Maytansinoid-BODIPY conjugates: Application to microscale determination of drug extinction coefficients and for quantification of maytansinoid analytes, *Mol. Pharm.*, 2015, **12**(6), 1745–1751, DOI: 10.1021/mp500843r.

242 G. Menchon, A. E. Prota and D. Lucena-Agell, *et al.*, A fluorescence anisotropy assay to discover and characterize ligands targeting the maytansine site of tubulin, *Nat. Commun.*, 2018, **9**(1), 2106, DOI: 10.1038/s41467-018-04535-8.

243 P. Marzullo, Z. Boiarska and H. Pérez-Peña, *et al.*, Maytansinol Derivatives: Side Reactions as a Chance for New Tubulin Binders, *Chem. – Eur. J.*, 2022, **28**(2), e202103520, DOI: 10.1002/chem.202103520.

244 Z. Boiarska, H. Pérez-Peña and A.-C. Abel, *et al.*, Maytansinol Functionalization: Towards Useful Probes for Studying Microtubule Dynamics, *Chem. – Eur. J.*, 2023, **29**(5), e202203431, DOI: 10.1002/chem.202203431.

245 C. P. Bold, D. Lucena-Agell and M. Á. Oliva, *et al.*, Synthesis and Biological Evaluation of C(13)/C(13′)-Bis(desmethyl)-disorazole Z, *Angew. Chem., Int. Ed.*, 2023, **62**(5), e202212190, DOI: 10.1002/anie.202212190.

246 D. G. Corley, R. Herb and R. E. Moore, *et al.*, Laulimalides. New potent cytotoxic macrolides from a marine sponge and a nudibranch predator, *J. Org. Chem.*, 1988, **53**(15), 3644–3646, DOI: 10.1021/jo00250a053.

247 E. Quinoa, Y. Kakou and P. Crews, Fijianolides, polyketide heterocycles from a marine sponge, *J. Org. Chem.*, 1988, **53**(15), 3642–3644, DOI: 10.1021/jo00250a052.

248 S. L. Mooberry, G. Tien and A. H. Hernandez, *et al.*, Laulimalide and isolaulimalide, new paclitaxel-like microtubule-stabilizing agents, *Cancer Res.*, 1999, **59**(3), 653–660.

249 L. M. West, P. T. Northcote and C. N. Battershill, Peloruside A: a potent cytotoxic macrolide isolated from the new zealand marine sponge Mycale sp, *J. Org. Chem.*, 2000, **65**(2), 445–449, DOI: 10.1021/jo991296y.

250 K. A. Hood, L. M. West and B. Rouwé, *et al.*, Peloruside A, a novel antimitotic agent with paclitaxel-like microtubule-stabilizing activity, *Cancer Res.*, 2002, **62**(12), 3356–3360.

251 O. Pineda, J. Farràs and L. Maccari, *et al.*, Computational comparison of microtubule-stabilising agents laulimalide and peloruside with taxol and colchicine, *Bioorg. Med. Chem. Lett.*, 2004, **14**(19), 4825–4829, DOI: 10.1016/j.bmcl.2004.07.053.

252 J. T. Huzil, J. K. Chik and G. W. Slysz, *et al.*, A Unique Mode of Microtubule Stabilization Induced by Peloruside A, *J. Mol. Biol.*, 2008, **378**(5), 1016–1030, DOI: 10.1016/j.jmb.2008.03.026.

253 E. Hamel, B. W. Day and J. H. Miller, *et al.*, Synergistic Effects of Peloruside A and Laulimalide with Taxoid Site Drugs, but Not with Each Other, on Tubulin Assembly, *Mol. Pharmacol.*, 2006, **70**(5), 1555–1564, DOI: 10.1124/mol.106.027847.

254 M. J. Bennett, K. Barakat and J. T. Huzil, *et al.*, Discovery and Characterization of the Laulimalide-Microtubule Binding Mode by Mass Shift Perturbation Mapping, *Chem. Biol.*, 2010, **17**(7), 725–734, DOI: 10.1016/j.chembiol.2010.05.019.

255 T. L. Nguyen, X. Xu and R. Gussio, *et al.*, The Assembly-Inducing Laulimalide/Peloruside A Binding Site on Tubulin: Molecular Modeling and Biochemical Studies with [^{3}H]Peloruside A, *J. Chem. Inf. Model.*, 2010, **50**(11), 2019–2028, DOI: 10.1021/ci1002894.

256 J. Estévez-Gallego, B. Álvarez-Bernad and B. Pera, *et al.*, Chemical modulation of microtubule structure through the laulimalide/peloruside site, *Structure*, 2023, **31**(1), 88–99, DOI: 10.1016/j.str.2022.11.006.

257 S. Vermeulen, S. Ernst and E. Blondeel, *et al.*, Pelophen B is a non-taxoid binding microtubule-stabilizing agent with

promising preclinical anticancer properties, *Sci. Rep.*, 2024, **14**(1), 30188, DOI: 10.1038/s41598-024-80672-z.

258 I. Paterson, D. Menche and A. E. Håkansson, *et al.*, Design, synthesis and biological evaluation of novel, simplified analogues of laulimalide: modification of the side chain, *Bioorg. Med. Chem. Lett.*, 2005, **15**(9), 2243–2247, DOI: 10.1016/j.bmcl.2005.03.018.

259 M. A. McGowan, C. P. Stevenson and M. A. Schiffler, *et al.*, An Enantioselective Total Synthesis of (+)-Peloruside A, *Angew. Chem., Int. Ed.*, 2010, **49**(35), 6147–6150, DOI: 10.1002/anie.201002177.

260 X. Liao, Y. Wu and J. K. D. Brabander, Total Synthesis and Absolute Configuration of the Novel Microtubule-Stabilizing Agent Peloruside A, *Angew. Chem., Int. Ed.*, 2003, **42**(14), 1648–1652, DOI: 10.1002/anie.200351145.

261 S. Kobayashi, K. Tsuchiya and T. Harada, *et al.*, Pironetin, a novel plant growth regulator produced by Streptomyces sp. NK 10958. I. Taxonomy, production, isolation and preliminary characterization, *J. Antibiot.*, 1994, **47**(6), 697–702, DOI: 10.7164/antibiotics.47.697.

262 S. Kobayashi, K. Tsuchiya and T. Kurokawa, *et al.*, Pironetin, a novel plant growth regulator produced by Streptomyces sp. NK10958. II. Structural elucidation, *J. Antibiot.*, 1994, **47**(6), 703–707, DOI: 10.7164/antibiotics.47.703.

263 S. Kobayashi, K. Tsuchiya and M. Nishide, *et al.*, Pironetin, a novel plant growth regulator produced by Streptomyces sp. NK10958. III. Biosynthesis, *J. Antibiot.*, 1995, **48**(8), 893–895.

264 M. Kondoh, T. Usui and S. Kobayashi, *et al.*, Cell cycle arrest and antitumor activity of pironetin and its derivatives, *Cancer Lett.*, 1998, **126**(1), 29–32, DOI: 10.1016/S0304-3835(97)00528-4.

265 M. Kondoh, T. Usui and T. Nishikiori, *et al.*, Apoptosis induction via microtubule disassembly by an antitumour compound, pironetin, *Biochem. J.*, 1999, **340**(2), 411–416.

266 S. Matthew, Q.-Y. Chen and R. Ratnayake, *et al.*, Gatorbulin-1, a distinct cyclodepsipeptide chemotype, targets a seventh tubulin pharmacological site, *Proc Natl. Acad. Sci. U. S. A.*, 2021, **118**(9), e2021847118, DOI: 10.1073/pnas.2021847118.

267 Q.-Y. Chen, R. Ratnayake and R. Hortigüela, *et al.*, Probing a distinct druggable tubulin binding site with gatorbulins 1–7, their metabolic and physicochemical properties, and pharmacological consequences, *Bioorg. Med. Chem.*, 2023, **95**, 117506, DOI: 10.1016/j.bmc.2023.117506.

268 T. Mühlethaler, L. Milanos and J. A. Ortega, *et al.*, Rational Design of a Novel Tubulin Inhibitor with a Unique Mechanism of Action, *Angew. Chem., Int. Ed.*, 2022, **61**(25), e202204052, DOI: 10.1002/anie.202204052.

269 A. Rai, T. Liu and E. A. Katrukha, *et al.*, Lattice defects induced by microtubule-stabilizing agents exert a long-range effect on microtubule growth by promoting catastrophes, *Proc Natl. Acad. Sci. U. S. A.*, 2021, **118**(51), e2112261118, DOI: 10.1073/pnas.2112261118.

270 C. M. Berg, V. A. van den, Volkov and S. Schnorrenberg, *et al.*, CSPP1 stabilizes growing microtubule ends and damaged lattices from the luminal side, *J. Cell Biol.*, 2023, **222**(4), e202208062, DOI: 10.1083/jcb.202208062.

271 G. L. Sala, N. Olieric and A. Sharma, *et al.*, Structure, Thermodynamics, and Kinetics of Plinabulin Binding to Two Tubulin Isotypes, *Chem*, 2019, **5**(11), 2969–2986, DOI: 10.1016/j.chempr.2019.08.022.

272 D. Lucena-Agell, Ó. Fernández, R. París-Ogáyar, *et al.*, An Atlas of Microtubule Lattice Parameters Regulated through Ligand Binding to the Microtubule Stabilizing Sites. 2025, DOI: 10.1101/2025.11.11.687833.

273 F. Bonato, R. París-Ogáyar, A. Soliman, *et al.*, Dissecting Structural and Functional Determinants of Microtubule Stabilization through Guided Chemical Modulation. 2025, DOI: 10.1101/2025.10.23.684077.

274 J. F. Díaz and J. M. Andreu, Kinetics of dissociation of the tubulin-colchicine complex. Complete reaction scheme and comparison to thermodynamic measurements, *J. Biol. Chem.*, 1991, **266**(5), 2890–2896, DOI: 10.1016/S0021-9258(18)49931-0.

275 S. Glauser, R. París-Ogáyar, D. Lucena-Agell, V. Palomo, J. F. Díaz and K. H. Altmann, Synthesis and Early Assessment of Epothilone-Derived Fluorescent Probes for Microtubule Imaging, *ChemMedChem*, 2026, **21**(2), e202500947, DOI: 10.1002/cmdc.202500947.